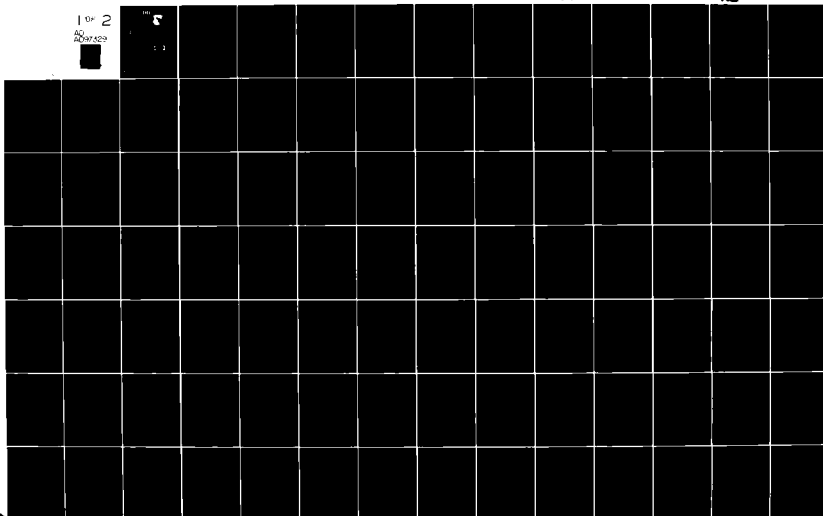


AD-A097 329 CONNECTICUT UNIV STORRS DEPT OF ELECTRICAL ENGINEERING--ETC F/8 5/9
HUMAN OPERATOR MODELING FOR AERIAL TRACKING.(U)
DEC 80 J KORN, A R EPHRAH, D L KLEINMAN F33615-78-C-0517
UNCLASSIFIED EECS-TR-79-16 AFAMRL-TR-80-44 NL

1 of 2
AD
A097 329



LEVEL II

12

AD A 097329

AFAMRL-TR-80-44



HUMAN OPERATOR MODELING FOR AERIAL TRACKING

**JONATHAN KORN
ARYE R. EPHRATH
DAVID L. KLEINMAN**

DECEMBER 1980

**DTIC
ELECTE
S APR 3 1981 D
B**

Approved for public release; distribution unlimited.

UNC FILE COPY

**AIR FORCE AEROSPACE MEDICAL RESEARCH LABORATORY
AEROSPACE MEDICAL DIVISION
AIR FORCE SYSTEMS COMMAND
WRIGHT-PATTERSON AIR FORCE BASE, OHIO 45433**

81 4 3 131

NOTICES

When US Government drawings, specifications, or other data are used for any purpose other than a definitely related Government procurement operation, the Government thereby incurs no responsibility nor any obligation whatsoever, and the fact that the Government may have formulated, furnished, or in any way supplied the said drawings, specifications, or other data, is not to be regarded by implication or otherwise, as in any manner licensing the holder or any other person or corporation, or conveying any rights or permission to manufacture, use, or sell any patented invention that may in any way be related thereto.

Please do not request copies of this report from Air Force Aerospace Medical Research Laboratory. Additional copies may be purchased from:

National Technical Information Service
5285 Port Royal Road
Springfield, Virginia 22161

Federal Government agencies and their contractors registered with Defense Documentation Center should direct requests for copies of this report to:

Defense Documentation Center
Cameron Station
Alexandria, Virginia 22314

TECHNICAL REVIEW AND APPROVAL

AFAMRL-TR-80-44

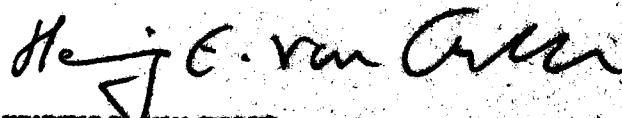
The experiments reported herein were conducted according to the "Guide for the Care and Use of Laboratory Animals," Institute of Laboratory Animal Resources, National Research Council.

The voluntary informed consent of the subjects used in this research was obtained as required by Air Force Regulation 169-3.

This report has been reviewed by the Office of Public Affairs (PA) and is releasable to the National Technical Information Service (NTIS). At NTIS, it will be available to the general public, including foreign nations.

This technical report has been reviewed and is approved for publication.

FOR THE COMMANDER



HENNING E. VON GIERKE
Director
Biodynamics and Bioengineering Division
Air Force Aerospace Medical Research Laboratory

SECURITY CLASSIFICATION OF THIS PAGE (When Data Entered)

19 REPORT DOCUMENTATION PAGE		7 READ INSTRUCTIONS BEFORE COMPLETING FORM
1 REPORT NUMBER AFAMRL-TR-80-44	2 GOVT ACCESSION NO. AD-A097329	3 REGISTRATION CATALOG NUMBER Technical Report
4 TITLE (and Subtitle) HUMAN OPERATOR MODELING FOR AERIAL TRACKING		5 DATE OF REPORT (Month-Year) 1 Oct 78 - 30 Sep 79 Technical Report
7 AUTHOR(s) Jonathan Korn Arye R. Ephrath David L. Kleinman		6 PERFORMING ORG. REPORT NUMBER Technical Report, 79-16 CONTRACT OR GRANT NUMBER(s) F33615-78-C-0517
9 PERFORMING ORGANIZATION NAME AND ADDRESS University of Connecticut Department of Electrical Engineering and Storrs, CT 06268 Computer Sciences		10 PROGRAM ELEMENT, PROJECT, TASK AREA & WORK UNIT NUMBERS 62202F, 6893, 02-16
11 CONTROLLING OFFICE NAME AND ADDRESS Air Force Aerospace Medical Research Laboratory Aerospace Medical Division, Air Force Systems Command, Wright-Patterson Air Force Base, OH 45433		12 REPORT DATE Dec 1980
14 MONITORING AGENCY NAME & ADDRESS (if different from Controlling Office)		13 NUMBER OF PAGES 123
		15 SECURITY CLASS. (of this report) UNCLASSIFIED
16 DISTRIBUTION STATEMENT (of this Report) Approved for public release; distribution unlimited.		15a DECLASSIFICATION DOWNGRADING SCHEDULE
17 DISTRIBUTION STATEMENT (of the abstract entered in Block 20, if different from Report)		
18 SUPPLEMENTARY NOTES		
19 KEY WORDS (Continue on reverse side if necessary and identify by block number) Tracking Air-to-air combat Acceleration Pilot performance Linear Acceleration G-Stress		
20 ABSTRACT (Continue on reverse side if necessary and identify by block number) Modern Optimal Control techniques are employed to investigate and model human performance degradation under sustained positive linear acceleration stress. The study, which combines both experimental and analytical programs, reaffirms the hypothesis that target tracking performance under G_z -stress deteriorates significantly. The empirical data exhibit trends which manifest this contention: G_z -stress effects slow tracking error recovery, lower magnitude of the human describing function, increased variability in tracking errors, a large increase in the pilot's control remnant, and significantly... (continued)		

DD FORM 1 JAN 73 1473 EDITION OF 1 NOV 65 IS OBSOLETE

SECURITY CLASSIFICATION OF THIS PAGE (When Data Entered)

417576

(block 20 continued)

-larger RMS tracking scores.

A normative performance G-model, based upon the Optimal Control Model (OCM), is developed. The model outputs include first-and second-order statistics of the various quantities in the tracking loop, such as tracking errors, control input time histories. Alternately, when a steady state situation is considered, the model predicts the human transfer function, control remnant and other related frequency measures. It is shown that under G_z -stress, the OCM is augmented with G-submodels and that model parameters depart from their nominal values.

PREFACE

This research project was funded by the Air Force Aerospace Medical Research Laboratory under contract No. F33615-78-C-0517 with the University of Connecticut. The technical monitor was Dr. Daniel W. Repperger, Acceleration Effects Branch of the Biodynamic and Bioengineering Division, AFAMRL. The support and assistance provided by Dr. Repperger and by the Air Force personnel associated with the Dynamic Environment Simulator system at AFAMRL were invaluable throughout the project effort.

At the University of Connecticut, principal investigators were Dr. David L. Kleinman and Dr. Arye R. Ephrath. Graduate Research Assistance was Mr. Jonathan Korn. Report preparation was done by Mrs. Sharon Smalley and Ms. Nancy Coderre.

Accession For	
NTIS GRA&I	<input checked="" type="checkbox"/>
DTIC TAB	<input type="checkbox"/>
Unannounced	<input type="checkbox"/>
Justification	
By	
Distribution/	
Availability Codes	
Avail and/or	
Dist	Special
A	

TABLE OF CONTENTS

<u>Chapter</u>	<u>Page</u>
I. OVERVIEW	6
1.1 Program Background.	6
1.2 Review of Physiological and Tracking Performance under Sustained Acceleration.	8
1.3 Experimental Phase.	13
1.4 Modeling Consideration.	15
II. REPETITIVE-G -- NONSTATIONARY TARGET PROFILE	29
2.1 Experimental Program.	29
2.2 Ensemble Data Analysis.	40
2.3 Modeling the Longitudinal Tracking Task	58
2.4 Modeling the Lateral Tracking Task.	82
III. FREQUENCY DOMAIN MEASURES OF HUMAN PERFORMANCE UNDER G-STRESS.	93
3.1 Experimental Design	94
3.2 Modeling Approach	99
3.3 Results and Discussion.	102
IV. CONCLUSIONS.	111
APPENDIX	113
REFERENCES	116

LIST OF ILLUSTRATIONS

<u>Figure</u>		
1	Positive Acceleration Induced on a Centrifuged Subject.	13
2	Closed-Loop Tracking Configuration	14
3	Optimal Control Model of Human Response.	17
4	Human Operator Modeling Hierarchy.	28
5	Closed-Loop Dynamic Tracking Configuration	29

LIST OF ILLUSTRATIONS (continued)

<u>Figure</u>		<u>Page</u>
6	Peak Profile $G_T(t)$	31
7	Peak Profile $G_T(t)$	31
8	Peak Profile $G_T(t)$	31
9	Longitudinal Tracking Geometry.	35
10	A 4th Order Lateral Tracking Model.	39
11	Mean Pitch Tracking Error, 0 Peak, Static G	43
12	Standard Deviation, 0 Peak, Static G.	43
13	Mean Pitch Tracking Error, 1 Peak, Static G	44
14	Standard Deviation Pitch Error, 1 Peak, Static G.	44
15	Mean Pitch Tracking Error, 5 Peaks, Static G.	45
16	Standard Deviation Pitch Error, 5 Peaks, Static G	45
17	Mean Pitch Tracking Error, 0 Peak, Dynamic G.	46
18	Standard Deviation Pitch Error, 0 Peak, Dynamic G	46
19	Mean Pitch Tracking Error, 1 Peak, Dynamic G.	47
20	Standard Deviation Pitch Error, 1 Peak, Dynamic G	47
21	Mean Pitch Tracking Error, 5 Peaks, Dynamic G	48
22	Standard Deviation Pitch Error, 5 Peaks, Dynamic G.	48
23	Mean Heading Tracking Error, 1 Peak, Static G	49
24	Standard Deviation Heading Error, 1 Peak, Static G.	49
25	Mean Heading Tracking Error, 1 Peak, Dynamic G.	50
26	Standard Deviation Heading Error, 1 Peak, Dynamic G	50
27	Commanded G_z Mean, Static G	51
28	Commanded G_z Mean, Dynamic G.	51
29	Subject Attained G Mean, Dynamic G.	52
30	95% Confidence Interval for $(\bar{e}_S - \bar{e}_D)$ Under Null Hypothesis . . .	54

LIST OF ILLUSTRATIONS (continued)

<u>Figure</u>		<u>Page</u>
31	95% Confidence Interval for $\frac{\sigma_z^2}{\sigma_{\bar{e}}^2}$	54
32	95% Confidence Interval for $(\bar{\sigma}_{\bar{e}} - \bar{\sigma}_{\bar{e}})$ Under Null Hypothesis.	55
33	95% Confidence Interval for $\frac{\sigma_z}{\sigma_{\bar{e}}}$	55
34	Pitch Error Threshold Time History	68
35	Mean Pitch Tracking Error, 1 Peak, Static G.	72
36	Standard Deviation Tracking Error, 1 Peak, Static G.	72
37	Mean Pitch Tracking Error, 1 Peak, Dynamic G	73
38	Standard Deviation Tracking Error, 1 Peak, Dynamic G	73
39	Commands G_z , Dynamic G Condition	74
40	Attained G_z Profile.	74
41	Model-VS-Data, Pitch Error Mean, Static G.	75
42	Model-VS-Data, Pitch Error SD, Static G.	76
43	Model-VS-Data, Pitch Error Mean, Dynamic G	77
44	Model-VS-Data, Pitch Error SD, Dynamic G	78
45	Model-VS-Data, Commanded G_z , Static G Condition.	79
46	Model-VS-Data, Commanded G_z , Dynamic G Condition	80
47	Motor Noises in the Lateral Tracking Task.	88
48	Standard Deviation Heading Error, 1 Peak, Static G	91
49	Standard Deviation Heading Error, 1 Peak, Dynamic G.	91
50	Model-VS-Data, Heading Error SD, Static G.	92
51	Model-VS-Data, Heading Error SD, Dynamic G	92
52	Tracking Task Configuration.	94
53	Pilot Describing Function Magnitude, $ H(j\omega) $, Static Condition.	106
54	Pilot Describing Function Magnitude, $\angle H(j\omega)$ Static Condition.	106
55	Control Remnant $R(\omega)$, Static Condition	107

LIST OF ILLUSTRATIONS (continued)

<u>Figure</u>		<u>Page</u>
56	Pilot Describing Function Magnitude $ H(j\omega) $, Dynamic Condition.	107
57	Pilot Describing Function Phase $\angle H(j\omega)$ Dynamic Condition	108
53	Control Remnant $R(\omega)$, Dynamic Condition	108
59	Pilot Describing Function Magnitude $ H(j\omega) $, Post Run Condition.	109
60	Pilot Describing Function Phase $\angle H(j\omega)$, Post Run Condition	109
61	Control Remnant $R(\omega)$, Post Run Condition.	110

LIST OF TABLES

<u>Table</u>		
1	Summary of Frequency Components	95
2	RMS Scores.	105
3	Model Parameters.	105

1. OVERVIEW

1.1 Program Background

Linear acceleration forces are encountered frequently in high-performance aircraft during rapid turns and pullouts from dives. It has long been recognized that these forces subject the pilot to a psycho-physiological stress that could degrade his performance.⁺ The problems associated with acceleration forces acting on pilots became even more pronounced with the development of the supersonic high-performance aircraft.

There is a wide spectrum of acceleration environments that may be encountered in a flying aircraft; the direction of the acting acceleration constitute its major distinctive characteristic. A comparative nomenclature for the various conventions used to describe the acceleration environment, largely referred to as G, may be found in the literature (Roth et al. [2]). The subject of the current study was the special linear acceleration which is known as positive acceleration, i.e., an acceleration acting in the head-to-foot direction. Often, it is referred to as $+G_z$ or vertical acceleration.

A vast amount of research has dealt with the effects of linear accelerations on pilots. These studies can be divided into two categories: Elementary research pertaining to the psycho-physiological response of the human under G-stress, and research dealing directly with the effects of sustained acceleration on human performance, as expressed explicitly by degraded tracking capabilities and loss of flight control. A survey of these research efforts follows in a subsequent section.

⁺ According to Brown [1], pilots in the Schneider Trophy Race of 1930 were the first to have experienced the visual effects of sustained acceleration.

These past research efforts were mostly empirical. Some descriptive models of human response to G-stress have been postulated, usually via experimental data reduction and statistical analysis techniques. In order to complement these research efforts, and to evaluate pilot performance under G-stress analytically, a normative performance model has become a developmental goal. That is, an analytical model, capable of predicting human performance decrements under G-stress is sought. This type of a prescriptive model can be utilized in a variety of applications, such as the optimization of fighter-cockpit design, or the definition of aircraft state augmentation requirements.

Accordingly, a research program supported by the USAF and performed concurrently at the Air Force Aerospace Medical Research Laboratory and at CYBERLAB the University of Connecticut, was undertaken. Through this combined experimental/analytical program, we have sought to investigate and model the following issues:

- 1) The effects of G-stress on human performance in a longitudinal air-to-air compensatory tracking task. Specifically, experiments were carried out with closed-loop sustained accelerations where the subject's pitch rate commands were also the driving signals to the centrifuge on which the positive acceleration was simulated.
- 2) The effects of G-stress on pilot performance of a secondary task. Along with the longitudinal air-to-air tracking under G-stress, the subjects performed a lateral tracking task as well. This task represented essentially a side-task as there were no target aircraft motions in the horizontal plane; the tracking error was induced solely by the pilot's involuntary roll commands. The experimental results obtained at AMRL show a significant degradation in performing this secondary task when under G-stress. Our analytical efforts duplicate these results, thus validating the performance model that has been developed.

- (3) Changes in pilot describing function when operating under G-stress. In the second year of the project a new set of experiments was devised. These experiments involved steady-state tracking under G-stress and they facilitated frequency domain analysis of human response. Both the experimental and the analytical phase of this work explore the changes in the pilot transfer function (between the observed tracking error and the control stick input) under sustained G-stress.
- (4) Changes in tracking scores and pilot's input-uncorrelated control (remnant). One facet of performance-degradation under G-stress is higher RMS values of tracking error and of control remnant. It is shown by model-data comparison that the performance-model parameters are perturbed from their nominal values when G-stress is introduced.
- (5) Model parameters. A comprehensive identification program was developed at CYBERLAB and greatly facilitated the development of the G-model. The algorithm was implemented in software on our PDP 11/60 computer and provided a mechanized, efficient and objective means for identifying the values of the model parameters.

Prior to addressing these sub-tasks, a literature survey pertinent to the effects of sustained accelerations on human beings was undertaken.

1.2 Review of Physiological and Tracking Performance under Sustained Accelerations.

1.2.1 Cardiovascular Response: Perhaps the most fundamental of a person's physiological response to sustained positive G_z -stress is the increase in the hydrostatic pressure gradient in the vascular system. The blood, being the most mobile tissue in the human body, is shifted from the upper parts of the body, notably the head, and is concentrated in the abdomen and the lower extremities. These observations were recognized as a serious problem by Code et al [3], and by Wood et al. [4], and further confirmed by Lindberg and Wood [5]. and

Fraser [6]. These articles report a consistent pattern of changes to the cardiovascular system when subjected to G-stress. According to these studies, there are two distinct periods in the cardiovascular response to positive acceleration with onset rate of about 1 G/Sec: (1) a period of progressive failure, and (2) a subsequent period of compensation. During the cardiovascular failure the following phenomena occur:

1. Decrease in arterial pressure at head level;
2. Increase in arterial and venous pressures at the lower extremities;
3. Increase in intra-abdominal and intrarectal pressures (approximately linear with G_z);
4. Increase in heart rate (this observation was also ascertained by Little et al. [7], and by Smedal et al. [8], although the latter considered mainly linear acceleration in the transverse direction);
5. Decrease in ear-blood volume;
6. Decrease in the arterial pressure pulse amplitude at ear level;
7. Severe interference with blood-tissue oxygenation, vision, cerebral activity and nervous system functions.

Following this period (~ 7 sec) is a subsequent period of compensations. Pressor reflex triggered by the fall in arterial pressure in the carotid sinus initiates partial recovery; it produces hypertension at the heart level that brings the hydrostatic pressure distribution in the vascular system close to normal levels. These dramatic changes in the cardiovascular system profoundly affect other physiological systems, as described below:

1.2.2 Vision: Human visual capabilities are extremely susceptible to variations in the eye blood supply. Degradation of vision is further aggravated by the additional reduction in blood circulation in the eyes due to changes in the intraocular pressure gradient. The gross effects of positive sustained acceleration on vision are as follows [9]:

1. An immediate consequence of decrement in the eye blood supply is retinal hypoxia. Photographs of the retina under sustained positive acceleration can be found in an article by Newson and Leverett [10];
2. Gross limitations in visual fields: tunnel vision (loss of peripheral vision), greyout, blackout. This, too, is a direct result of the reduction of blood circulation in the eye. This phenomenon has been observed and reported by many researchers (White [11], York [12] et al.);
3. Impairment of visual acuity, as reported by Frankenhaeuser [13], White and Jorve [14], and others;
4. Increase in brightness discrimination thresholds, reported by Braunstein and White [15];
5. It has been observed by Smedal et al. [8] that pupillary dilation occurs with the loss of peripheral vision.
6. The oculomotor mechanism is affected. According to White and Monty [16] limited ocular mobility, under sustained positive acceleration, has been observed due to mechanical changes in eye orbital tissues. These limitations can be overcome (with considerable effort), but may result in ataxic eye movements.
7. Smedal et al. [8] furnished photographs of the cornea, under transverse acceleration. It is evident that it is mechanically deformed, resulting perhaps in blurred vision.

1.2.3 Pulmonary-Respiratory Response: Physiological phenomena related to prolonged accelerations occur in the pulmonary and respiratory systems. Along with the increase in the pressure differences in the vascular system, there is an independent increase in the arterial and venous pressure gradients along the lungs' base-to-apex axis. These findings are mentioned by Lindberg and Wood [5] and Fraser [6]. This increase is followed by hypoxemia, which increases in severity with repeated exposures to vertical G, as reported by Barr [17]. Lindberg and Wood [5] observed that displaced internal organs, under sustained positive G, pull the diaphragm downward, causing difficulties in breathing. York et al. [12] and Smedal et al. [8] reported evident cases of dyspnea (shortness of breath) under transverse accelerations ($+G_x$). Smedal et al. [8] also reported reduction in the vital capacity, increase in respiratory rate, diminished alveolar ventilation (hypoxia) and hypercapnia.

1.2.4 Psychomotor Performance: It is quite obvious that under sustained acceleration, motor performance (as expressed in manual movements and manipula-

tion tasks) would be disturbed. Indeed, Brown and Lechner, in their survey of research, report changes in the forces that both arms can exert when under G-stress [1]. Canfield et al. [18] conducted experiments proving that movement time and reaching errors increase with increase in G. Similar results were shown by Cohen [19,20], Kaehler and Meehan [21], Little et al. [7], and Frankenhaeuser [13].

An increase in human reaction time to various stimuli comprise another symptom of sustained acceleration. These findings are reported by several researchers (Frankenhaeuser [13], Canfield et al. [22,23], Kaehler and Meehan [21].)

1.2.5 Other: The following are among some other side effects of positive G:

1. Degradation in intellectual performance, resulting probably from acceleration effects on the central neural system (Grether [9], Frankenhaeuser [13], Ross and Chambers [24], Miller et al. [25]).
2. Variations in time perception with different levels of G (Frankenhaeuser [13]).
3. Effects on the vestibular, kinesthetic and proprioceptive senses (Brown and Lechner [1]). These are attributed mainly to the centrifugation side effects, and are usually not present during linear acceleration in real flight situations.

1.2.6 Tracking Performance

It is our conviction that some, if not most, of the psycho-physiological responses to sustained positive acceleration lead ultimately to variations in tracking task performance. It was necessary, therefore, to review the findings related to this problem.

First reports concerning tracking performance and flight control did not appear, as noted by Grether [9], until 1958. Since then, research in this area has been extensive, although no modeling efforts using modern control theory have ever been attempted. The majority of these studies has been oriented toward transverse ($+G_x$) direction. Some studies, however, do deal with tracking performance (not necessarily air-to-air tracking) under $+G_z$ stress.

Brown and Collins [26] and Brown [27] pioneered in closed-loop centrifuge simulation of air-to-air tracking tasks. They found a significant increase in what they called "average tracking scores," mostly in the longitudinal axis, when performing under vertical acceleration stress. Piranian [28] and Smiles [29] also reported that sustained $+G_z$ up to 6 G had appreciable effects, degrading air-to-air tracking performance. Similar results, for an open-loop centrifugation with various levels of $+G_z$, in pursuit tracking experiments were reported by Fletcher et al. [30]. Kaehler [31], Little et al. [7], and Middleton et al. [32] conducted various tracking experiments and, although they considered transverse accelerations only, their results generally agree with the $+G_z$ experiment results.

Creer et al. [33] conducted tracking experiments that simulated a re-entry vehicle piloting task. One of their findings was that an increase in tracking deficiency occurred when performing under $+G_z$ acceleration, vs. $+G_x$ or $-G_x$ stress conditions. In addition, they observed a marked deterioration in pilot tracking performance during the onset of the acceleration, i.e., during active \dot{G} . They explained this by "vertigo sensations caused by the angular rotations of the centrifuge gondola as the centrifuge was brought up to the desired operating speed."

There is a general agreement among the various reports, relating to the effects of acceleration feedback on tracking performance. This type of informational feedback is usually categorized as motion cues. Chambers [34] reported a noted improvement in performance when the centrifuge was engaged in a closed-loop operation vs. static conditions. However, this was found for low levels of acceleration only. Brown and Collins [26] reported pronounced improvement in dynamic vs. static tracking scores when a coordinated flight simulation was employed. Guercio and Wall [35] also emphasize the importance of congruent

motion in compensatory tracking. They showed that the presence of motion cues resulted in lower tracking errors.

1.3 Experimental Phase

Experiments investigating the effects of positive acceleration on pilots were conducted as early as the mid 1930's. These studies were carried out in real aircraft. Continuing research interests motivated the construction of the first human centrifuge systems, for aviation studies, in the U.S. and in Germany. The basic human centrifuge is a gimbal-mounted cab at the end of a rotating arm. The cab is free to rotate, independently of the rotating arm, in two axes. It is possible, therefore, for a pilot seated in the cab to perform a task while subjected to a wide variety of acceleration patterns. Later models of the human centrifuge were able to replicate air-to-air combat situations successfully. A detailed description of a human centrifuge can be found in the literature [4,26].

One way of inducing a sustained positive (z-axis) acceleration on a centrifuged subject is to spin the apparatus around the central axis of rotation, while tilting the cab inward. This is shown in Figure 1.

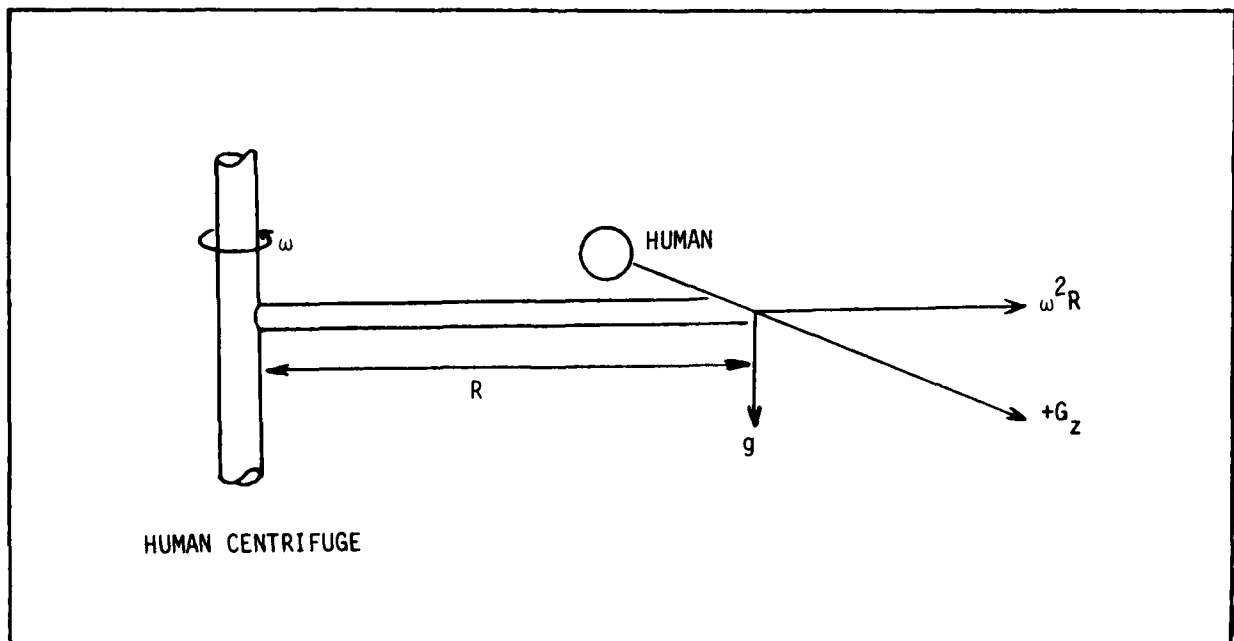


Fig 1 POSITIVE ACCELERATION INDUCED ON A CENTRIFUGED SUBJECT

In order to achieve the desired (or commanded) vertical acceleration, the angle α and the radial velocity ω are adjusted according to equations 1.1-1.2, R being the radius of rotation:

$$\omega^2 R \cos \alpha + g \sin \alpha = G_z \quad (1.1)$$

$$\omega^2 R \sin \alpha + g \cos \alpha = 0 \quad (1.2)$$

This is the technique employed in the high-G experiments that were conducted on the Dynamic Environment Simulator (DES) facility at the Air Force Aerospace Medical Research Laboratory.

The AMRL experiments simulated an air-to-air combat scenario. The centrifuged subjects were instructed to track a stylized target aircraft image using a cross-hair reticle sight. The target motion followed either a predetermined or a pseudo-random pattern in either the longitudinal or the lateral plane. The closed-loop configuration of the tracking task is schematically depicted in Figure 2.

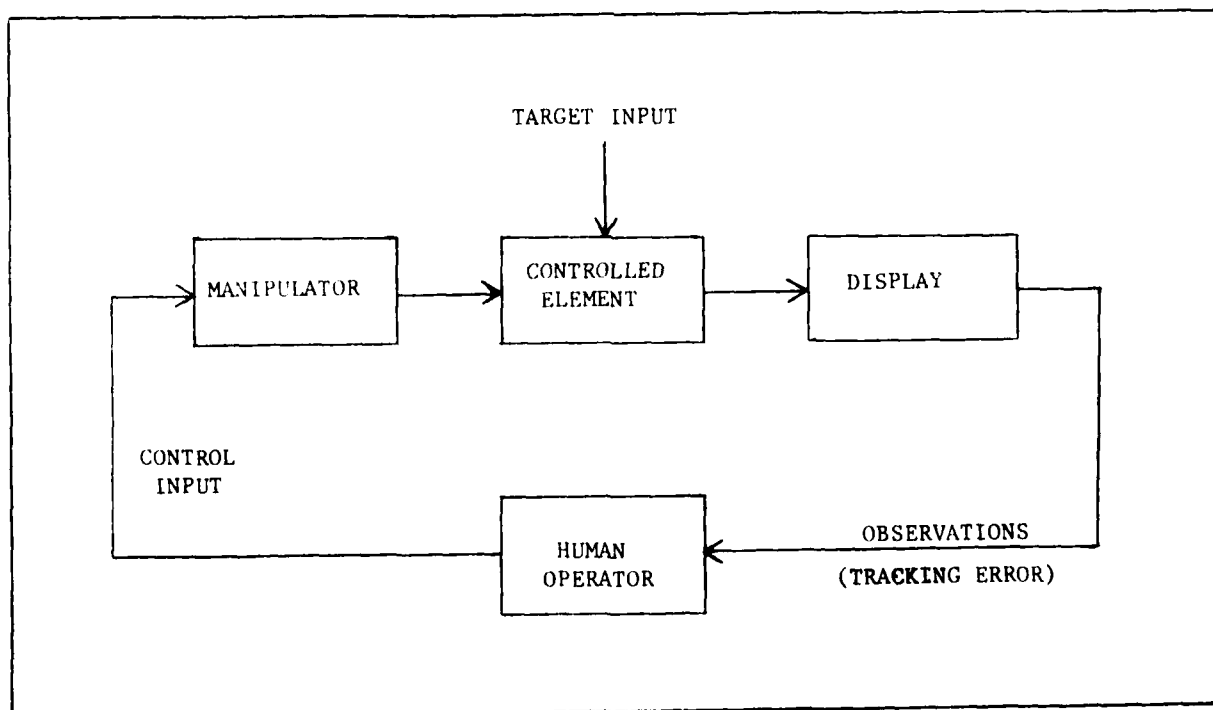


Fig. 2 CLOSED-LOOP TRACKING CONFIGURATION

In order to segregate the effects that G_z forces have on the pilot's tracking performance, two experimental conditions are employed. In the first case, denoted here as static-G, the subjects tracked the target with the centrifuge at rest. In the second experimental condition, denoted here as dynamic-G, the DES was in motion. In addition, a third condition was included in one set of experiments (Chapter III). In these experiments the cumulative G-effects were investigated. Thus, every G-stress run was immediately followed by a static tracking session. These were denoted as post-static runs.

The recorded data included the time histories of tracking errors, the subject-commanded and attained-G, his control inputs and other auxiliary variables. In addition, physiological variables were recorded, heart rate, systolic and diastolic pressures, etc. The raw data analysis included across-subject ensemble averaging and FFT analysis on stationary data.

A detailed description of the experimental program as well as of the data analysis techniques involved follows in Sections 2.1 and 3.1.

1.4 Modeling Considerations

The modeling efforts in the present study have been based upon the well-known Optimal Control Model (OCM) (Kleinman et al. [36], Baron et al. [37], and Kleinman et al. [38]). The main contribution of the modeling phase was the adjustment and the modification of the OCM to include the effects of G_z -stress on pilot performance. A major reason for using the OCM as opposed to some other human performance model, is that the parameters of this model are descriptive of human limitations. Thus, they have shown a remarkable invariance over different task specifications, input disturbances or commands, and controlled-vehicle dynamics. It therefore follows that changes in the "nominal" OCM in a sustained acceleration environment are induced almost entirely by the G_z stress.

1.2.4 Modeling Approach

Figure 3 shows the structure of the OCM. The vehicle dynamics are represented in state space form

$$\begin{aligned}\dot{x}_o(t) &= A_o x_o(t) + b_o u(t) + E_o w_o(t) + F_o z(t) \\ v(t) &= C x_o(t) + d_o u(t)\end{aligned}\quad (1.3)$$

where $w_o(t)$ is usually a white-Gaussian disturbance with covariance W_o and $z(t)$ is a deterministic vehicle trajectory. The displayed information $y(t)$ consists of tracking error $e(t)$ and error-rate $\dot{e}(t)$, as well as other auxiliary variables and their rate of change.

The visual assumption in the OCM is that the human perceives a delayed and noisy replica of $y(t)$, viz.,

$$\underline{y}_p(t) = \underline{y}(t-\tau) + \underline{v}_y(t-\tau) \quad (1.4)$$

where the white-Gaussian observation noise $v_{yi}(t)$ of the i -th indicator has covariance

$$v_{yi}(t) = \frac{\pi_D y_i}{f_i(t) N(a_i)} E \left\{ y_i^2(t) \right\} \quad (1.5)$$

In these equations τ is the pilot's lumped time-delay, v_{yi} is the observation noise/signal ratio, $f_i(t)$ is the fraction of attention the human is allocating to each observation[†], and $N(a_i)$ is the equivalent "gain" of the visual/indifference threshold a_i . The gain $N(a_i)$ is obtained via statistical linearization derived from Random Input Describing Function Theory, and is also a function of the mean and the standard deviation of $y_i(t)$.

Assuming that the system state estimate, \hat{x}_o , is given, then the human develops an optimal control strategy by minimizing the quadratic cost functional,

[†]Total attention f_{TOT} is assumed = 1. This is subdivided across axes of control, and further subdivided among instruments per axis.

OPTIMAL CONTROL MODEL OF HUMAN RESPONSE

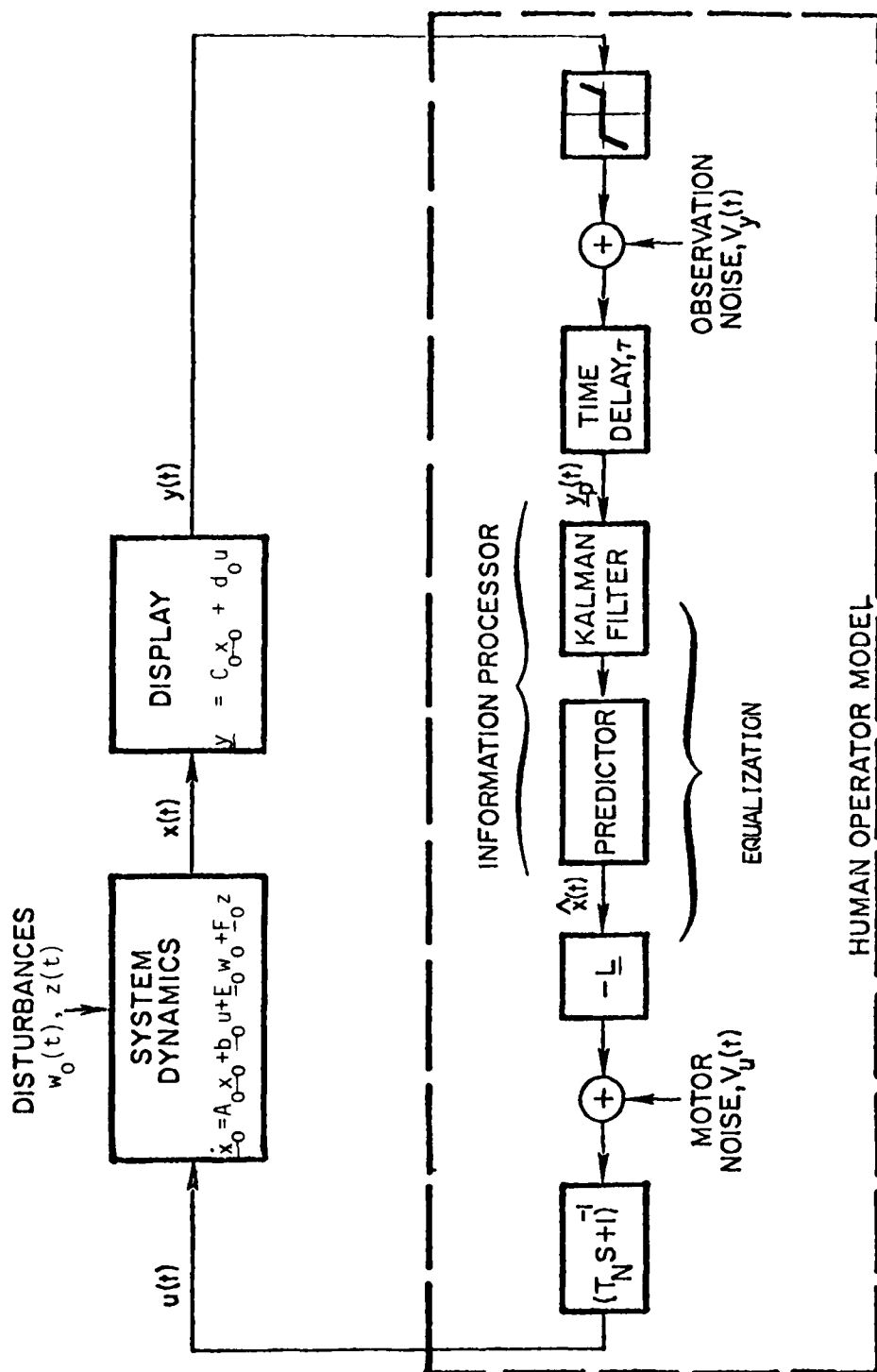


Fig. 3 OPTIMAL CONTROL MODEL OF HUMAN RESPONSE

$$J(u) = \lim_{T \rightarrow \infty} \frac{1}{T} E \left\{ \int_0^T (\underline{y}'(t) Q_y \underline{y}(t) + g \dot{u}^2(t)) dt \right\} \quad (1.6)$$

where $Q_y = \text{diag}(q_{yi})$ are the relative weightings on the observations and g is the control-rate weighting[†]. Usually, the tracking error weighting coefficient, q_e , is non-zero, since the objective is to minimize the observed error. By augmenting the state estimate with the control u , viz.,

$$\underline{\hat{x}} = \begin{bmatrix} \hat{x}_0 \\ u \end{bmatrix} \quad (1.7)$$

this strategy results in the optimal control gains, \underline{L}_1 , arising from the pertinent steady-state Riccati equation, such that

$$\dot{\underline{\hat{x}}}(t) = -\underline{L}_1' \begin{bmatrix} \hat{x}_0 \\ u \end{bmatrix} \triangleq -\underline{L}_1' \underline{\hat{x}}(t)$$

If we define $\underline{L}_1' \triangleq \begin{bmatrix} \tau_N^{-1} \underline{L}'_{opt} & \tau_N^{-1} \end{bmatrix}$ and include motor noise in the pilot's control, the optimal control, $u(t)$, obeys the equation

$$\tau_N \dot{u} + u = -\underline{L}'_{opt} \hat{x}_0 + v_u(t) \triangleq u_c(t) + v_u(t) \quad (1.8)$$

or with $\underline{L}' \triangleq \begin{bmatrix} \underline{L}'_{opt} & 0 \end{bmatrix}$

$$\tau_N \dot{u} + u = \underline{L}' \hat{\underline{x}} + v_u(t) = u_c(t) + v_u(t) \quad (1.9)$$

The parameter τ_N can be interpreted as a "neuromotor" time constant. Usually, τ_N is specified and g is adjusted accordingly, as there is a one-to-one correspondence between the two.

The motor noise $v_u(t)$ is assumed to be white and Gaussian with covariance

We assume that the subject seeks a control strategy that would minimize control-rate rather than control.

that scales with the covariance of $u(t)$,

$$V_u(t) = \pi \rho_u \text{cov}[u(t)]. \quad (1.10)$$

The coefficient ρ_u represents the motor-noise/signal ratio.

Next, it is necessary to examine the other blocks of the human information processing unit (Figure 2). That is, how does the subject estimate the state $\hat{x}(t-\tau)$, and how does he predict $\hat{x}(t)$ from $\hat{x}(t-\tau)$. The augmented state $\underline{x}'(t) = [\underline{x}_0'(t), u(t)]$ obeys now the differential equation

$$\dot{\underline{x}}(t) = A \underline{x}(t) + \underline{b}u_c(t) + E\underline{w}(t) + Fz(t) \quad (1.11)$$

where

$$A = \begin{bmatrix} A_o & \underline{b}_o \\ - & - \\ 0 & -\tau_N - 1 \end{bmatrix}, \underline{b} = \begin{bmatrix} 0 \\ - \\ \tau_N - 1 \end{bmatrix}, E = \begin{bmatrix} E_o & 0 \\ - & - \\ 0 & \tau_N - 1 \end{bmatrix}, F = \begin{bmatrix} F_o \\ - \\ 0 \end{bmatrix} \quad (1.12)$$

$$\text{and } \underline{w}(t) = \begin{bmatrix} w_o(t) \\ v_u(t) \end{bmatrix} \text{ with the covariance } W = \begin{bmatrix} W_o & 0 \\ - & - \\ 0 & V_u \end{bmatrix} \quad (1.13)$$

It is not difficult to show, that

$$\hat{\underline{x}}(t) = e^{A\tau} \hat{\underline{x}}(t-\tau) + \int_{t-\tau}^t e^{A(t-\sigma)} \underline{b}u_c(\sigma) d\sigma \quad (1.14)$$

In Equation (1.14) the subject will use the estimate $\hat{\underline{x}}(t-\tau) \triangleq \underline{p}(t)$. This state estimate is obtained from the Kalman filter, via

$$\dot{\underline{p}}(t) = A\underline{p}(t) + \underline{b}u_c(t-\tau) + G(t) [\underline{y}_p(t) - C\underline{p}(t)] \quad (1.15)$$

where

$$p(t) = E \left\{ \underline{x}(t-\tau) | \underline{y}_p(\sigma), \sigma \leq t \right\} \quad (1.16)$$

The filter gain $G(t)$ is

$$G(t) = \Sigma(t) C' V_y^{-1}(t) \quad , \quad V_y(t) = \text{diag} [V_{yi}(t)] \quad (1.17)$$

where $\Sigma(t)$ is generated from the solution of the Riccati equation

$$\dot{\Sigma} = A\Sigma + \Sigma A' - \Sigma C' V_y^{-1} C \Sigma + EWE' + W_d(t) \quad (1.18)$$

Three observations should be made with regard to Equation (1.18).

1. The matrix $W_d(t)$ is a "pseudo-noise" covariance matrix and arises from the deterministic signal $z(t)$. It is chosen in such a way that the filter adapts to the changing characteristics of the trajectory $z(t)$. At present,

$$W_d(t) = \tau_{\text{cor}} \underline{F} z^2(t-\tau) \underline{F}' \quad (1.19)$$

where τ_{cor} is linked to the human short-term memory, or alternately, is dependent on the $z(t)$ profile's bandwidth.

2. In the absence of the deterministic target motion, $W_d(t)=0$ and $\dot{\Sigma}=0$. That is, the steady-state Riccati equation is solved.
3. In the case when the noisy disturbance $w_o(t)=0$, the term EWE' becomes

$$\begin{bmatrix} 0 & 0 \\ - & - & -2 & - \\ 0 & \tau_N & V_u \end{bmatrix} \quad (1.20)$$

1.4.2 Model Application

Basically, modeling efforts utilizing the OCM can be approached in two ways:

1. Time-varying (nonstationary) mode
2. Steady-state mode.

1.4.2.1 Nonstationary Model

In the time-varying case, the target's profile is deterministic, i.e., $z(t) \neq 0$ and $w_0(t) = 0$. This modeling technique usually involves a comparison of experimental data time histories (first- and second-order statistics) with the model-predicted ones. In this case, it is required to develop the process mean and covariance propagation equations which arise from the non-random component $z(t)$ in the process model. These equations have been thoroughly documented (e.g., [38], [39], [40]), and the basic continuous time equations are repeated here without proofs for completeness.

If one defines

$$\begin{aligned}\bar{\underline{\hat{x}}} &= E(\underline{\hat{x}}) \\ \bar{\underline{x}} &= E(\underline{x}) \\ \underline{e}_1(t) &= \underline{x}(t-\tau) - \underline{p}(t) = \text{filtering error} ; \quad \bar{\underline{e}}_1 = E(\underline{e}_1) \\ \underline{e}_2(t) &= \underline{x}(t) - \underline{\hat{x}}(t) = \text{prediction error} ; \quad \bar{\underline{e}}_2 = E(\underline{e}_2) \\ \bar{\underline{y}} &= E(\underline{y})\end{aligned}\quad (1.21)$$

then the process mean and covariance are computed from the following time equations:

$$\dot{\bar{\underline{\hat{x}}}}(t) = \bar{\underline{A}} \bar{\underline{\hat{x}}}(t) + \bar{\underline{G}} \bar{\underline{C}} \bar{\underline{e}}_1(t) ; \quad \bar{\underline{A}} \triangleq \underline{A} - \underline{b} \underline{L}', \bar{\underline{G}} \triangleq \underline{e}^{A\tau} \underline{G} \quad (1.22)$$

$$\dot{\bar{\underline{e}}}_1(t) = \tilde{\underline{A}} \bar{\underline{e}}_1(t) + \underline{F} z(t) ; \quad \tilde{\underline{A}} \triangleq \underline{A} - \underline{G} \underline{C} \quad (1.23)$$

$$\bar{\underline{e}}_2(t) = \int_{t-\tau}^t \underline{e}^{A(t-\sigma)} \underline{F} z(\sigma) d\sigma ; \quad (1.24)$$

$$\bar{\underline{x}}(t) = \bar{\underline{\hat{x}}}(t) + \underline{e}^{A\tau} \bar{\underline{e}}_1(t) + \bar{\underline{e}}_2(t) \quad (1.25)$$

$$\bar{\underline{y}}(t) = \underline{C} \bar{\underline{x}}(t) \quad (1.26)$$

The boundary conditions are appropriately chosen at time $t=\tau$.

Next, if we let \hat{X} , E_1 , E_2 , X and Y be the covariance matrices of \hat{x} , e_1 , e_2 , x and y respectively, and

$$M(t) \triangleq E \left[(\hat{x}(t) - \bar{x}(t)) (e_1(t) - \bar{e}_1(t))' \right] = \text{cross covariance}, \quad (1.27)$$

one can show that

$$X(t) = \hat{X}(t) + e^{A\tau} M'(t) + M(t) e^{A'\tau} + e^{A\tau} E_1(t) e^{A'\tau} + E_2(t) \quad (1.28)$$

$$E_2(t) = \int_{t-\tau}^t e^{A(t-\sigma)} \left[EW(\sigma)E' + W_d(\sigma) \right] e^{A'(t-\sigma)} d\sigma \quad (1.29)$$

$$\dot{E}_1(t) = \bar{A}E_1(t) + E_1(t)\bar{A}' + G\bar{V}_y(t-\tau)G' + EW(t-\tau)E' + W_d(t-\tau) \quad (1.30)$$

$$\dot{M}(t) = \bar{A}M(t) + M(t)\bar{A}' + \bar{G}C \left[E_1(t) - \bar{x}(t) \right] \quad (1.31)$$

$$\dot{\hat{X}} = \bar{A}\hat{X} + \hat{X}\bar{A}' + \bar{G}CM'(t) + M(t)C'\bar{G}' + \bar{G}\bar{V}_y(t-\tau)\bar{G}' \quad (1.32)$$

$$Y = CXC' \quad (1.33)$$

Notice that since we assume in this case $w_o(t)=0$, the matrix $W(t)$ is a zero matrix except for the lower right 1×1 corner entry which is $\tau_N^{-1}V_u(t)$ (see Section 1.4.1).

1.4.2.2 Steady-State Mode

In the steady-state mode $z(t)=0$, and the target input is driven by a stationary colored noise. The usual practice is to describe the disturbance $w_o(t)$ as a white-Gaussian noise, and to augment the system with the dynamics of a noise shaping filter that characterizes the driving noise. The stationary approach is most suitable for frequency domain analysis of human response. The model equations are represented in the frequency domain, so that various performance measures can be

predicted. The model outputs include any of several possible describing functions associated with the subject, the vehicle, or the overall closed-loop system. Also available are power density spectra of any pertinent system variable that show both correlated (i.e., input-related) and remnant (i.e., human-related) components. In addition, the performance scores (RMS values) are predicted. Among the quantities that are considered in the present study are

1. Pilot describing function,
2. Pilot control remnant, and
3. Tracking scores: RMS values of the tracking error and control.

This modeling approach is most suitable for model identification from frequency domain data. The model is applied in conjunction with fourier-transformed experimental data, and measures such as described above can be compared.

The frequency domain equations are summarized here. A more detailed theoretical background can be found in the literature (e.g. [41]).

We assume the model of Equation (1.11) with $z(t)=0$. All initial conditions are ignored since steady-state situation is assumed. The major transfer function of interest initially is that between $y(s)$ and $u_c(s)$:

$$u_c(s) = \underline{H}'(s) \underline{y}(s) \quad (1.34)$$

This function is obtained by taking the Laplace transform of the equations of Section 1.4.1. The following relationships result:

$$\underline{H}'(s) = \left[1 + \Gamma(s) \right]^{-1} \underline{L}' e^{(A-sI)\tau} (sI-\tilde{A})^{-1} G \quad (1.35)$$

$$\Gamma(s) = \underline{L}' \left\{ e^{(A-sI)\tau} \left[(sI-\tilde{A})^{-1} - (sI-A)^{-1} \right] + (sI-A)^{-1} \right\} \underline{b} \quad (1.36)$$

The overall input-output human transfer function is thus

$$u(s) = -(s + \tau_N^{-1})^{-1} \underline{H}'(s) \underline{y}(s) \triangleq \underline{I}'(s) \underline{y}(s) \quad (1.37)$$

where we note that $(s + \tau_N^{-1})^{-1}$ is obtained from the lower right 1×1 corner of $(sI - A)^{-1}$. Next, we also require the decomposition of all closed-loop signals \underline{x} , \underline{y} and u_c into their two major components. The first is that part linearly correlated with the independent input disturbance $w_o(t)$. The second is that part due to the human-injected remnant v_y and v_u . Thus, with $\underline{E}_o' = [\underline{E}_o', 0]$, we obtain

$$u_c(s) = -\underline{H}'(s) \underline{C} \underline{x}(s) - \underline{H}'(s) v_y(s) \quad (1.38)$$

$$\underline{x}(s) = (sI - A + b \underline{H}' \underline{C})^{-1} \underline{E}_o' w_o(s) + (sI - A + b \underline{H}' \underline{C})^{-1} b \left[\underline{H}' v_y(s) + \tau_N^{-1} v_u(s) \right] \quad (1.39)$$

$$\underline{y}(s) = \underline{C} \underline{x}(s) \quad (1.40)$$

Following these equations the human transfer function of (1.37) can be obtained. This describing function is of interest to us since it can be measured experimentally. It is defined, relative to the disturbance $w_o(t)$, as a ratio of the transfer function between u and noise w_o to the transfer function between the observed tracking error e and noise w_o . Thus

$$\frac{u(s)}{e(s)} = \frac{u(s)/w_o(s)}{e(s)/w_o(s)} \quad (1.41)$$

To compute this human describing function we use

$$\begin{aligned} \frac{e(s)}{w_o(s)} &= \left[\underline{C} (sI - A + b \underline{H}' \underline{C})^{-1} \underline{E}_o' \right]_e \\ \frac{u(s)}{w_o(s)} &= \left[(sI - A + b \underline{H}' \underline{C})^{-1} \underline{E}_o' \right]_u \end{aligned} \quad (1.42)$$

It is recognized that $v_y(t)$ does not strictly have a Laplace transform. This, however, is not a problem since we are interested in the uncorrelated spectra.

The subscripts e and u in (1.42) indicate that the tracking error- and control-related components of the describing function are considered.

Finally we require power spectral densities of the various variables in the loop. These are obtained from Equations (1.38-1.40). For any signal the spectrum is decomposed into input and remnant related components, (superscripts c and uc respectively) and the spectral densities $\Phi(\cdot)$ are obtained, viz.,

$$\Phi_{x_k}^{uc}(\omega) = \frac{1}{\pi} \sum_{i=1}^{N_y} |\psi_{ki}^2(j\omega)| V_{yi} + \frac{1}{\pi} |\phi_k^2(j\omega)| V_u \quad (1.43)$$

$$\Phi_{x_k}^c(\omega) = \frac{1}{\pi} |\beta_k^2(j\omega)| W_0 \quad (1.44)$$

where,

x_k = k-th state component

ψ_{ki} = ki-th element of $(sI - A + b\bar{h}'C)^{-1}b\bar{h}'$

ϕ_k = k-th component of $(sI - A + b\bar{h}'C)^{-1}b\bar{\tau}_N^{-1}$

N_y = number of observed variables (dimension of $\underline{y}(t)$)

β_k = k-th element of $(sI - A + b\bar{h}'C)^{-1}\bar{E}_0$

Similar expressions are easily obtained for $\Phi_{y_k}^c(\omega)$, $\Phi_{y_k}^{uc}(\omega)$, $\Phi_u^c(\omega)$ and $\Phi_u^{uc}(\omega)$. The spectral density $\Phi_u^{uc}(\omega)$ is of special interest in this study as it represents the human input-uncorrelated control. It will be shown in Chapter III that the magnitude of $\Phi_u^{uc}(\omega)$ in G-stress conditions is significantly larger than it is in no-G situations. This

is an excellent indicator of the human's motor randomness which increases in the presence of sustained linear accelerations.

1.4.3 Model Development

The baseline model adopted in this work was, as noted previously, the Optimal Control Model of human performance. The approach taken in the G-stress modeling process was to develop a "G submodel" that can be embedded in the general structure of the OCM. The steps taken in this direction included a development of technology to isolate and identify the effects on tracking error and pilot control of target motion versus those associated with G-stress. The effects of target motion were studied via static (no G) experiments. If a pilot model is first tuned accurately to this case, then our hypothesis was that any data-vs-model mismatch in the dynamic-G tracking case is attributable to the effects of the G-stress. The subsequent identification process to model the mismatch consisted of four steps:

1. Sensitivity analysis: A comprehensive sensitivity analysis of model to OCM parameter variations was undertaken.
2. Development of generic structural formulae that relate pilot parameters to instantaneous and/or antecedent load factor (G and $\int G$);
3. a. Adjustment (tuning) of the free parameters within the OCM:
 τ , τ_N , a_i , ρ_{yi} and ρ_u ;
3. b. Tuning of the free parameters within the structural submodels so as to best match given data;
4. An identification program that performed the final fine-tuning adjustments to the OCM and the G submodel parameters.

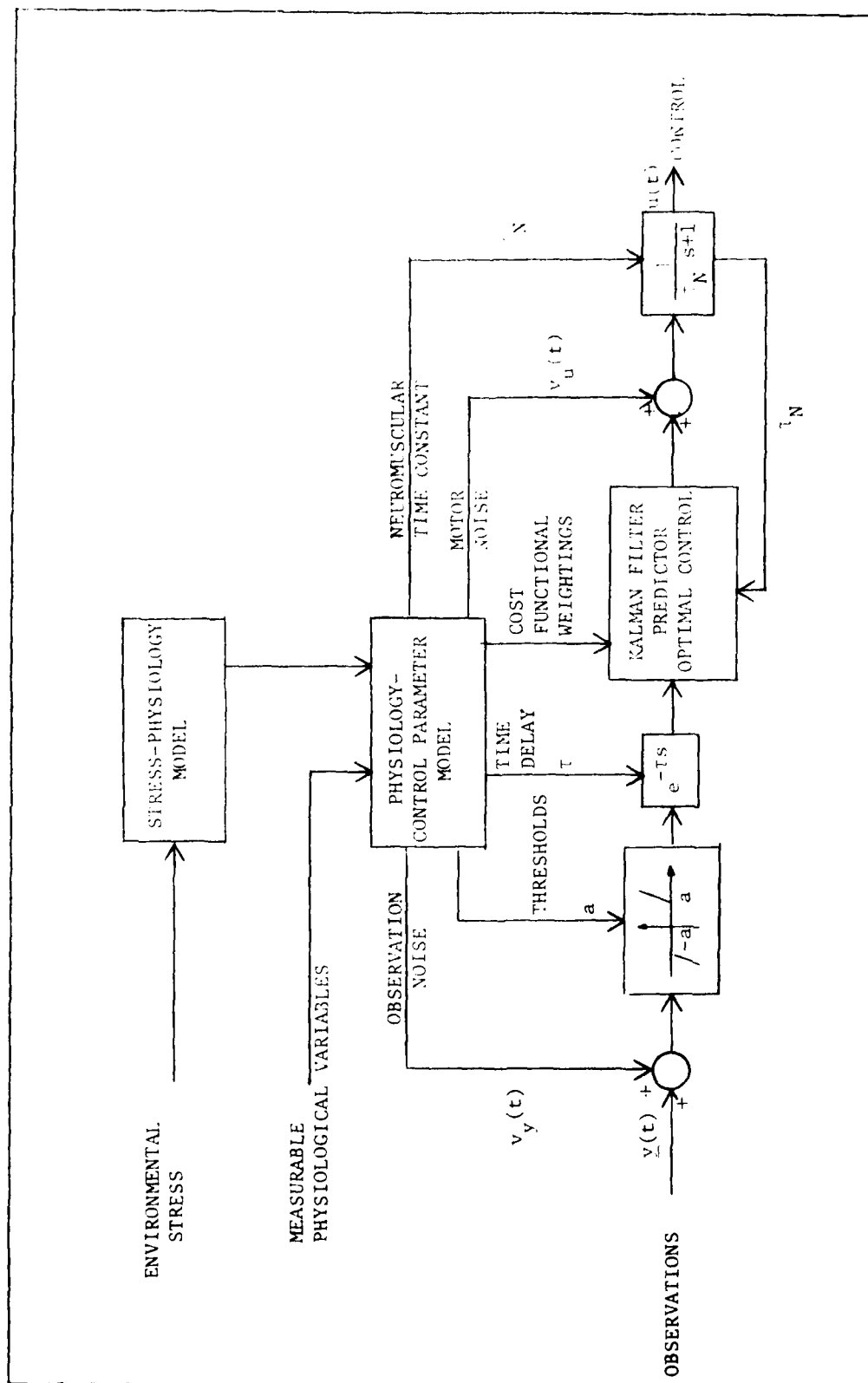
In addition to obtaining a performance model, this modeling approach provides a potentially powerful method of obtaining physiological correlates of performance under acceleration stress. We believe, therefore, that an ultimate

modeling hierarchy which defines in succession the functional relationships between

1. Stress and physiology
2. Physiology and control parameters
3. Control parameters and tracking performance (via OCM)

will provide maximal flexibility for future work. This hierarchy is shown schematically in Figure 4. It should be noted, however, that even a failure to obtain the submodels of levels 1 and/or 2 does not hinder the general success of such approach. This "robustness" of the technique is significant since research in the area of modeling physiological factors has traditionally been painfully slow and, to date, not very fruitful. It is always possible to consolidate the first two levels into a single augmented G-stress-control parameters model, circumventing the physiological variables altogether.

In the following chapter, the experimental and modeling phases of this project are detailed.



II. REPETITIVE - G -- NONSTATIONARY TARGET PROFILE

In the first year of the program, our efforts were directed towards analyzing the Repetitive-G ensemble data, followed by the development of an analytical model. The Repetitive-G experiments were performed on the DES facility at AMRL, and provided the data base for our nonstationary, time-domain, G-Stress performance model.

2.1 Experimental Program

Repeated trials of a compensatory tracking task were performed on the DES at AMRL. The subjects were seated in the centrifuge cab and were instructed to track a simulated, triangular-shaped target aircraft image that was displayed on a graphics screen. The target motion followed a predetermined pattern in the longitudinal plane. There was no target input in the lateral plane, but the operator had to correct horizontal tracking errors that were induced by his own inherent motor randomness. Figure 5 shows the structure of the visual/motion loops. $G_p(s)$ and $G_r(s)$ represent the controlled vehicle dynamics in the pitch and the roll axes respectively; these are discussed later.

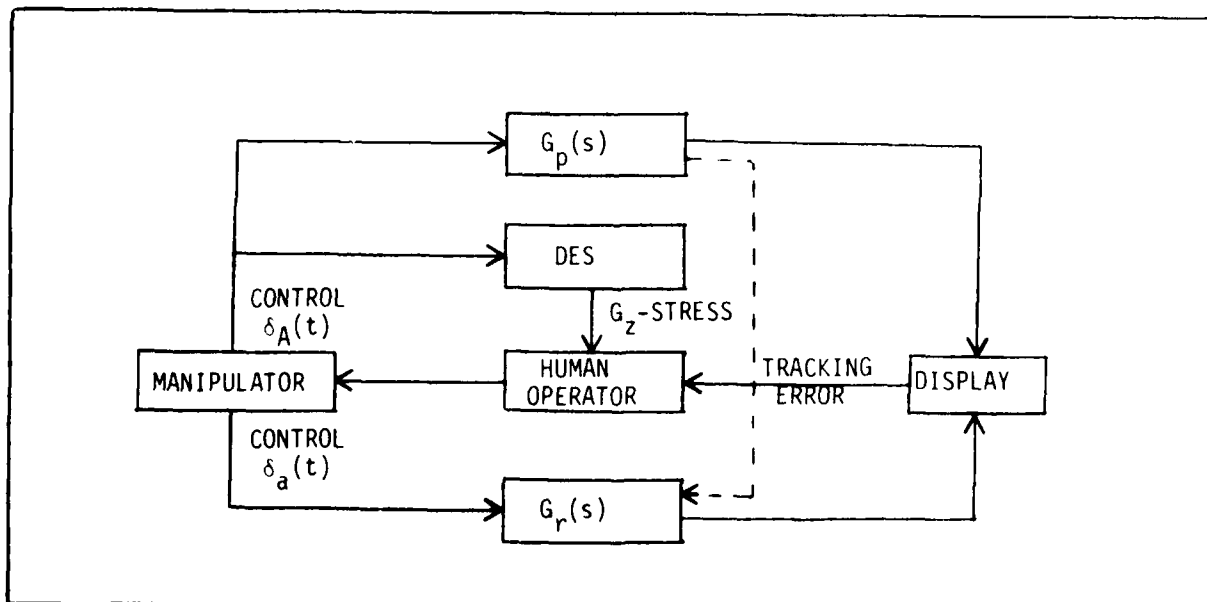


Fig. 5 CLOSED-LOOP DYNAMIC TRACKING CONFIGURATION

2.1.1 Target Profiles

The typical target maneuver in the longitudinal (pitch) plane is represented in terms of the induced vertical acceleration $G_T(t)$. Three different target trajectories, employing trapezoidally-shaped acceleration profiles were used;

- (a) No Peaks: Shown in Figure 6; runtime = 103.34 seconds
- (b) One Peak: Shown in Figure 7; runtime = 121.33 seconds
- (c) Five Peaks: Shown in Figure 8; runtime = 260. seconds.

The target profiles are characterized by the following features:

- (1) The peak levels are 7G and are sustained for a period of 10 seconds.
- (2) There is a 10 second rest period (1.5G) between two successive peaks.
- (3) The rate of onset of $G_T(t)$ from the 1.5G level to the 7G peak level is 0.75 G/Sec.
- (4) There is a 90 second final period of a constant 4G level plateau for each of the three profiles. The subjects' performance was scored during these periods only.

The profile $G_T(t)$ can be interpreted as "commanded-G" input to the human-tracker. If the human operator (HO) were to track with zero error, $G_T(t)$ would equal the acceleration forces he would experience. Actually, the subject's "attained vertical acceleration," $G_A(t)$, would be a filtered version of $G_T(t)$ because of the lag inherent in the HO-System-DES dynamics. Since the aircraft's attained G level is directly proportional to its pitch rate, one may envision the simulated scenario as a pursuit-evasion task in a circular path with a changing radius. The general equation that relates the aircraft pitch rate to its attained G is given by

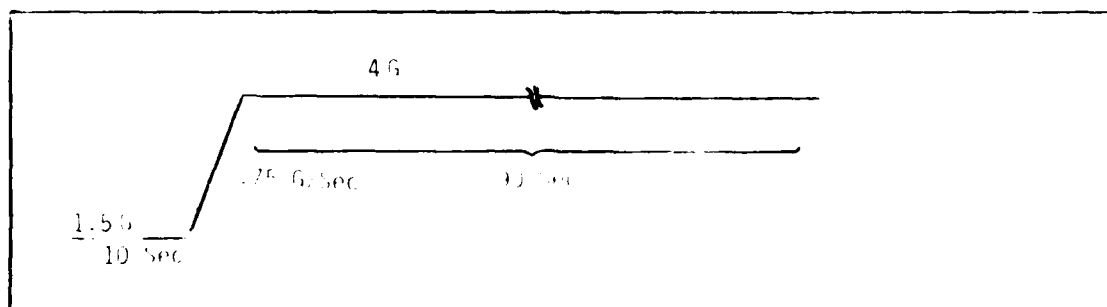


Fig. 6 PEAK PROFILE $G_T(t)$

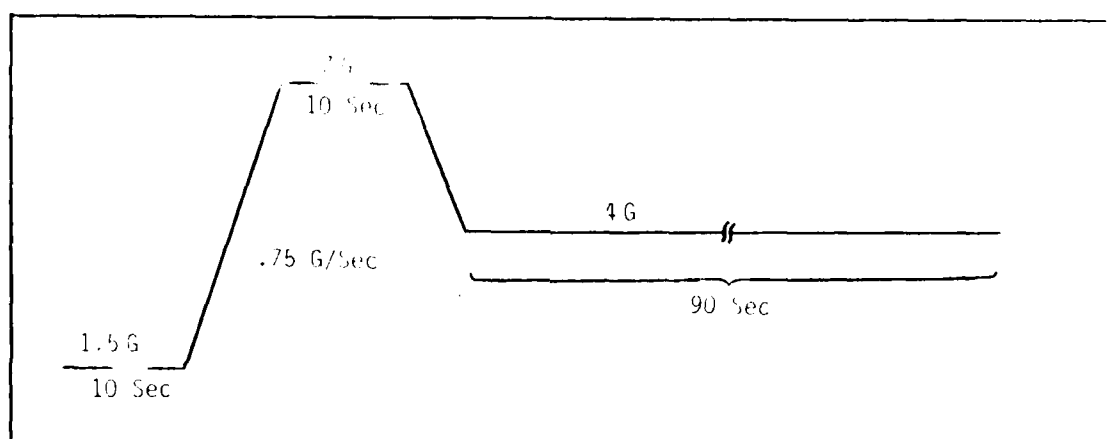


Fig. 7 PEAK PROFILE $G_T(t)$

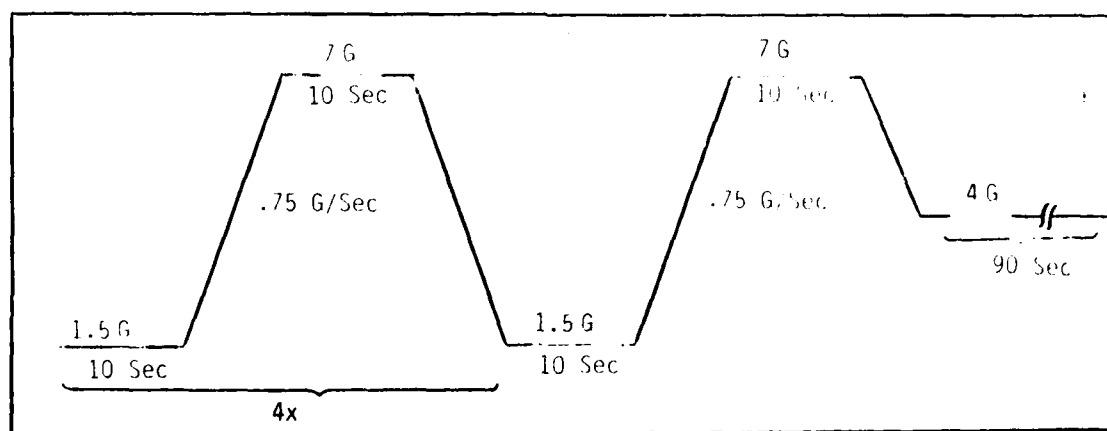


Fig. 8 PEAKS PROFILE $G_T(t)$

$$G(t) = \frac{Vq(t)}{g} + 1 \quad (2.1)$$

where V is the aircraft's velocity (assumed constant) $q(t)$ is its pitch rate, and $g = 32.2$ ft/sec. The 1 accounts for the (fixed) acceleration of gravity.

2.1.2 Experimental Conditions

The major goal in the design of these experiments was to detect any performance degradation under sustained G-stress. Therefore, two experimental conditions had to be employed.

1. Static-G: The subjects tracked the target with the centrifuge at rest.
2. Dynamic-G: The DES was engaged in a closed-loop mode. The subjects, responding to a pitch error stimulus, generated a command control input in order to reduce the tracking error. By this action, they induced a positive, time varying G_z stress upon themselves by increasing or by decreasing the angular velocity of the centrifuge (see also Figure 5).

Note that the roll error existed only in the visual loop and no off-normal (G_y) accelerations were generated by the pilot's roll commands.

As a consequence, a 3x2 factorial design was utilized. Each of the subjects tracked three different trajectories, and each trajectory was tracked both under conditions of "Static-G" and "Dynamic-G."

2.1.3 Subjects

The AMRL hazardous duty panel provided the personnel for these experiments. Eight male subjects were trained, and each provided approximately six runs per target trajectory per experimental condition.

2.1.4 Aircraft Longitudinal (pitch) Dynamics:

The basic set of longitudinal equations being used for the attacker's aircraft is the short-period dynamics. They are the perturbation equations written about straight and level flight, $\theta_0 = 0$.

$$\dot{\alpha}_A = q_A + Z_{\alpha} \alpha_A + Z_{\delta} \delta_A \quad (2.2)$$

$$\dot{q}_A = M_{\alpha} \alpha_A + M_{\dot{\alpha}} \dot{\alpha}_A + M_q q_A + M_{\delta} \delta_A \quad (2.3)$$

$$\dot{\theta}_A = q_A \quad (2.4)$$

Where θ_A is the attacker's pitch angle, q_A is the pitch rate, α_A is the angle of attack and δ_A is the elevator deflection (all perturbation values). The normalized stability derivatives, Z_{α} , Z_{δ} , M_{α} , $M_{\dot{\alpha}}$, M_q and M_{δ} are generally functions of the nominal angle of attack α_0 and dynamic pressure. The range of validity of Equations (2.2)-(2.3) with constant parameters may be small, contributing to modeling errors in an air-to-air problem. Also, the choice of equilibrium condition may vary.

In Equation (2.2) the parameter Z_{δ} is usually small and sometimes neglected. The same is sometimes true for $M_{\dot{\alpha}}$. The analysis that follows will assume

$$M_{\dot{\alpha}} = Z_{\delta} = 0 \quad (2.5)$$

as this corresponds to the assumptions made in the simulations. It should be noted that this does not compromise the results; non-zero choice presents no analytic difficulties.

The transfer functions q_A/δ_A and α_A/δ_A are, with Equation (2.5)

$$\frac{q_A}{\delta_A} = \frac{M_\delta s - M_\delta Z_\alpha}{\Delta(s)} \quad (2.6)$$

$$\frac{\alpha_A}{\delta_A} = \frac{M_\delta}{\Delta(s)} \quad (2.7)$$

where

$$\Delta(s) = s^2 - (Z_\alpha + M_q) s + M_q Z_\alpha - M_\alpha \quad (2.8)$$

Acceleration Forces

The acceleration normal to the flight path due to an incremental flight-path angle is

$$G_z = V \dot{\gamma}_A \quad (2.9)$$

where V = aircraft velocity (assumed constant) and γ_A = (incremental) flight path angle. Noting that

$$\alpha_A + \gamma_A = \theta_A \quad (2.10)$$

or equivalently

$$\dot{\gamma}_A = q_A - \dot{\alpha}_A, \quad (2.11)$$

and using Equations (2.2) and (2.11) one obtains

$$G_z = -V Z_\alpha \alpha_A \text{ ft/sec}^2 \quad (2.12)$$

Thus, the transfer function G_z/δ_A is

$$\frac{G_z}{\delta_A} = -V \frac{Z_\alpha M_\delta}{\Delta(s)} \quad (2.13)$$

From the transfer function parameters given in the HAC study, $\Delta(s) = s^2 + 9.9s + 38$
and

$$M_\delta = 11, \quad Z_\alpha = -25/11, \quad V = 1000 \text{ ft/sec}$$

$$M_q = -7.63, \quad M_\alpha = -20.66$$

Geometric Considerations

Figure 9 shows the geometry of air-to-air tracking in the longitudinal plane. The variables with subscripts A relate to the attacker and those with T to the target aircraft. There are no gunsight dynamics, i.e. the sight is fixed and aligned with the aircraft body axis. For the case of gunsight lead, etc., see Harvey and Dillow [42].

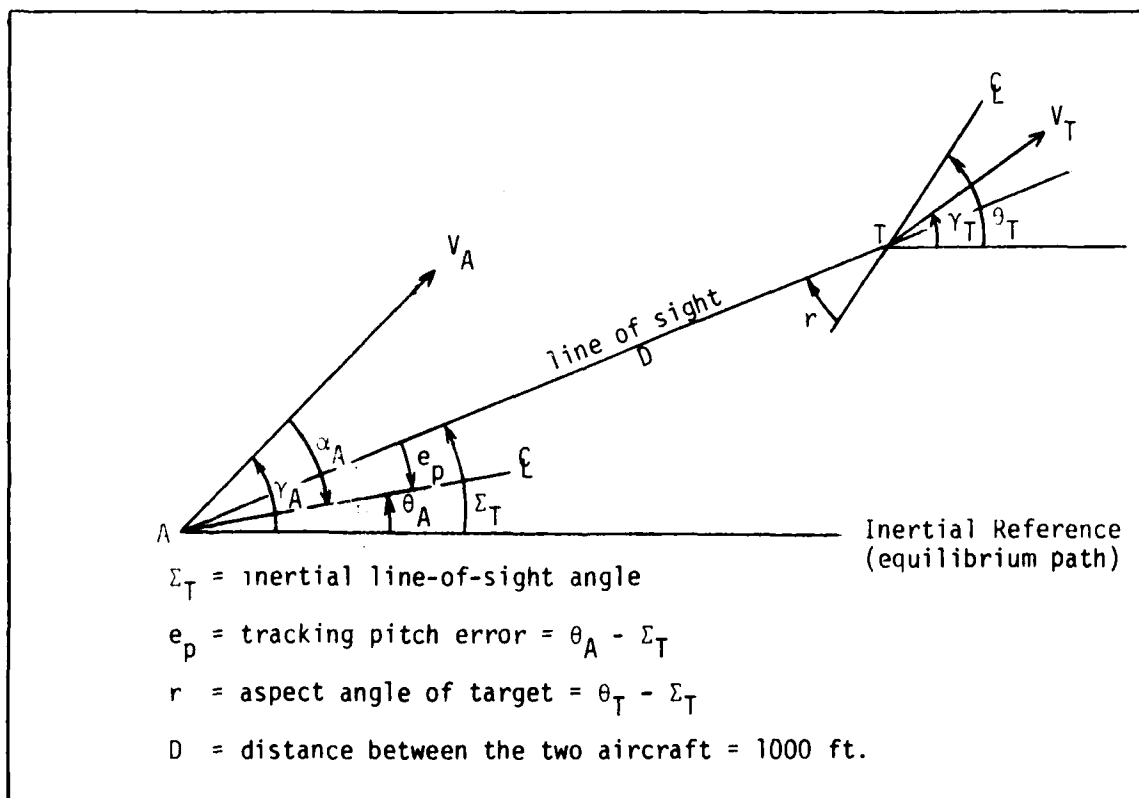


Fig. 9 LONGITUDINAL TRACKING GEOMETRY

Assuming $V_A \approx V_T = V$ and small (relative) angles it has been shown [42] that

$$\dot{\Sigma}_T = \frac{V}{D} (\gamma_T - \gamma_A) \quad (2.14)$$

for constant V and D . Since the explicit second order response of the target is not important for modeling the attacker, we conveniently assume

$$\dot{q}_T(t) = z(t) \quad (2.15)$$

where $z(t)$ is a function of target profile as shown in Figures 6 - 8 and described in Section 2.1.1. By referring to Equation (2.1), one may also recognize $z(t)$ as

$$z(t) = \frac{g}{V} \dot{G}_T(t) \quad (2.16)$$

2.1.5 Aircraft Lateral (roll) Dynamics

The lateral tracking task represents essentially a side-task as there are no target aircraft motions in the horizontal plane. In order to model the lateral task, the dynamics between aileron deflection, δ_a , and tracking error, e_r , must be defined. The implementation of the lateral tracking task assumes the following:

1. Roll angle, ϕ , is small so that $\cos\phi \approx 1$ and $\sin\phi \approx \phi$. This enables us to treat the lateral and longitudinal modes as uncoupled. Moreover, the longitudinal tracking task is not dependent on ϕ in this case.
2. The attacker angle-of-attack α_A and sideslip angle β_A are negligible. Thus, the attacker velocity vector is always aligned with the body axis. This greatly simplifies the system representation in the horizontal plane.
3. All turns are coordinated, i.e. the G vector is aligned with the aircraft's z -body axis.

For a level, coordinated, turn

$$\dot{\psi} = g \frac{\phi}{V} \quad (2.17)$$

and when the aircraft is pitching

$$\dot{\psi} = (q + \frac{g}{V}) \phi \quad ; \quad g = 32.2 \text{ ft/sec}^2 \quad (2.18)$$

where ψ , q , and V are aircraft heading angle, pitch rate and velocity, respectively. By the above assumptions $q \approx \dot{\gamma}$ for the vertical axis, γ being the flight-path angle. Thus

$$\dot{\psi}_T \approx (\dot{\gamma}_T + \frac{g}{V}) \phi_T \quad (2.19)$$

and

$$\dot{\psi}_A \approx (\dot{\gamma}_A + \frac{g}{V}) \phi_A \quad (2.20)$$

where the subscripts T and A again denote the target and the attacker, respectively. Since we are interested only in the deviations between attacker and target aircraft motions, it is convenient to consider an attacker-centered coordinate system. Thus, we set $\phi_T=0$ and $\dot{\psi}_T=0$. It is convenient to define

$$\phi \triangleq \phi_A - \phi_T = \text{relative roll angle} \quad (2.21)$$

$$\psi \triangleq \psi_A - \psi_T = \text{relative headings} \quad (2.22)$$

so that,

$$\dot{\psi} = (\dot{\gamma}_A + \frac{g}{V}) \phi \quad (2.23)$$

The time-varying quantity $\dot{\gamma}_A$ affects the motion in the lateral axis. In fact,

if we consider $\dot{\gamma}_A = \text{constant}$ then Equation (2.23) represents a dynamic linearization. In the present problem $\dot{\gamma}_A$ is a random variable, with a mean and variance that are functions of time. It is more convenient to use $\dot{\gamma}_T$ in Equation (2.23), since this will be a "cleaner" signal. The approximation is valid to first-order as $(\dot{\gamma}_T - \dot{\gamma}_A) \phi \approx 0$. Thus,

$$\dot{\psi} = (\dot{\gamma}_T + \frac{g}{V}) \phi \quad (2.24)$$

The next equation specifies the relationship between heading error ψ and lateral tracking error $e_r(t)$. It is easy to show that

$$\dot{e}_r = \frac{V}{D} \psi \quad (2.25)$$

where D = distance between the two aircraft.

The final equation reflects the aircraft roll axis dynamics which is essentially a roll-rate command system

$$\tau_\phi \ddot{\phi} + \dot{\phi} = \delta_a \quad (2.26)$$

In the present simulations $\frac{1}{\tau_\phi} = 5.55$, $D = 1000$ ft and $V = 1000$ ft/sec.

Equations (2.24)-(2.26) show that the response between δ_a and $e_r(t)$ is like $1/s^3$. This is a very difficult system for a human to control, depending on the visual information. The block diagram of this system is shown in Figures 10. Note that $V\dot{\gamma}_T + g$ is the target normal acceleration in ft/sec^2 . For convenience, this open-loop gain has been made into an equivalent gain $K(t)$ at the input. With these equations, the system description in both the longitudinal ($G_p(s)$) and the lateral ($G_r(s)$) axes is complete.

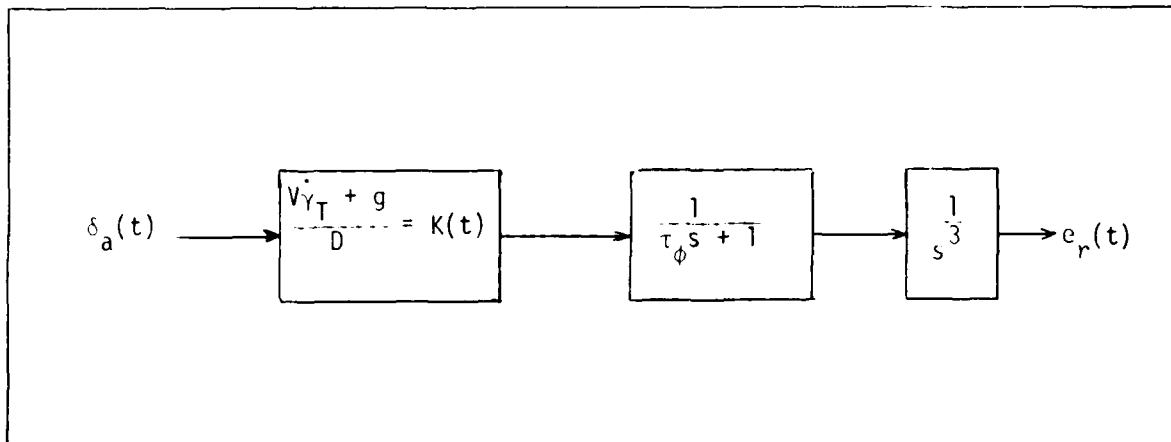


Fig. 10 A 4th ORDER LATERAL TRACKING MODEL

2.1.6 Data Acquisition

The data supplied by AMRL consisted of the time histories of

1. Longitudinal (pitch) axis tracking error
2. Lateral (roll) axis tracking error
3. Commanded G_z (input to DES)
4. Attained G_z
5. Pilot longitudinal-axis stick input
6. Pilot lateral-axis stick input.

These were provided for the 0-peak, 1-peak and 5-peak trajectories. Two magnetic tapes were provided, one for each experimental condition (Static-G and Dynamic-G).

The sampling interval in the real-time operation of the formal experimental runs was 0.06 seconds. The data were collected every other time step, providing

a sample of each of the six variables every time frame of 0.12 seconds. This produced, for every recorded variable, the following:

1. 862 datum points in the 0-peak profile.
2. 1012 datum points in the 1-peak profile.
3. 2168 datum points in the 5-peak profile.

The total number of complete runs that were suitable for reduction and analysis was:

- Static Condition: 0-peak , N=41.
 1-peak , N=38.
 5-peak , N=32.
- Dynamic Condition: 0-peak , N=37.
 1-peak , N=36.
 5-peak , N=24.

2.2 Ensemble Data Analysis

The raw data obtained on the DES, in conjunction with the repetitive-G tracking experiments, have been analyzed via aggregation using an ensemble averaging method. This has been done for subsequent model-data detailed comparisons, and for covariance modeling modifications.

An extensive set of software was developed for processing the single-run data. Tape conversion programs were written on UConn Computer Center's IBM 360/65 to read the AMRL tapes and to rewrite them in a form compatible with our laboratory's DEC PDP-11 system. The PDP-11 system was used for the averaging process, as it enabled a hands-on, interactive analysis. Accordingly, programs were written for averaging the data in a serial, or sequential, manner. In this way the editing, addition, or removal of a single run could be done iteratively, without having to re-average the

entire ensemble. This is an extremely useful approach for treating outlier runs not satisfying a t-test criterion. Specifically, the following equations were employed to reduce the empirical data process:

1. The ensemble mean $\bar{x}_{k+1}(i)$ of the i-th point of k+1 runs is computed from $\bar{x}_k(i)$ by

$$\bar{x}_{k+1}(i) = (\bar{x}_k(i) \cdot k + x_{k+1}(i)) / (k+1) \quad (2.27)$$

where $x_{k+1}(i)$ is the value of the i-th point ($t = 0.12i$ sec) of the (k+1)-th run.

2. The ensemble mean-square $\overline{x_{k+1}^2}(i)$ was computed similarly from

$$\overline{x_{k+1}^2}(i) = (\overline{x_k^2}(i) \cdot k + x_{k+1}^2(i)) / (k+1) \quad (2.28)$$

and the unbiased estimate of the ensemble variance, $V_k(i)$, was then found in the usual manner

$$V_k(i) = (\overline{x_k^2}(i) - \bar{x}_k^2(i)) \cdot k / (k-1) \quad (2.29)$$

This, of course, resulted in the ensemble mean and ensemble standard deviation, viz.,

$$\bar{x}(t) = \frac{1}{N} \sum_{k=1}^N x_k(t) \quad (2.30)$$

$$\sigma_x(t) = \left\{ \frac{1}{N-1} \sum_{k=1}^N [x_k(t) - \bar{x}(t)]^2 \right\}^{1/2} \quad (2.31)$$

The resulting time histories are plotted as follows:

- Figures 11 - 12 : Mean and SD of Longitudinal Tracking Error, Static-G, 0-peak.

- Figures 13 - 14 : Mean and SD of Longitudinal Tracking Error, Static-G, 1-peak
- Figures 15 - 16 : Mean and SD of Longitudinal Tracking Error, Static-G, 5-peak.
- Figures 17 - 18 : Mean and SD of Longitudinal Tracking Error, Dynamic-G, 0-peak.
- Figures 19 - 20 : Mean and SD of Longitudinal Tracking Error, Dynamic-G, 1-peak.
- Figures 21 - 22 : Mean and SD of Longitudinal Tracking Error, Dynamic-G, 5-peak.

In Figures 23 - 29 only the initial 60-second period of the 1-peak profile is considered.

- Figures 23 - 24 : Mean and SD of Lateral Tracking Error, Static-G.
- Figures 25 - 26 : Mean and SD of Lateral Tracking Error, Dynamic-G.
- Figure 27 : Commanded G_z Mean, Static-G.
- Figure 28 : Commanded G_z Mean, Dynamic-G.
- Figure 29 : Subject-Attained G Mean, Dynamic-G.,

Notice that not all variables are plotted here. This is done mainly for practical reasons. For example, the Commanded G_z for the 5-peak trajectory was an exact replica of the 1-peak case. The SD of this variable is of no great consequence since it is virtually zero. Also, the stick inputs in both axes were unreadable from the supplied tapes. These variables, however, are of minor interest in the modeling process.

The next step in the processing of the ensemble data was statistical analysis. Since the air-to-air experiments were performed under two experimental conditions (Static-G vs. Dynamic-G), statistical tests had to be employed in order to detect any

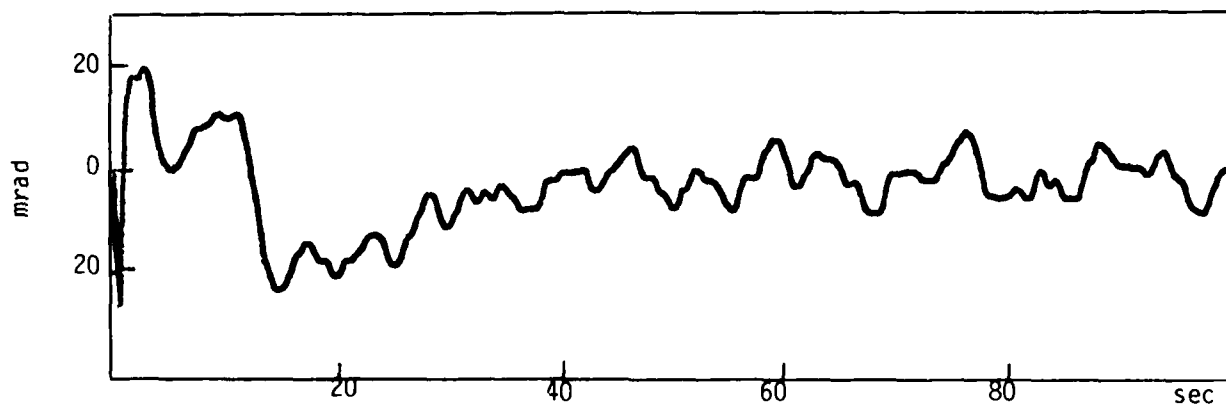


Fig. 11 MEAN PITCH TRACKING ERROR, 0 PEAK, STATIC G

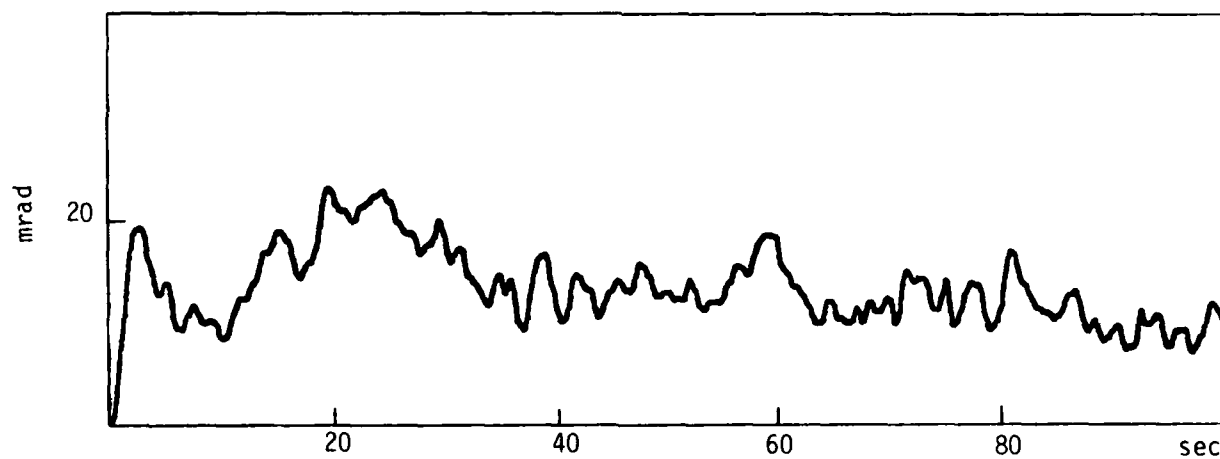


Fig. 12 STANDARD DEVIATION, 0 PEAK, STATIC G

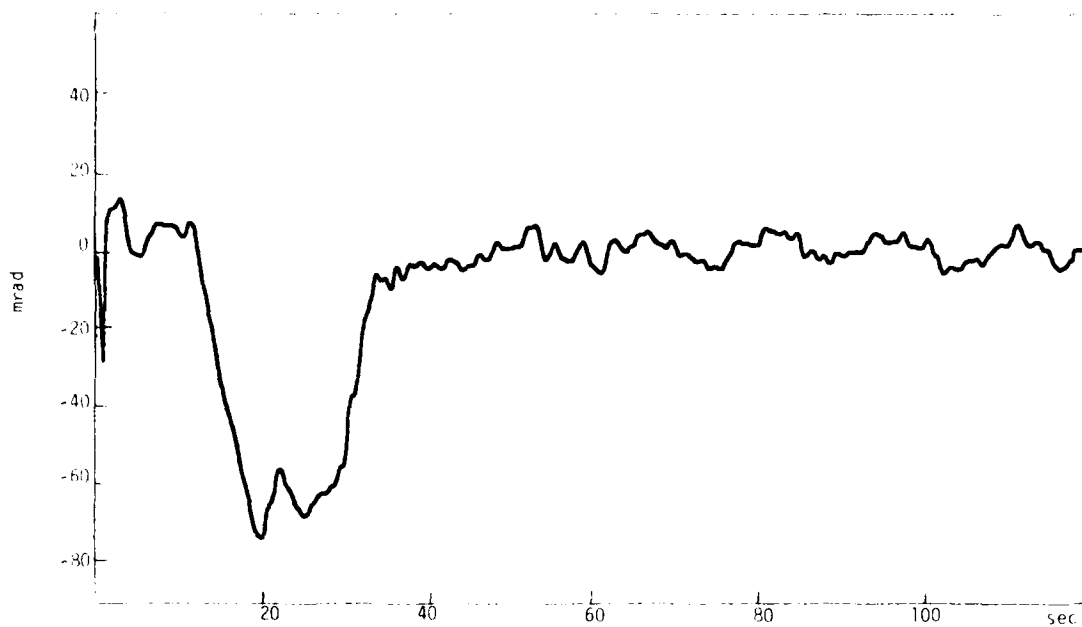


FIG. 13 MEAN PITCH TRACKING ERROR, 1 PEAK, STATIC G

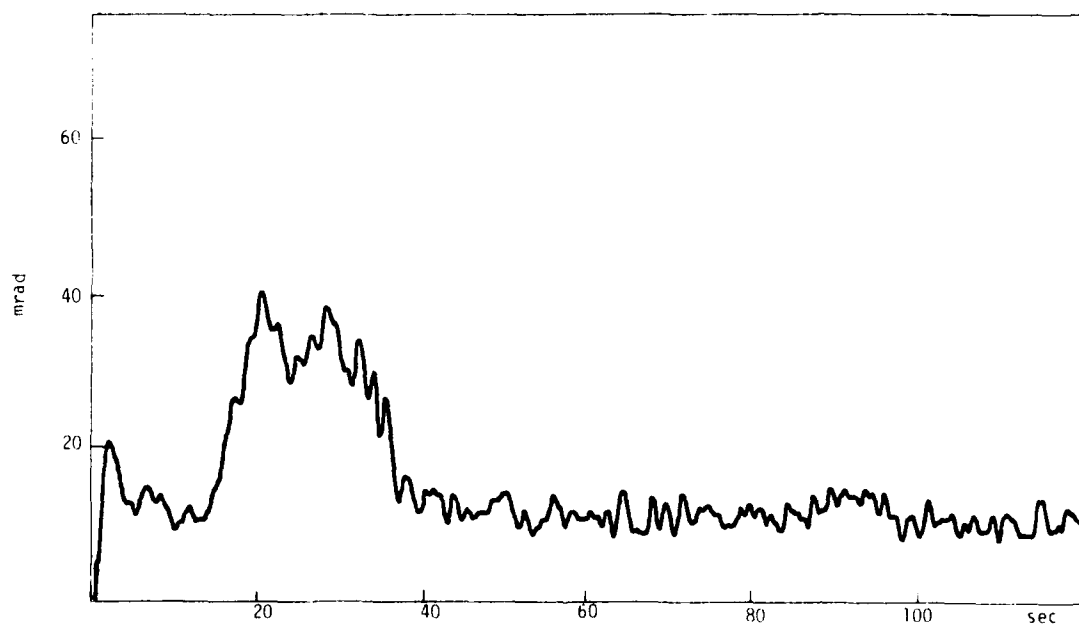


FIG. 14 STANDARD DEVIATION PITCH ERROR, 1 PEAK, STATIC G

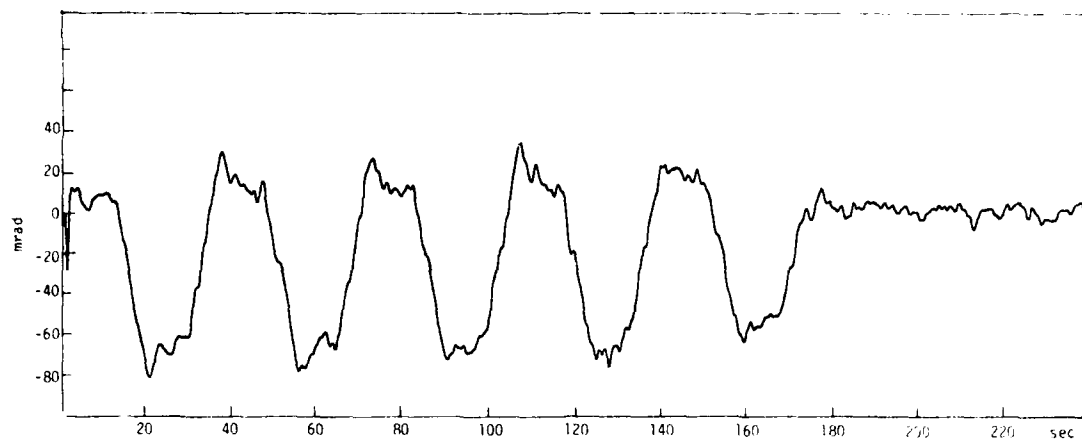


FIG. 15 MEAN PITCH TRACKING ERROR, 5 PEAKS, STATIC G

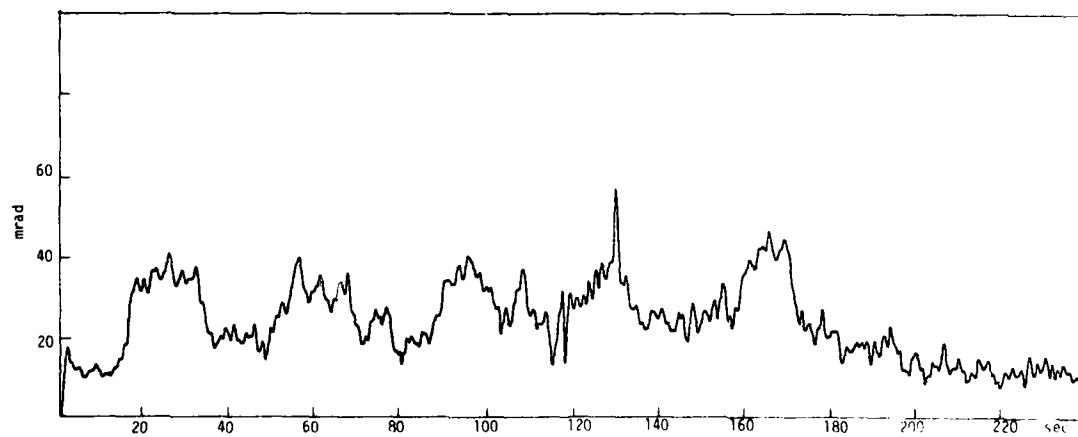


FIG. 16 STANDARD DEVIATION PITCH ERROR, 5 PEAKS, STATIC G

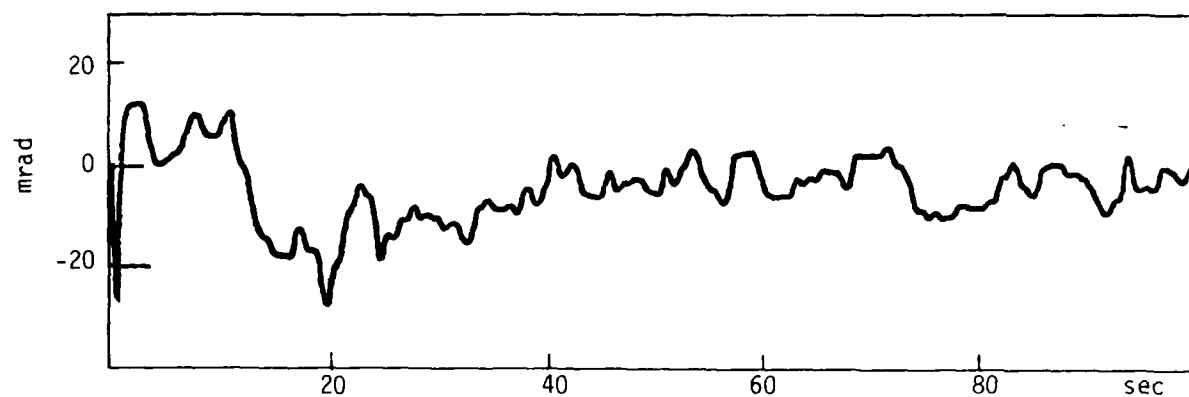


Fig. 17 MEAN PITCH TRACKING ERROR, 0 PEAK, DYNAMIC G

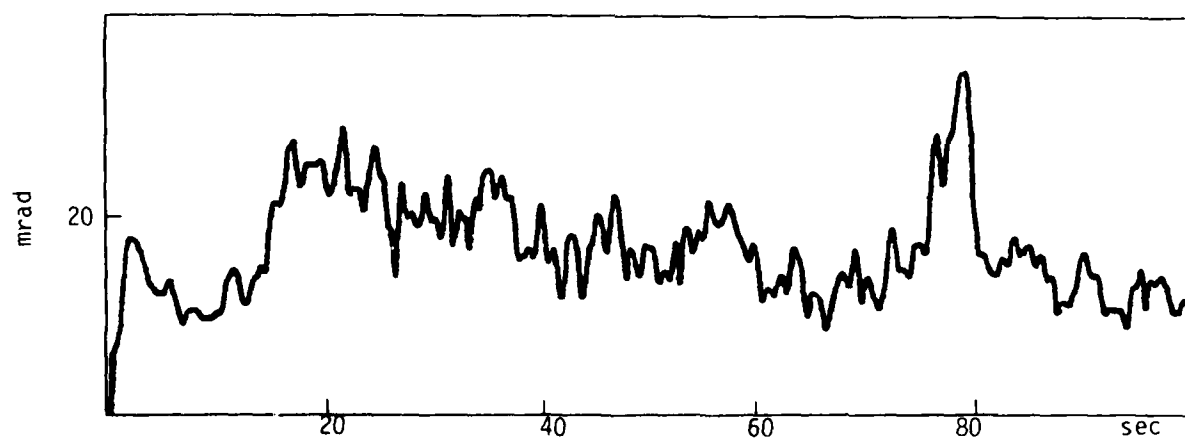


Fig. 18 STANDARD DEVIATION PITCH ERROR, 0 PEAK, DYNAMIC G

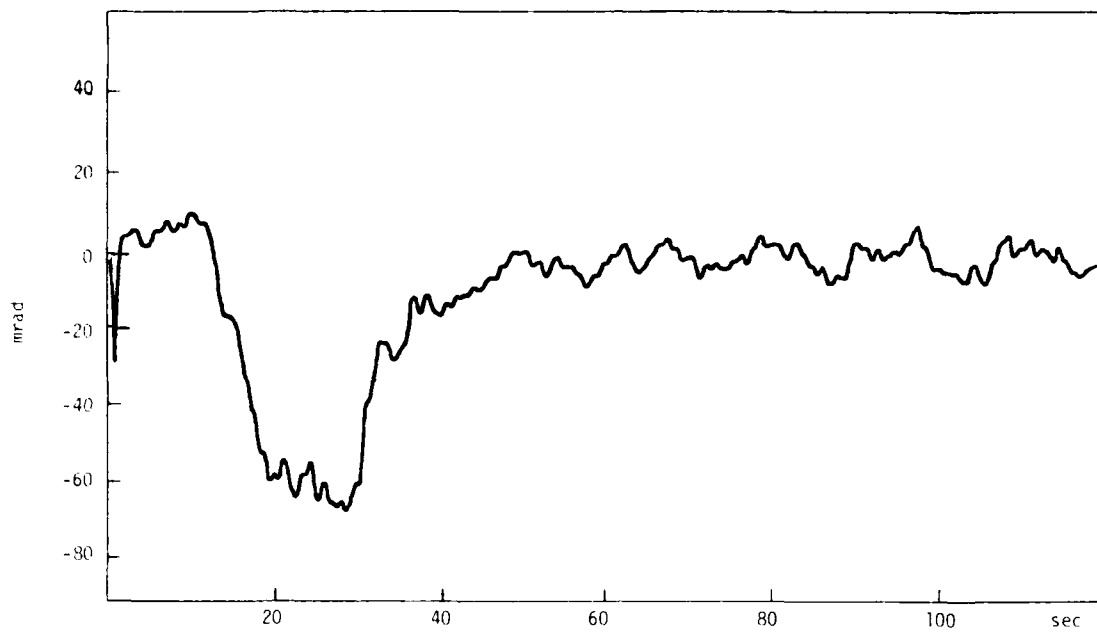


FIG. 17 MEAN PITCH TRACKING ERROR, 1 PEAK, DYNAMIC G

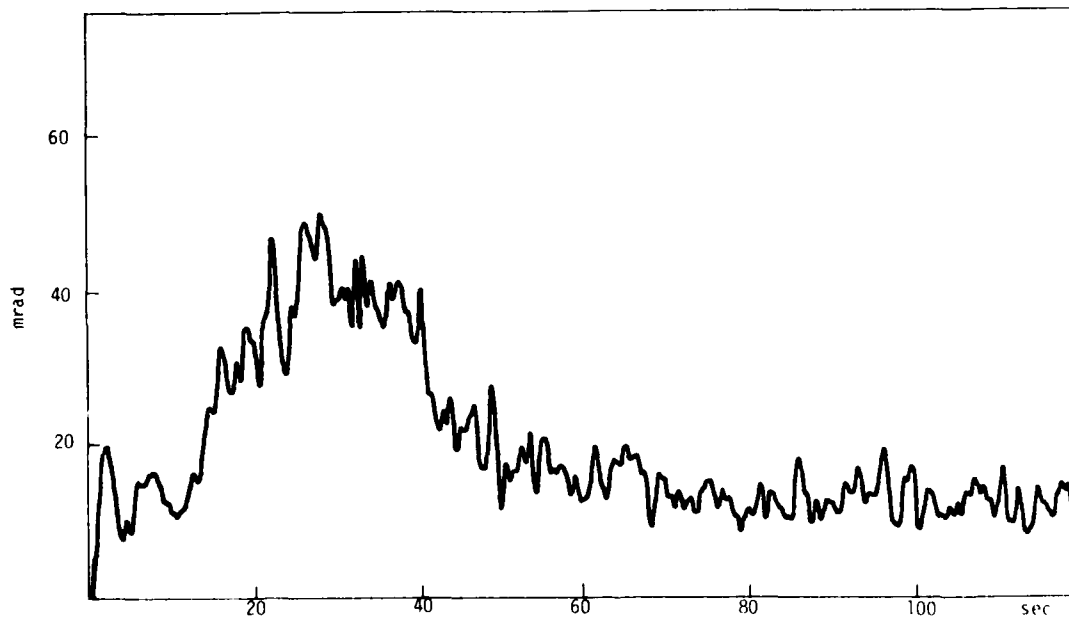
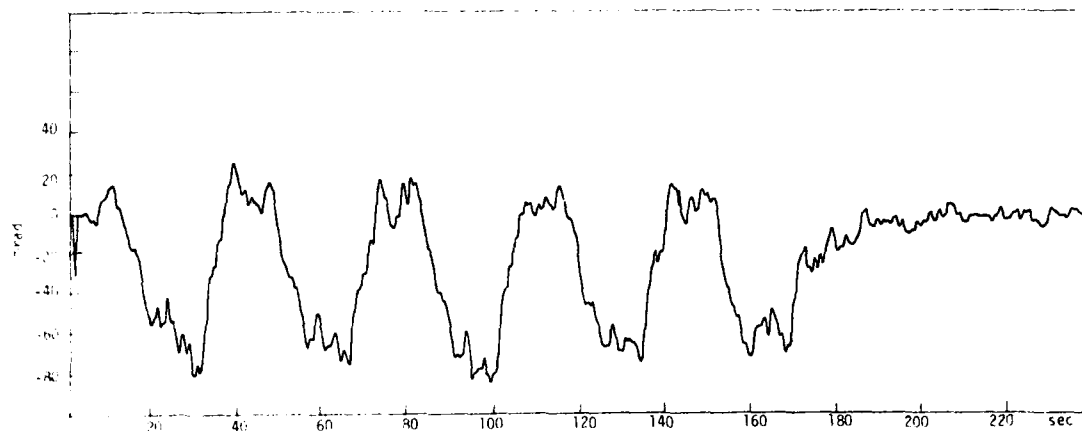
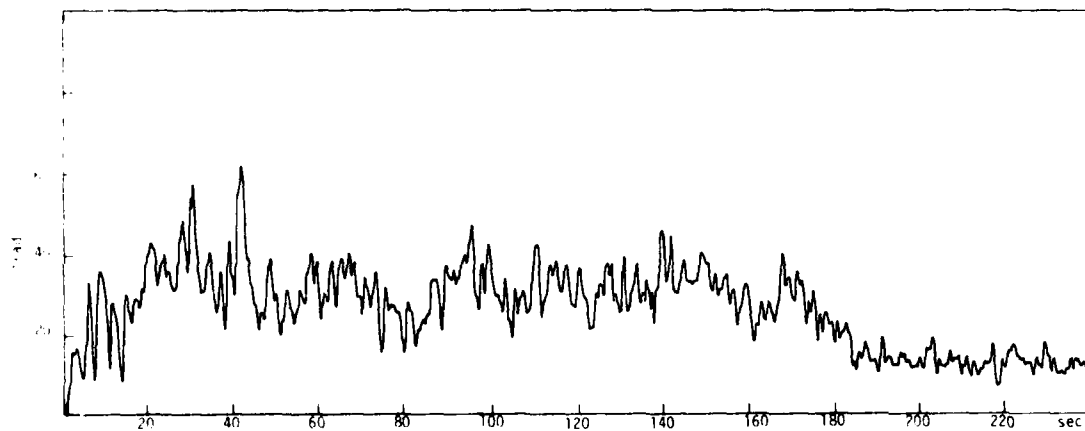


FIG. 20 STANDARD DEVIATION PITCH ERROR, 1 PEAK, DYNAMIC G



MEAN PITCH TRACKING ERROR, 5 PEAKS, DYNAMIC G



STANDARD DEVIATION PITCH ERROR, 5 PEAKS, DYNAMIC G

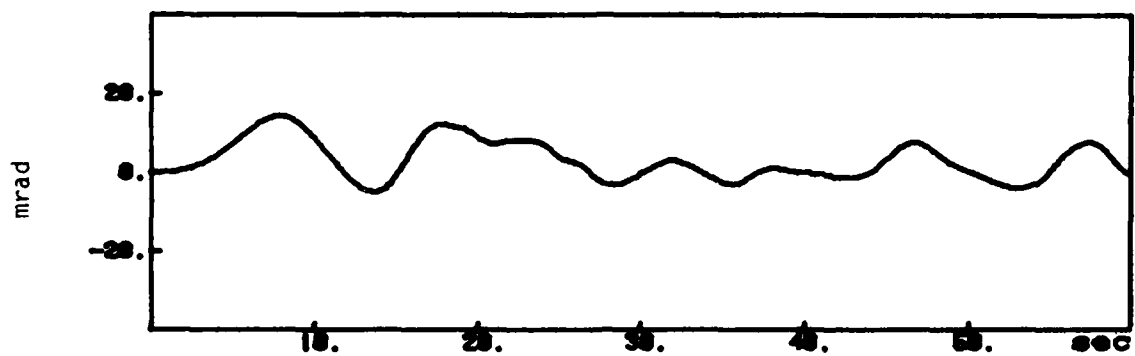


Fig. 23 MEAN HEADING TRACKING ERROR, 1 PEAK, STATIC G

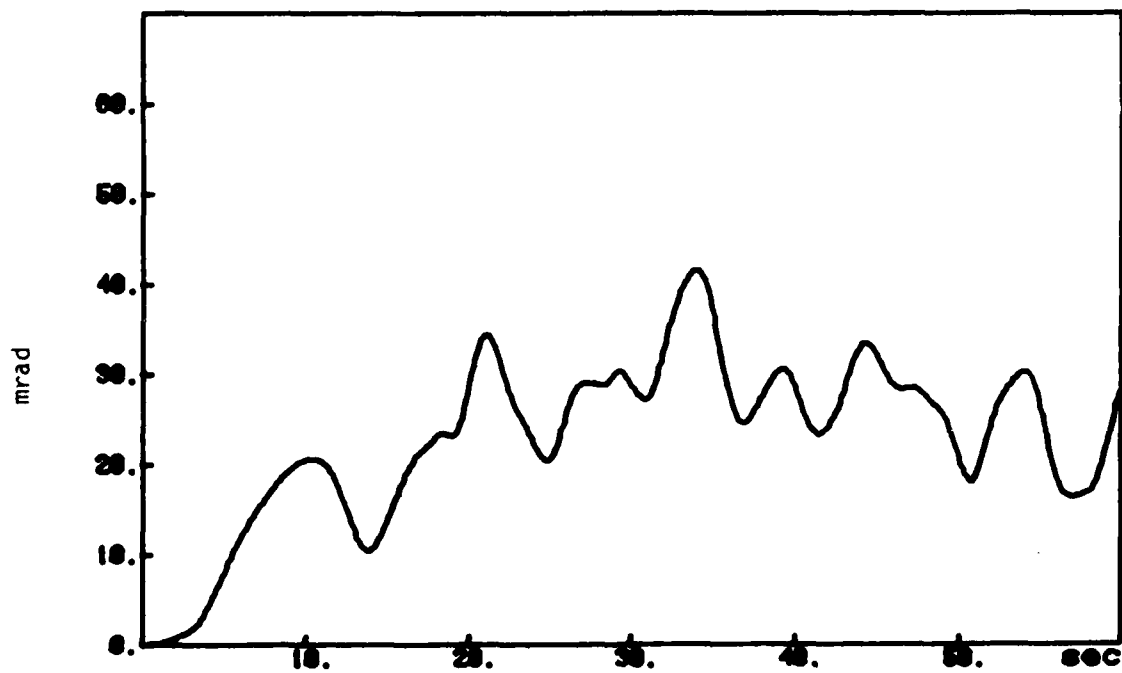


Fig. 24 STANDARD DEVIATION HEADING ERROR, 1 PEAK, STATIC G



Fig. 25 MEAN HEADING TRACKING ERROR, 1 PEAK, DYNAMIC G

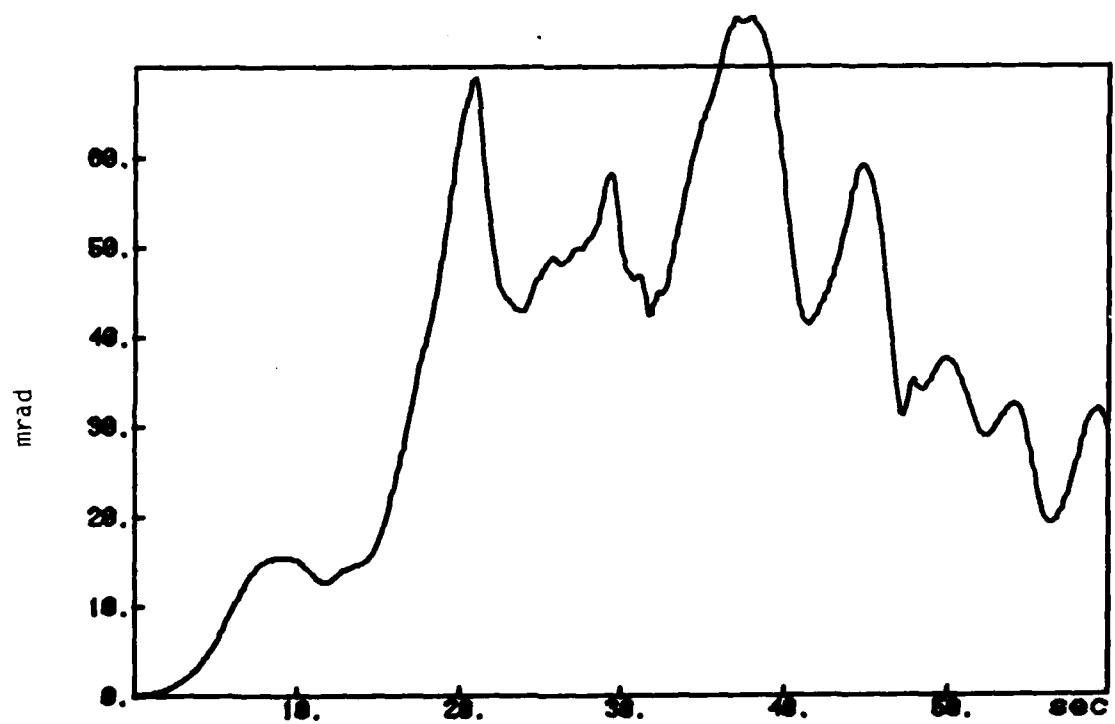


Fig. 26 STANDARD DEVIATION HEADING ERROR, 1 PEAK, DYNAMIC G

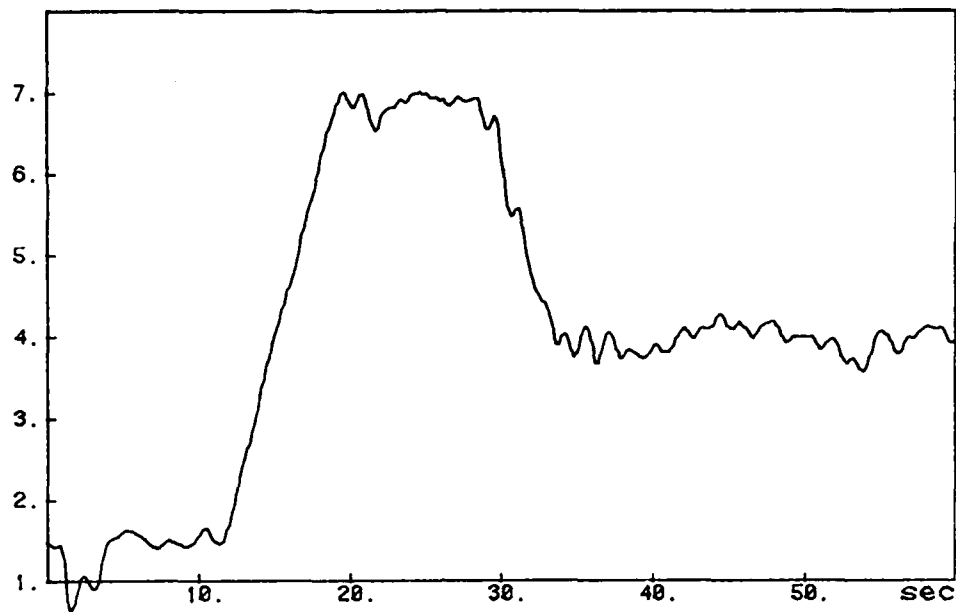


Fig. 21. COMMANDED G_z MEAN, STATIC G

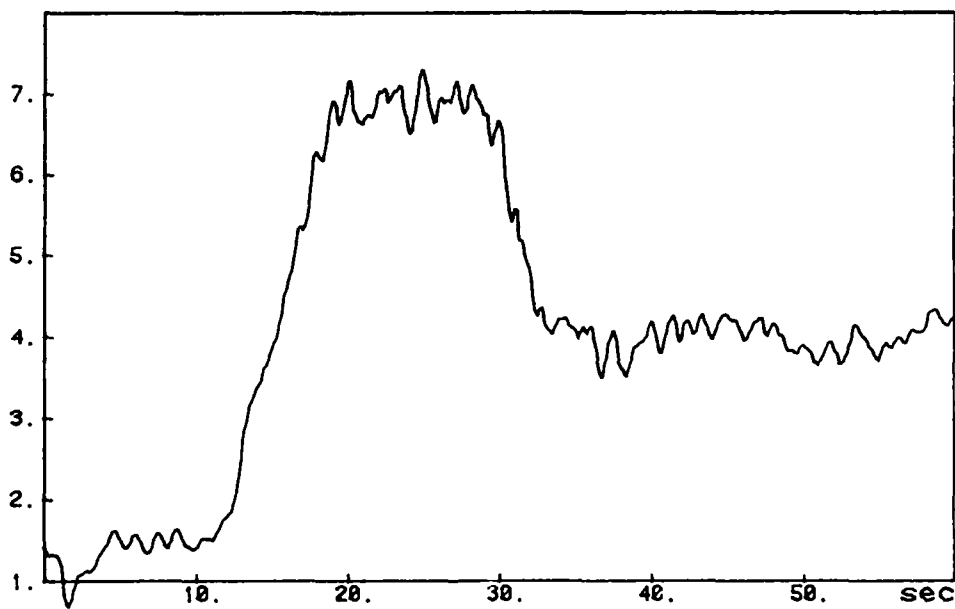


Fig. 22. COMMANDED G_z MEAN, DYNAMIC G

9

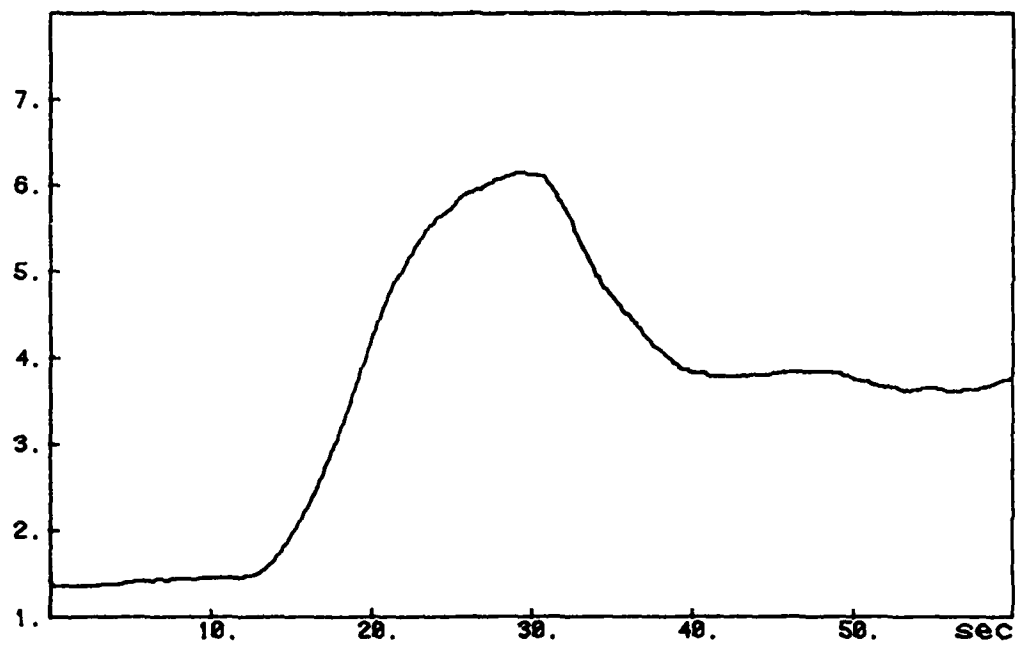


Fig. 29 SUBJECT ATTAINED G MEAN, DYNAMIC G

statistical difference among the ensemble means and variances. For convenience, only the first 60 seconds of the 1-peak trajectory are considered, but the results can be generalized for the other target profiles. The following hypotheses were examined:

- (1) Longitudinal tracking error ensemble means are equal under both experimental conditions. (Welch-test[†]) (Figure 30).
- (2) Longitudinal tracking error variances are equal under both experimental conditions (F-test) (Figure 31).
- (3) Same as (1) for the lateral data (Figure 32).
- (4) Same as (2) for the lateral data (Figure 33).

Application of the statistical tests and inspection of Figures 30 - 33 unveils the following:

- a. We reject hypothesis (1). A comparison of Figure 30 with Figures 7 and 29 (target's G-profile (G_T) and attacker's attained G (G_A), respectively) shows that there is a significant difference ($P < .05$) between the means during active \dot{G}_T (12-18th second of the run) and during high G_A (around the 30th second of the run) periods.
- b. We reject hypothesis (2). It is evident that the variances are significantly different ($P < .05$) during a part of the active \dot{G}_T period (11-16th second) and during most of the period that immediately follows the peak G interval.
- c. We fail to reject hypothesis (3). This result is obvious since there is no target input in the horizontal axis. Also, the acceleration forces are perpendicular to this plane.

[†] In order to test the null hypothesis of equality of means, one would normally use the t-test only when equality of variances is assumed. In our case, however, the null hypothesis does not assume to deal with the same population, since the variances prove to be significantly different (see (2) and (4)). In such a case Welch test is usually employed. In the event, both t and Welch tests gave almost identical results.

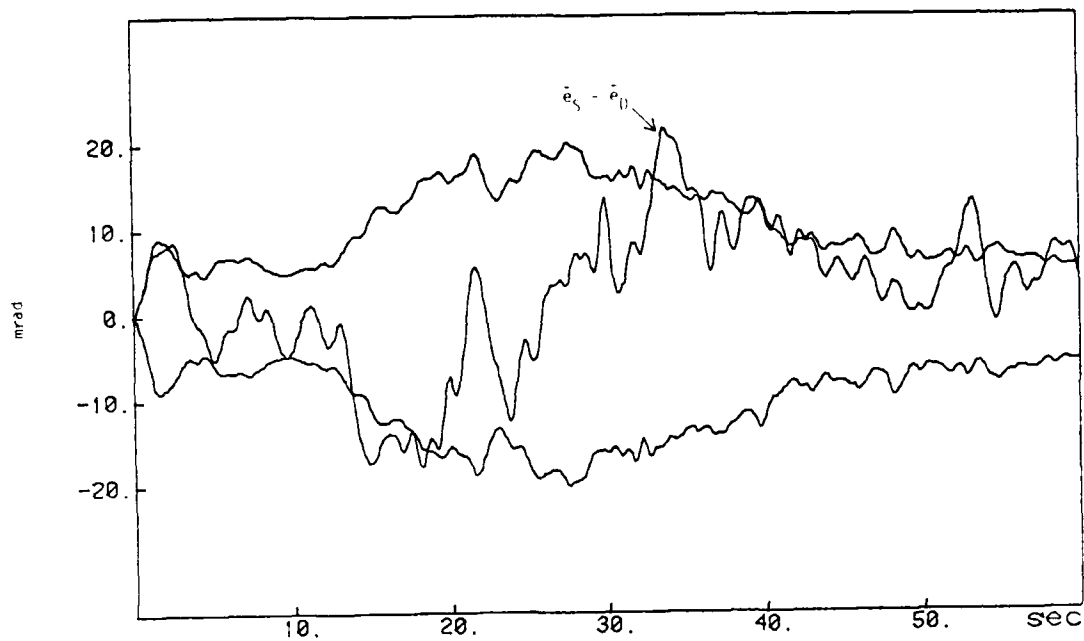


Fig. 30: 95% CONFIDENCE INTERVAL FOR $(\bar{e}_S - \bar{e}_D)$ UNDER NULL HYPOTHESIS

\bar{e}_S = LONGITUDINAL TRACKING ERROR MEAN (STATIC-G)

\bar{e}_D = LONGITUDINAL TRACKING ERROR MEAN (DYNAMIC-G)

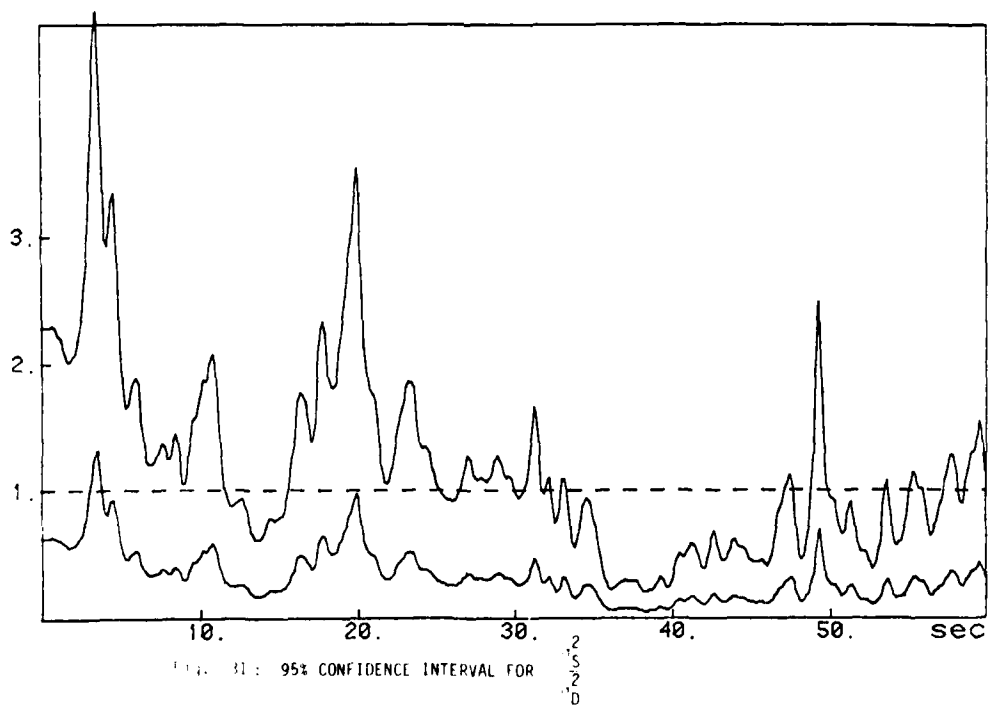


Fig. 31: 95% CONFIDENCE INTERVAL FOR

σ_S^2 = LONGITUDINAL TRACKING ERROR VARIANCE (STATIC-G)

σ_D^2 = LONGITUDINAL TRACKING ERROR VARIANCE (DYNAMIC-G)

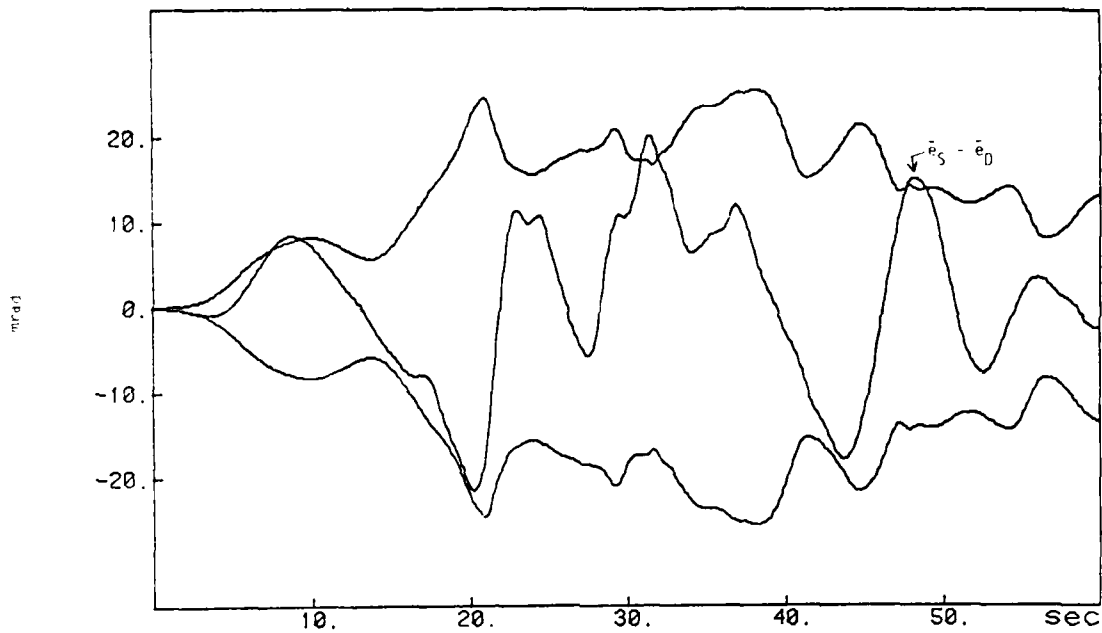


FIG. 3: 95% CONFIDENCE INTERVAL FOR $(\bar{e}_S - \bar{e}_D)$ UNDER NULL HYPOTHESIS

\bar{e}_S = LATERAL TRACKING ERROR MEAN (STATIC-G)

\bar{e}_D = LATERAL TRACKING ERROR MEAN (DYNAMIC-G)

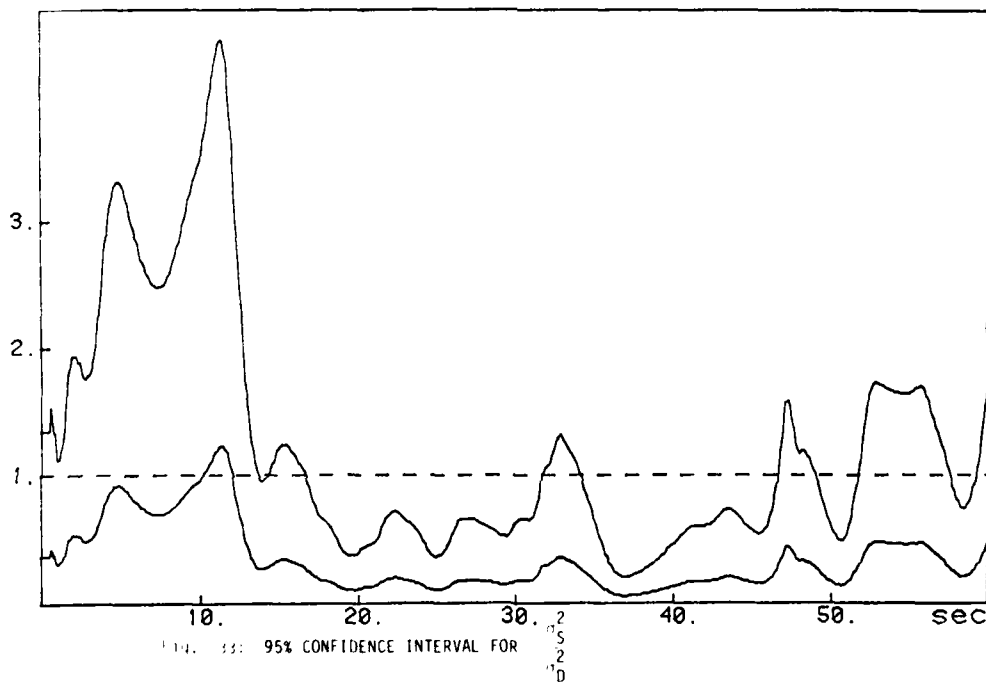


FIG. 3: 95% CONFIDENCE INTERVAL FOR

e_S^2 = LATERAL TRACKING ERROR VARIANCE (STATIC-G)

e_D^2 = LATERAL TRACKING ERROR VARIANCE (DYNAMIC-G)

- d. We reject hypothesis (4) ($P < .05$). A significant difference between the lateral tracking error variances is evident (Figure 33).

An inspection of the aggregated data indicates the following.

1. In general, the quality of the data is excellent. There is a sufficient number of runs to form a "good" ensemble average. Moreover, unlike the previous High Acceleration Cockpit (HAC) studies, the averages are relatively smooth, tend to be more believable statistically, and provide a good cornerstone for G-modeling efforts.
2. The G vs. no-G comparisons of the longitudinal tracking errors and of the standard deviations ($\bar{e}_p(t)$ and $\bar{\sigma}_{ep}(t)$, respectively) show that the magnitudes of $\bar{e}_p(t)$ are not very different. There is, however, an increase in $\sigma_{ep}(t)$ for the G-present versus the static runs. This is in agreement with past acceleration research wherein performance decrements are observed with sustained G-stress.
3. It is noted that the effective time-constant of $\bar{e}_p(t)$ in going from the last 7 G peak to the 4 G tracking phase is smaller in the static vs. the dynamic runs. Thus, the time required for $\bar{e}_p(t) \rightarrow 0$ is longer with the G-stress present. Similar time-constant differences can be observed in the $\sigma_{ep}(t)$. This slower pilot response is again compatible with previous G-stress results.
4. The static tracking \bar{e}_p data for the 1- or 5-peak trajectory show a tendency for the error to return towards zero immediately following a target pull-up maneuver. Thus, the peak (negative) error exhibits a positive slope tendency.
5. The same $\bar{e}_p(t)$ tracking data for the G-stress case show a diametrically opposed trend! During the peak error period there is a further lagging trend in the subject's response, i.e. the error decreases. This tendency was

noted in the earlier HAC data, but could not be confirmed as being statistically significant. Indeed, it was suggested by some that this tendency was due to pilot anticipation of the target's upcoming pitch-rate reversal.

This explanation is not borne out by the new data, however. As we follow the ensemble average of $\bar{e}_p(t)$ through the 5 peaks this lagging tendency becomes diminished. If there were pilot anticipation it should have shown up throughout the run, possibly becoming more pronounced on subsequent peaks. Instead we see the opposite trend. It appears that the person may be becoming "acclimated" to the repetition of G-stress and local performance is improving. Put another way, the degrading effects of the G-stress are possibly being absorbed--the pilot's G threshold might actually increase.

6. The results do not appear to be tainted by the lateral axis control tasks. On the contrary: a valuable insight into the effects of G-stress on pilot performance is gained by the inclusion of this secondary task. The lateral tracking error means ($\bar{e}_r(t)$) are not substantial, which is natural as there is no target input in this axis. The standard deviation ($\sigma_{er}(t)$) magnitudes, however, are worth noticing. It is readily evident that $\sigma_{er}(t)$ in the G-stress condition is much larger. This is a testimony to the thesis that there is a substantial performance degradation when subjected to sustained G-stress.
7. It appears that the Attained G profile is a delayed and filtered version of the Commanded G. This is because of the slow dynamics of the DES, which can be approximated by a first order low-pass filter, with time constant ~ 4.5 sec.

2.3 Modeling the Longitudinal Tracking Task

2.3.1 Application of the Optimal Control Model

The Optimal Control Model (OCM), modified to treat deterministic target motion, assumes the system dynamics

$$\begin{aligned}\dot{\underline{x}}_O(t) &= A_O \underline{x}_O(t) + b_O \delta_A(t) + F_O z(t) \\ \underline{y}(t) &= C_O \underline{x}_O(t)\end{aligned}\tag{2.32}$$

where A_O, b_O, F_O and C_O are the pertinent system matrices, $\underline{x}(t)$ is the system state vector, $\delta_A(t)$ is the elevator deflection and $\underline{y}(t)$ are the observations available to the human operator (HO).

One of the difficult aspects of the modeling is the choice of state variables.

The criteria are

1. α and q for both aircraft should be retained as states.
2. The equations should be simple.
3. Other variables such as G_z, e_p, r , etc., should either be states or linear combinations of states.
4. No absolute (i.e. inertial) angles may be states
5. The rates \dot{e}_p and \dot{r} should be combinations of states.[†]

The last criterion indicates that a relative coordinate system is to be used.

After considering numerous possibilities, the following choices were made

[†] This condition is needed for subsequent pilot modeling.

$$\begin{aligned}
x_1 &= q_T \\
x_2 &= \alpha_T \\
x_3 &= q_A \\
x_4 &= \alpha_A \\
x_5 &= \theta_A - \theta_T \\
x_6 &= e_p = \theta_A - \Sigma_T
\end{aligned}
\tag{2.33}$$

Differentiating these quantities gives

$$\begin{aligned}
\dot{x}_1 &= M_\alpha^T x_2 + M_q^T x_1 + M_\delta^T \delta_T \\
\dot{x}_2 &= Z_\alpha^T x_2 + x_1 \\
\dot{x}_3 &= M_\alpha^A x_4 + M_q^A x_3 + M_\delta^A \delta_A \\
\dot{x}_4 &= Z_\alpha^A x_4 + x_3 \\
\dot{x}_5 &= x_3 - x_1 \\
\dot{x}_6 &= x_3 + \frac{V}{D} (x_2 - x_4 + x_5)
\end{aligned}
\left. \begin{array}{l} \\ \\ \\ \\ \end{array} \right\} \begin{array}{l} \text{Target dynamics} \\ \\ \text{Attacker dynamics} \end{array}
\tag{2.34}$$

The pilot observes the error $e_p(t)$ and aspect angle $r(t)$, plus their rates of change.

Therefore

$$\begin{aligned}
y_1 &= e_p = x_6 \\
y_2 &= \dot{e}_p = x_3 + \frac{V}{D} (x_2 - x_4 + x_5) \\
y_3 &= r = \theta_T - \chi_T = x_6 - x_5 \\
y_4 &= \dot{r} = \dot{x}_6 - \dot{x}_5 = x_1 + \frac{V}{D} (x_2 - x_4 + x_5)
\end{aligned}
\tag{2.35}$$

Also note that

$$G_z = V \dot{\gamma}_A = -V Z_\alpha^A \alpha_A \quad (2.36)$$

In order to simplify the modeling process we sought a reduced-order version of the model. Therefore we assumed that the attacker and the target aircraft flight path angles, γ_A and γ_T , equal θ_A and θ_T , respectively. Note that in this situation the state variables x_2 and x_4 can no longer be regarded as α_A and α_T , since, strictly speaking, $\alpha_A = \alpha_T = 0$. However, the 2nd order short period attacker dynamics remain as in Equation (2.34). The assumption $\gamma_A = \theta_A$ modifies only the equation for x_6 ,

$$\begin{aligned} \dot{x}_6 &= \dot{\theta}_A - \dot{\theta}_T = x_3 - \frac{V}{D} (\theta_T - \theta_A) \\ &= x_3 + \frac{V}{D} x_5 \end{aligned} \quad (2.37)$$

The result of the target simplification is that state x_2 does not enter the system equations, except for the target dynamics. If the explicit 2nd - order response of the target is not important for modeling, then it is convenient to replace the equation for x_1 with

$$\dot{x}_1 = z(t) \quad (2.38)$$

where $x_1 = q_T (= \dot{\gamma}_T)$ and $z(t)$ is the target's commanded flight path angle acceleration (i.e. pitching moment).

Taking these simplifications into account and redefining states to account for omission of x_2 , we find

$$\dot{\underline{x}} = \begin{bmatrix} 0 & 0 & 0 & 0 & 0 \\ 0 & M_q^A & M_\alpha^A & 0 & 0 \\ 0 & 1 & Z_\alpha^A & 0 & 0 \\ -1 & 1 & 0 & 0 & 0 \\ 0 & 1 & 0 & V/D & 0 \end{bmatrix} \underline{x} + \begin{bmatrix} 0 \\ M_\delta^A \\ 0 \\ 0 \\ 0 \end{bmatrix} \delta_A + \begin{bmatrix} 1 \\ 0 \\ 0 \\ 0 \\ 0 \end{bmatrix} z(t) \quad (2.39)$$

$$\underline{y} = \begin{bmatrix} 0 & 0 & 0 & 0 & 1 \\ 0 & 1 & 0 & V/D & 0 \\ 0 & 0 & 0 & -1 & 1 \\ 1 & 0 & 0 & V/D & 0 \end{bmatrix} \underline{x}$$

These modeling assumption are in accordance with the simulation setup at AMRL.

There is a subtlety involving the vertical acceleration G_z : while it is always true that G_z scales with $\dot{\gamma}_A$, it will not scale with α_A in this case. But since $\dot{\gamma}_A = q_A$, the vertical G_z force should be

$$G_z = Vq_A \quad (2.40)$$

Therefore, the vertical acceleration of the target aircraft --in g units-- is

$$G_T(t) = \frac{V}{g} \dot{\gamma}_T = \frac{V}{g} q_T = \frac{V}{g} x_1, \quad (2.41)$$

and the vertical acceleration commanded by the attacker is given by

$$G_A^c(t) = \frac{V}{g} q_A(t) + 1 = \frac{V}{g} x_2(t) + 1 \quad (2.42)$$

Because of distributed dynamic lags, nonlinear effects, etc., the actual acceleration, G_A , attained on the centrifuge, and hence that felt by the pilot is approximately

$$G_A \approx C(s) G_A^C, \quad (2.43)$$

where $C(s) = \frac{1}{1+4.5s}$ approximates the DES' transfer function.

2.3.2 G-Submodel for Longitudinal Tracking Task

The OCM assumes that the well-trained and well-motivated human operator adopts an optimal control strategy, subject to his various psycho-physiological limitations. The task of correctly specifying these limitations along with the resultant control strategy is not always easy since they depend heavily on environmental and experimental conditions. In the case at hand, the environmental condition is the level of G-stress the human is subjected to. Below we describe the major human limitations that are of concern in our modeling efforts.

Operator Time Delay: The various internal time delays associated with visual and central processing are represented by an equivalent time delay, τ . The sensitivity analysis that preceded the modeling phase had not uncovered any particular trends in the model predictions. It proved to be largely insensitive to this parameter. Therefore, the nominal value of $\tau = 0.25$ seconds was chosen for the Static-as well as for the Dynamic-G condition.

Threshold Effects: Nonlinear threshold effects associated with human information processing are the visual and the indifference thresholds (not distinguished by the model). We therefore associate with each displayed variable $y_i(t)$ a visual indifference threshold level, a_i . Thus, the (delayed and noisy) perceived signal is

$$y_{pi}(t) = F_i[y_i(t-\tau)] + v_{yi}(t-\tau) \quad i=1,2,3,4 \quad (2.44)$$

where $v_{yi}(t)$ is assumed to be a white-Gaussian observation noise (see the following paragraph), and the threshold function $F_i(\cdot)$ is

$$F_i(y) = \begin{cases} y_i + a_i & y_i < -a_i \\ 0 & -a_i \leq y_i \leq a_i \\ y_i - a_i & a_i \leq y_i \end{cases} \quad i=1, \dots, 4 \quad (2.45)$$

Since $y(t)$ is assumed Gaussian, we apply here the concept of the Random-Input-Describing-Function (RIDF) to statistically linearize $F(\cdot)$ [43]. The approximated perceived observation is given therefore by

$$y_{pi}(t) \approx N_i y_i(t-\tau) + v_{yi}(t-\tau) \quad i=1,2,3,4 \quad (2.46)$$

where $N_i = N_i(a_i, \bar{y}_i, \sigma_{yi})$ is the i -th effective display gain, \bar{y}_i being $E(y_i)$ and σ_{yi} being y_i 's standard deviation. The nominal values of a_2, a_3, a_4 were determined from the experimental setup and the displayed target size:

$$a_2 = 2 \text{ mrad/sec}, \quad a_3 = 50 \text{ mrad} \quad a_4 = 25 \text{ mrad/sec}$$

In both experimental conditions these values remained unchanged. The choice of the indifference threshold on the tracking error, a_1 , was a more subtle task, and it is discussed later in the section. It will be seen that a_1 is heavily dependent on the G-stress level the tracker is subjected to.

Observation and Motor Noise: The various sources of inherent human randomness are represented by observation noise, v_y , and motor noise, v_δ . These zero-mean white noises mainly account for errors in observing displayed variables and in generating control signals. The observation and motor noise covariances are

$$V_{yi}(t) = \pi \rho_{yi} \frac{[\bar{y}_i^2(t) + \sigma_{yi}^2(t)]}{f_i} \quad i=1, \dots, 4 \quad (2.47)$$

$$V_{\delta}(t) = \pi \rho_{\delta} \cdot \text{cov}[\delta_A(t)] \quad (2.48)$$

where

$\rho_y(\rho_{\delta})$ = observation (motor) noise ratio coefficient

f_i = fractional attention allocation to indicator i

The nominal values for the noise/signal coefficients were

$$\rho_{yi} = -21.5 \text{ dB} \quad i=1, 2, 3, 4$$

$$\rho_{\delta} = -18.0 \text{ dB}$$

These values were applied to the Static-G condition. In the Dynamic-G, ρ_{yi} remained unchanged but the motor-noise ratio coefficient, ρ_{δ} , had to be increased by ~ 40% (to -16.5 dB) to match the empirical data, yielding a 40% increase in the motor noise, $V_{\delta}(t)$.

Since there are four observation channels -- two for the longitudinal axis ($e_p(t)$ and $r(t)$), and two for the lateral ($e_r(t)$ and $\phi(t)$) -- the fractional attentions are assumed to be evenly divided among them. The result is $f_i = 1/4$, which increases the effective observation noise by 6 dB.

One may notice that in all the covariance propagation equations of Section 1.4, which involve $V_y = \text{diag}[V_{yi}]$, (Equations (1.18), (1.30) - (1.32)), only $C'V_y^{-1}C$ appears. If we let

$$N = \text{diag}(N_i) \quad (2.49)$$

and

$$v_y'(t) = \text{col}[v_{yi}(t)], \quad (2.50)$$

then Equation (2.46) becomes

$$\underline{y}_p(t) = NC\underline{x}(t-\tau) + \underline{v}_y(t) \quad (2.51)$$

It can be seen, therefore, that the matrix C has to be modified to NC. We preferred, however, to modify V_y viz.,

$$V_y^{-1} \rightarrow N'V_y^{-1}N. \quad (2.52)$$

The mathematical equivalent is,

$$y_{pi}(t) = y_i(t-\tau) + v_{yi}(t) \quad (2.53)$$

$$v_{yi}(t) = \pi \rho_{yi} \frac{[\bar{y}_i^2(t) + \sigma_{yi}^2]}{f_i \cdot N_i^2} \quad (2.54)$$

which corresponds to Equations (1.4)-(1.5). This interpretation of the visual channel is very significant. The net effect of the nonlinearity-equivalent gain N_i is to increase $V_{yi}(t)$, since from RIDF theory, $0 \leq N_i \leq 1$. In fact, N_i decreases with increasing threshold level a_i . It will be seen that the tracking error indifference threshold, a_i , increases with G , thus decreasing $N_i(a_i)$, which in turn increases the observation noise covariance of the tracking error, $V_{ep}(t) = V_{y1}(t)$.

Neuromotor Time Constant: Although it has been found that the model is quite insensitive to variations in the neuromotor time constant τ_N , we have chosen to adopt the values of $\tau_N = .18$ sec for the Static- and $\tau_N = .2$ sec for the Dynamic-G condition. This parameter, which governs the first-order lag in the human control

mechanism, has proven to be a key parameter in the steady-state G-model (Chapter III). A similar difference in the time-constant values between the two experimental condition was identified there.

Control Gains: In computing the optimal gains adopted by the human, we minimize the following cost functional,

$$J(\delta_A) = \lim_{T \rightarrow \infty} \frac{1}{T} E \left\{ \int_0^T [q_e e_p^2(t) + q_e \dot{e}_p^2(t) + g \dot{\delta}_A(t)] dt \right\} \quad (2.55)$$

where q_e , q_e and g are the (constant) weighting coefficients. The control rate weighting g is completely determined by the choice of τ_N , but q_e and q_e are subjective and represent the operators control strategy and error tradeoffs. We assume $q_e = q_e = 1$ in both conditions since in the longitudinal tracking task the subjective importance of the pitch error rate is no lesser than that of the pitch error.

In the Repetitive-G experiments, there were two major factors that influenced the performance of the subjects:

- (1) The specific instructions and training that guided the subjects in their task;
- (2) The attained positive acceleration (G_A) which resulted from the commanded input signal (G_A^C).

It is clear that coaching the subjects to adopt only certain prespecified control actions, and/or constraining their permissible command levels, should profoundly affect tracking performance. This was demonstrated by Brown and Collins [26] in experiments whereby subjects were required to perform a tracking task similar to ours. Prior to certain runs the subjects were instructed to fly the simulated air-

craft in a coordinated fashion, i.e., to maintain lateral acceleration at a minimum. The results proved that there was a significant difference in performance between these runs and those not preceded by the specific instructions.

The effect of such instructions is reflected in the human's control strategy, i.e. in the weightings in the cost functional $J(\cdot)$. In our experiments, the subjects were instructed (and trained) to track well, i.e., to minimize the tracking error, but only during the last stage of the run, namely, from the onset of the 4 G stress period. The subjects were scored only during the final 90 second period of the 4 G plateau. Preceding the 4 G period, the subjects were instructed to merely "keep the target on the screen."

One might well conclude from this experimental setup that the subjects' error indifference threshold level, a_1 , was changing during the tracking period, and that it had a profound effect on the relative error/error-rate weightings in the computation of the optimal gains. One plausible error threshold time history is shown in Figure 34. Figure 34 refers only to the 1-peak trajectory but similar threshold time-histories may be used for the other trajectories. During the first tracking interval, $a_1(t) = th_1$ = maximum angular error that corresponds to the graphics' total screen size = 150 mrad. During the $G_T = 4$ G plateau $a_1(t) = th_0$ = minimal threshold level inherent to the human, and dependent on the size of the pipper image simulated on the screen (= 20 mrad). We assume that the threshold changes gradually around $t_s = 30$ sec, where G_T decreases from 7 to 4 G. These assumption were applied, regardless of the experimental condition (i.e., for both Static- and Dynamic-G).

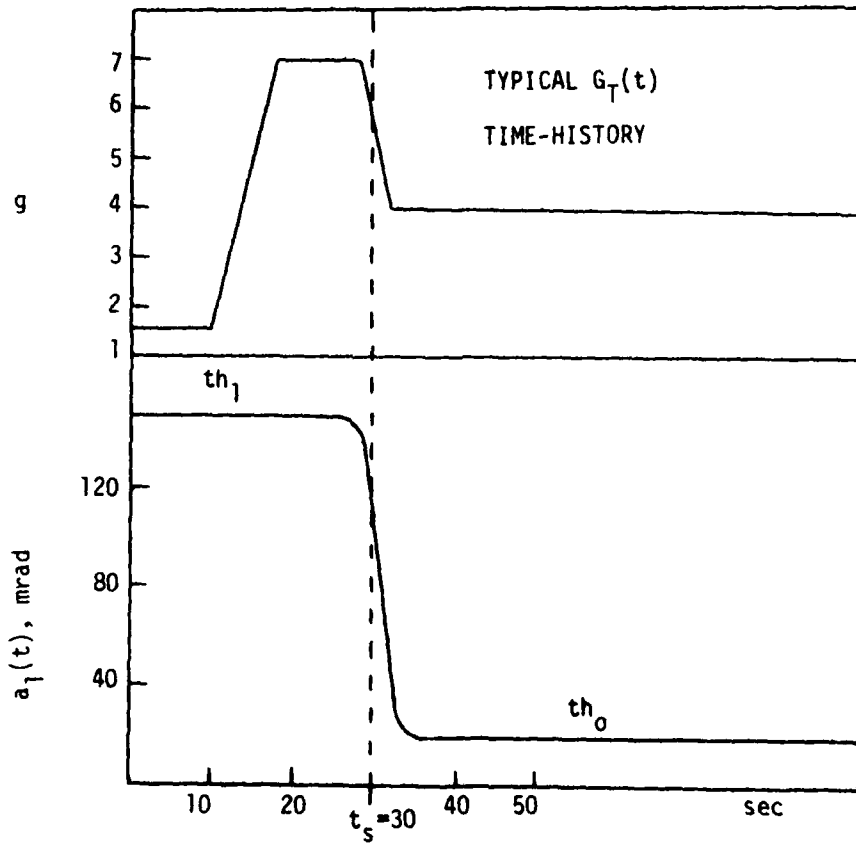


Fig. 34 PITCH ERROR THRESHOLD TIME HISTORY

With the above in mind, coupled with Equations (2.46) and (2.55), we replace the displayed pitch error $e_p(t)$ in the cost functional $J(\cdot)$ with the perceived error, namely,

$$e_p(t) \rightarrow N_1[a_1(t), \bar{e}_p(t), \sigma_{ep}(t)] e_p(t) \quad (2.56)$$

where

$$\bar{e}_p(t) = \bar{y}_1(t) \quad (2.57)$$

$$\sigma_{ep}(t) = \sigma_{y1}(t)$$

Thus, the cost functional to be minimized is now

$$J'(\delta_A) = \lim_{T \rightarrow \infty} \frac{1}{T} E \left\{ \int_0^T [q_e N_1^2 e_p^2(t) + q_e \dot{e}_p^2 + g \delta_A^2] dt \right\} \quad (2.58)$$

The error rate display gain is not included in $J'(\cdot)$ since we assume that the error rate threshold level, a_2 is negligible (≈ 2 mrad/sec) and time-invariant. This approach of weightings modification in the cost functional has been originally suggested by Kleinman and Baron [43], and it extends the preliminary modeling efforts of Korn et al [44].

One may argue that this approach has an inherent serious drawback. Since a_1 is now time dependent, the error weighting would vary in time which in turn implies that the optimal control gains would have to be computed continually. This would not be feasible. However, it has been found that only the error (x_5) gain depends strongly on the error weighting, and the remaining gains are virtually unaffected. With this fact, a functional relationship between the error gain and the error weighting has been found, and successfully applied.

The indifference threshold on the observed tracking error is further affected by the G-stress. We postulate that the human would tend to decrease the importance he assigns to the tracking performance when subjected to sustained physical stress. From Figures 17 - 22 it is apparent that the subjects exhibited a lagging tendency, which increased during the peak-G periods. The hypothesis is, therefore, that the acceleration stress would tend to increase the tracker's indifference threshold associated with the tracking error. Alternately, he would become less indifferent to his own psycho-physiological response.

To incorporate this threshold effect in our G-model we adopted an ad-hoc formula, such that,

$$a_1(t, G_A) = a_1(t) [1 + \rho_g \cdot \max^2(0, G_A - G_{\min})] \quad (2.59)$$

where $G_A = G_A(t)$ is the subject attained G_z (Equation (2.43)) and $G_{\min} = 4g = \text{minimal } G_z \text{ level}$, below which human performance is assumed not to be affected significantly. (We assume, of course, that the subject is wearing a G-suit). The value of the parameter ρ_g that gave the best data-model fits was $\rho_g = .5$.

The effect of the increase in a_1 under G_z -stress is twofold:

1. The equivalent display gain, N_1 , decreases under G-stress, further reducing the effective weighting on the tracking error, while the error-rate weighting remains unchanged. This, in turn, reduces the control gain on the error that is computed from Equation (2.58).
2. The decrease of N_1 increases the effective observation noise covariance associated with the pitch error ($V_{ep}(t)$) as can be observed in Equation (2.54).

2.3.3 Modeling Results of the Longitudinal Tracking Task

A good performance model is one that satisfactorily validates experimental data and can be applied reliably in a predictive mode. Moreover, it should be applicable to a wide range of manual control tasks. The OCM has proven its ability to model the air-to-air compensatory tracking task as demonstrated by the excellent data matches that follow.

In order to demonstrate the model predictions of the pertinent variables, we consider the 1-peak trajectory as a representative case. The 0-peak profile is of no real interest because of a limited target maneuver and the low G levels, and the 5-peak profile is basically a replica of the 1-peak as can be observed from the ensemble data. Moreover, most of the final period of constant 4 G can be discarded

since it is a period of zero \dot{q}_T ($z(t) = 0$). Therefore, it is sufficient to consider the first 60-second period of the 1-peak profile, in order to illustrate our modeling results.

In the following discussion we present the model prediction time histories. These are followed by figures which show the model-data comparisons.

- Figures 35 - 36: Mean and SD of tracking error, Static-G.
- Figures 37 - 38: Mean and SD of tracking error, Dynamic G.
- Figure 39: Commanded-G, Dynamic-G condition.
- Figure 40: Attained-G profile.

Comparisons:

- Figure 41: Tracking error mean, Static-G.
- Figure 42: Tracking error SD, Static-G.
- Figure 43: Tracking error mean, Dynamic-G.
- Figure 44: Tracking error SD, Dynamic-G.
- Figure 45: Commanded G, Static-G condition.
- Figure 46: Commanded G, Dynamic-G condition.

2.3.4 Discussion

The data-model fits are excellent. It should be emphasized that the base-line OCM parameters were unperturbed from their nominal values in the no-stress condition. Only in the G-stress situation was it necessary to formulate a G-submodel. To recapitulate the G-stress performance model, the model predictions have to be expounded:

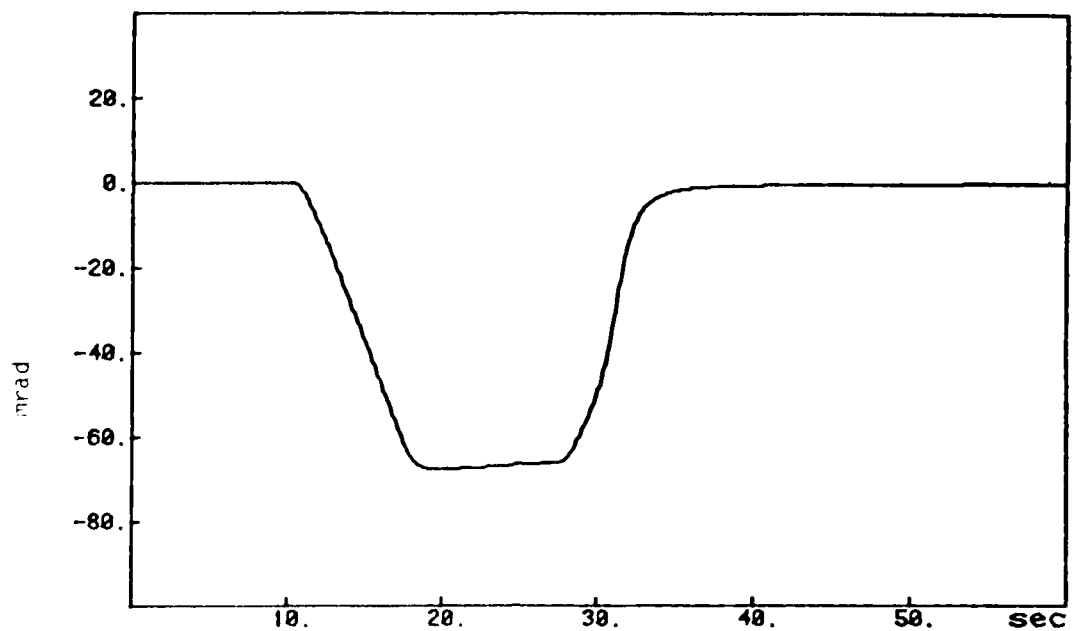


Fig. 35 MEAN PITCH TRACKING ERROR, 1 PEAK, STATIC G

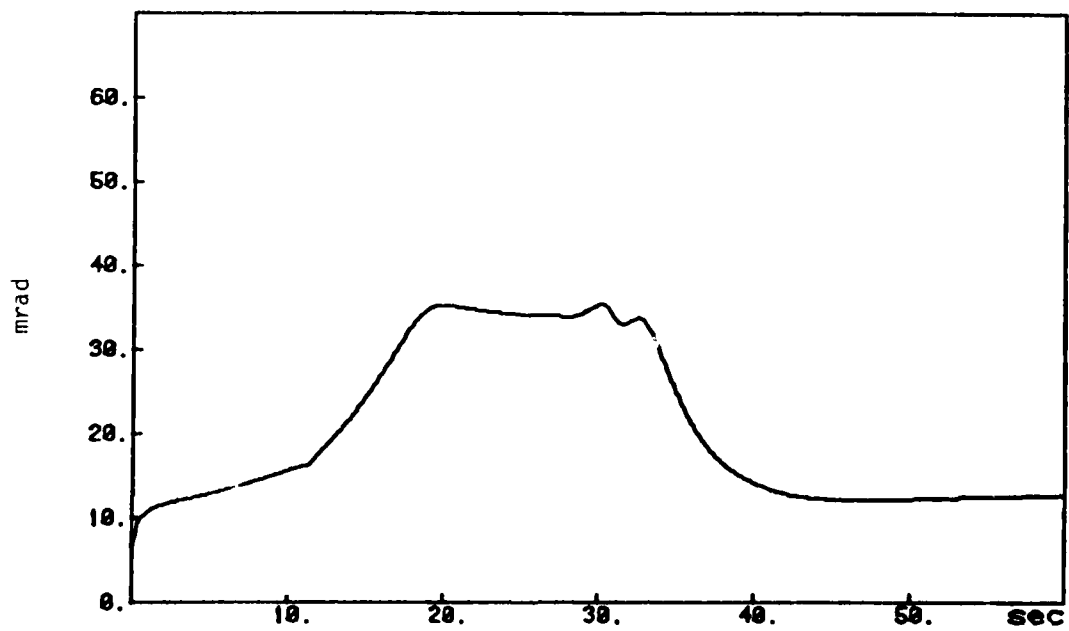


Fig. 36 STANDARD DEVIATION TRACKING ERROR, 1 PEAK, STATIC G

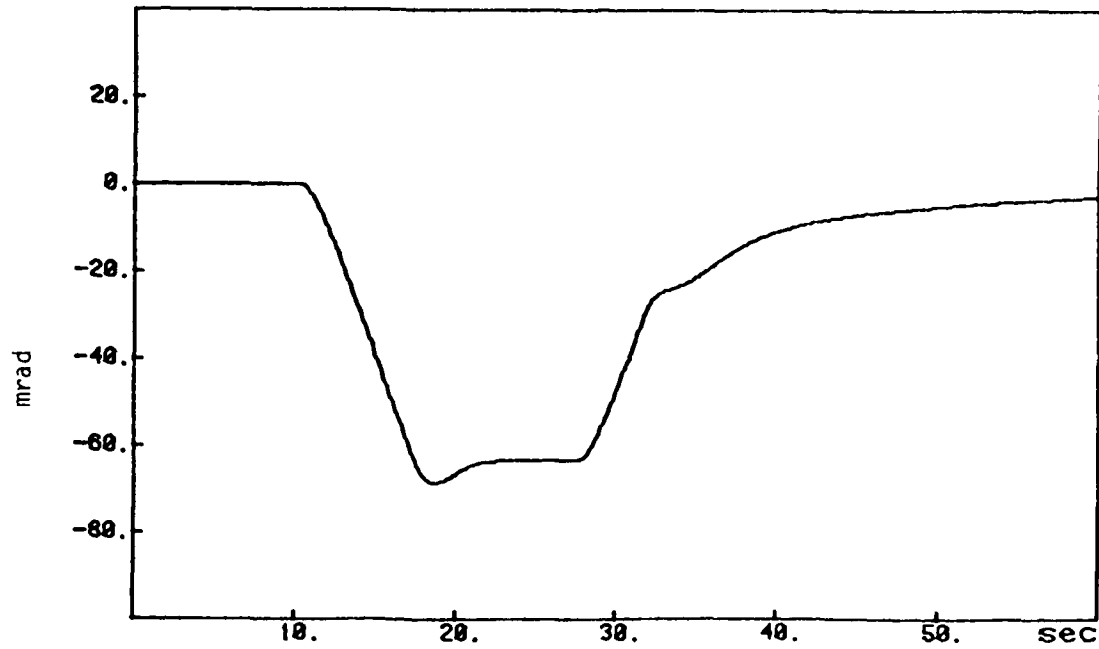


Fig. 37 MEAN PITCH TRACKING ERROR, 1 PEAK, DYNAMIC G

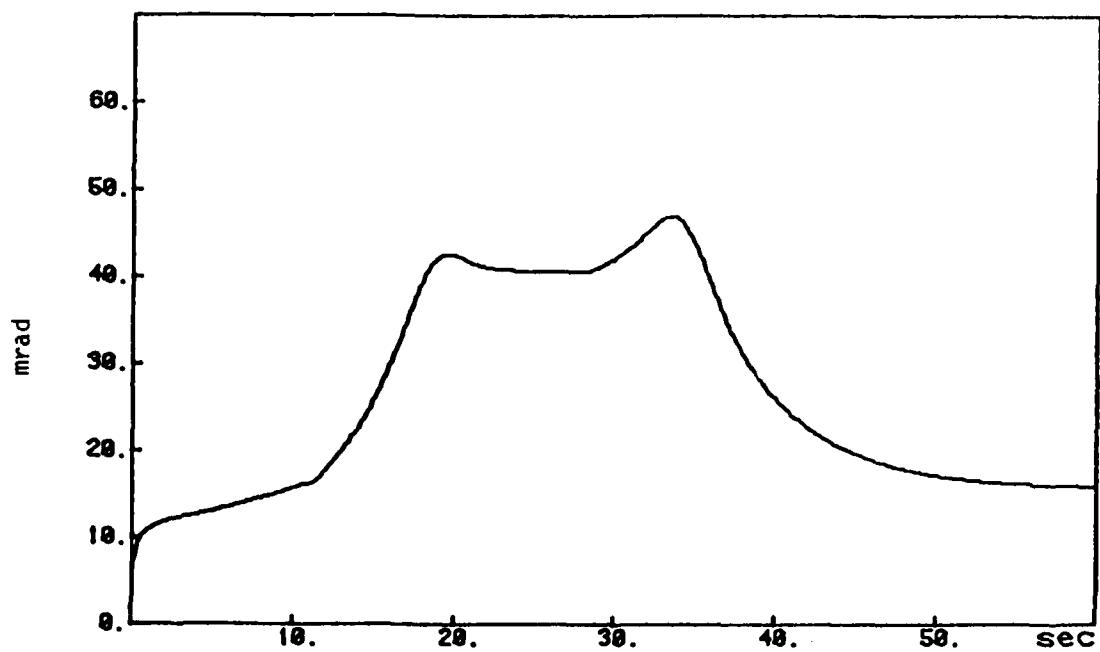


Fig. 38 STANDARD DEVIATION TRACKING ERROR, 1 PEAK, DYNAMIC G

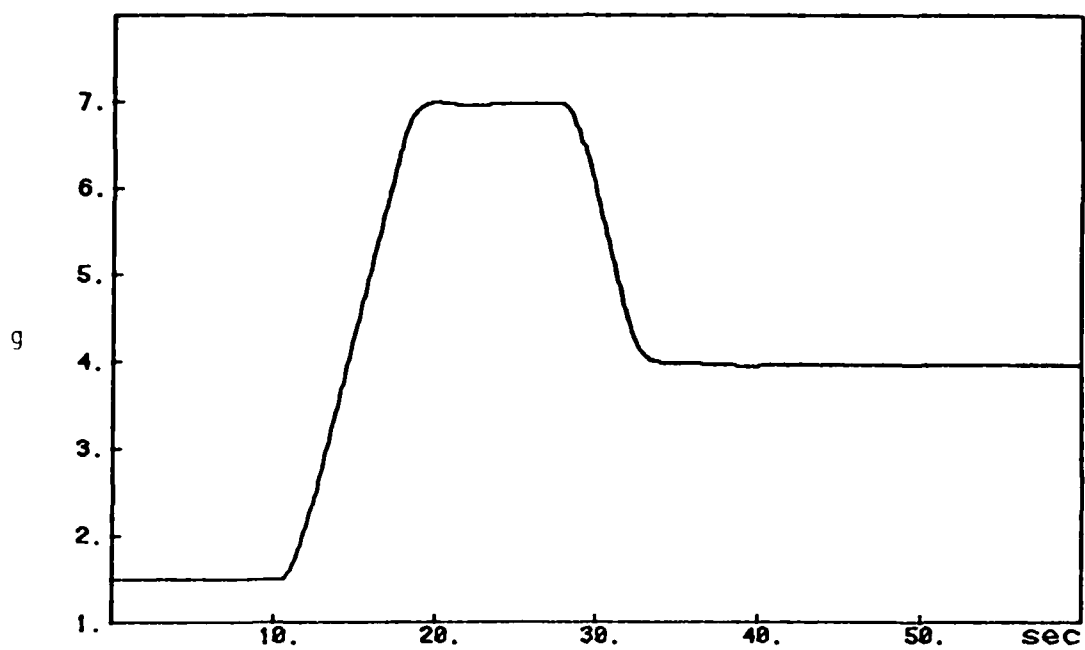


Fig. 39 COMMANDED G_z , DYNAMIC G CONDITION

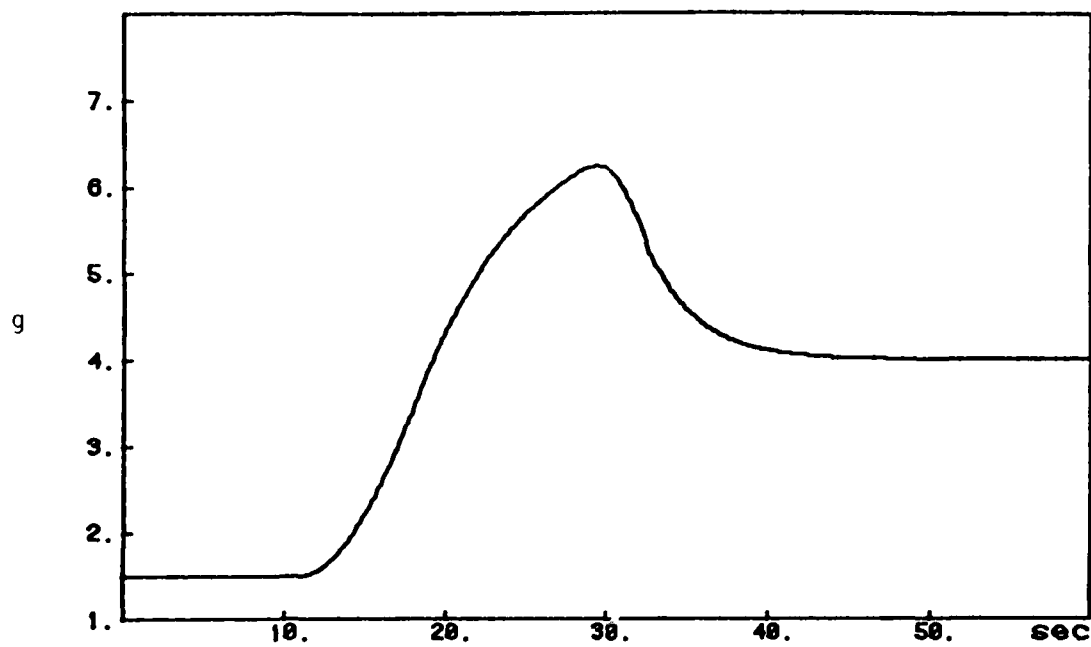


Fig. 40 ATTAINED G_z PROFILE

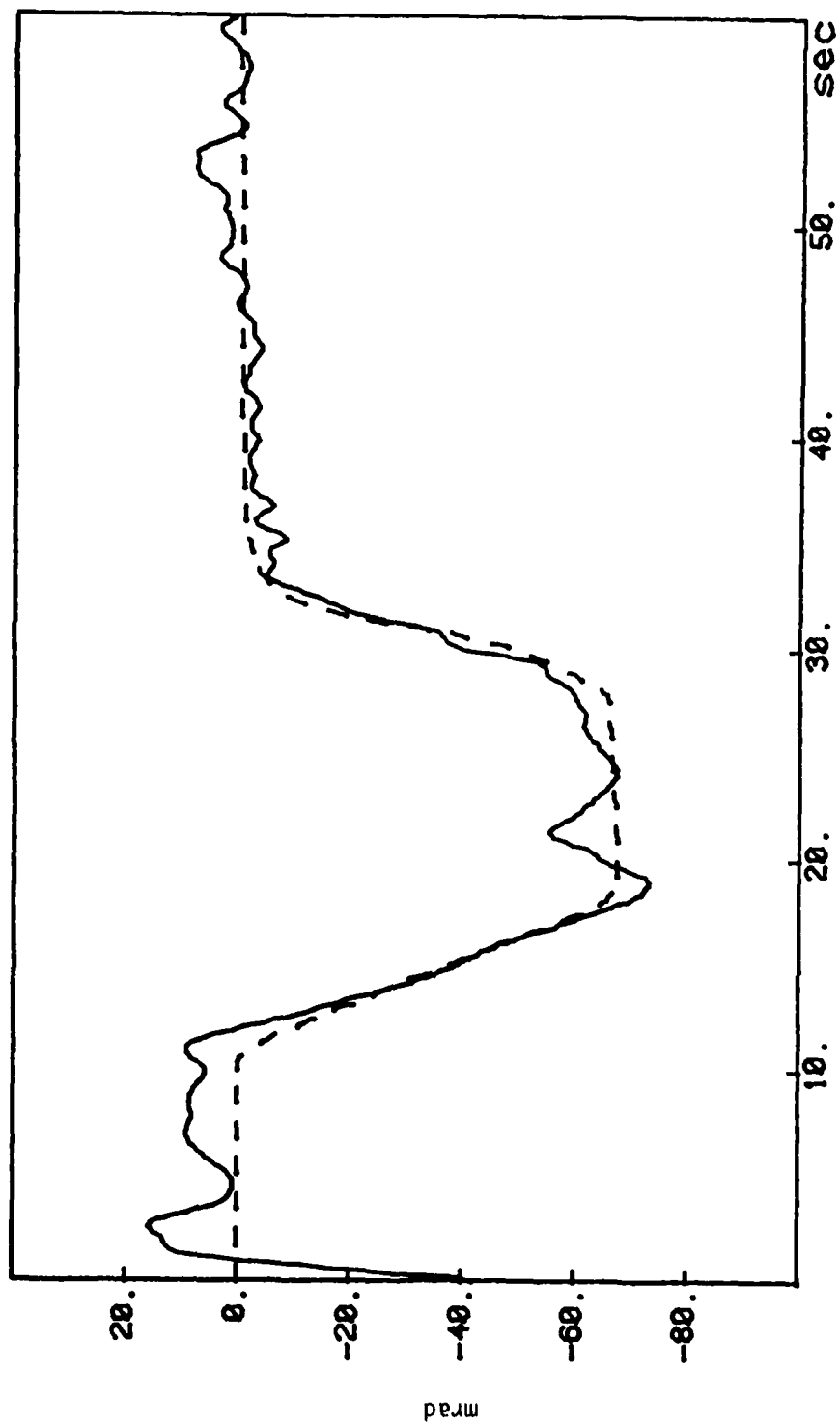


Fig. 41 MODEL-VS-DATA, PITCH ERROR MEAN, STATIC G

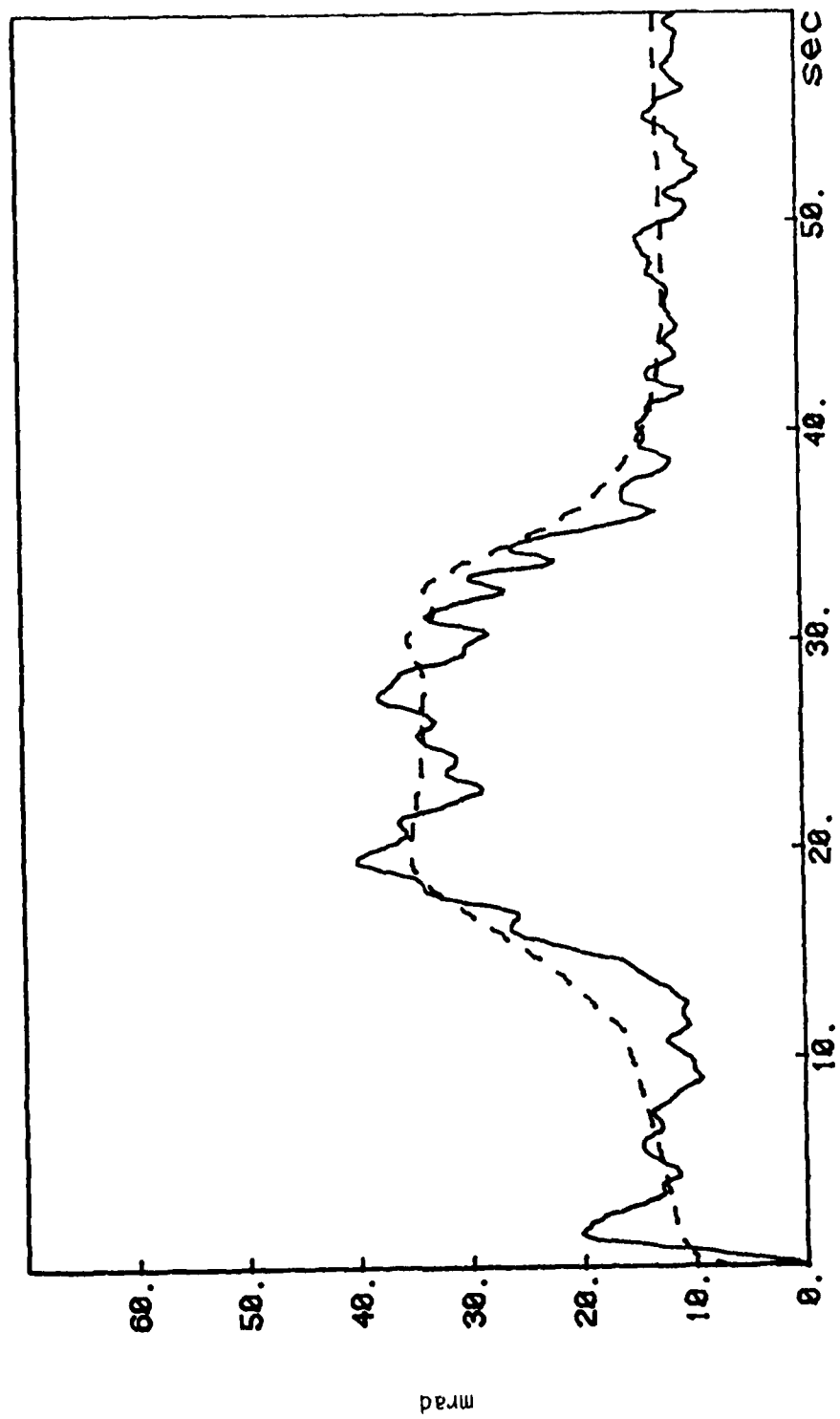


Fig. 42 MODEL-VS-DATA, PITCH ERROR SD, STATIC G

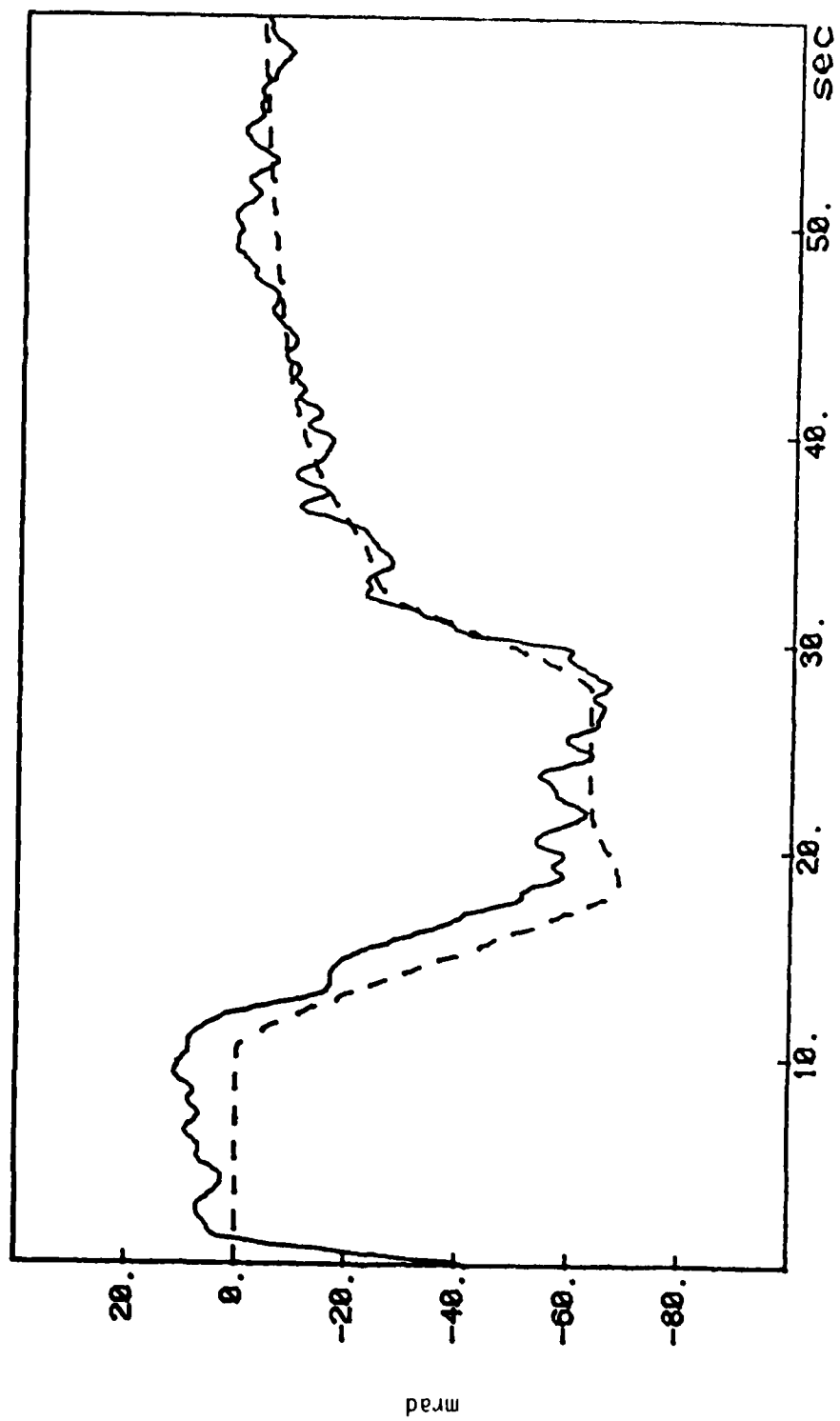


Fig. 43 MODEL-VS-DATA, PITCH ERROR MEAN, DYNAMIC G

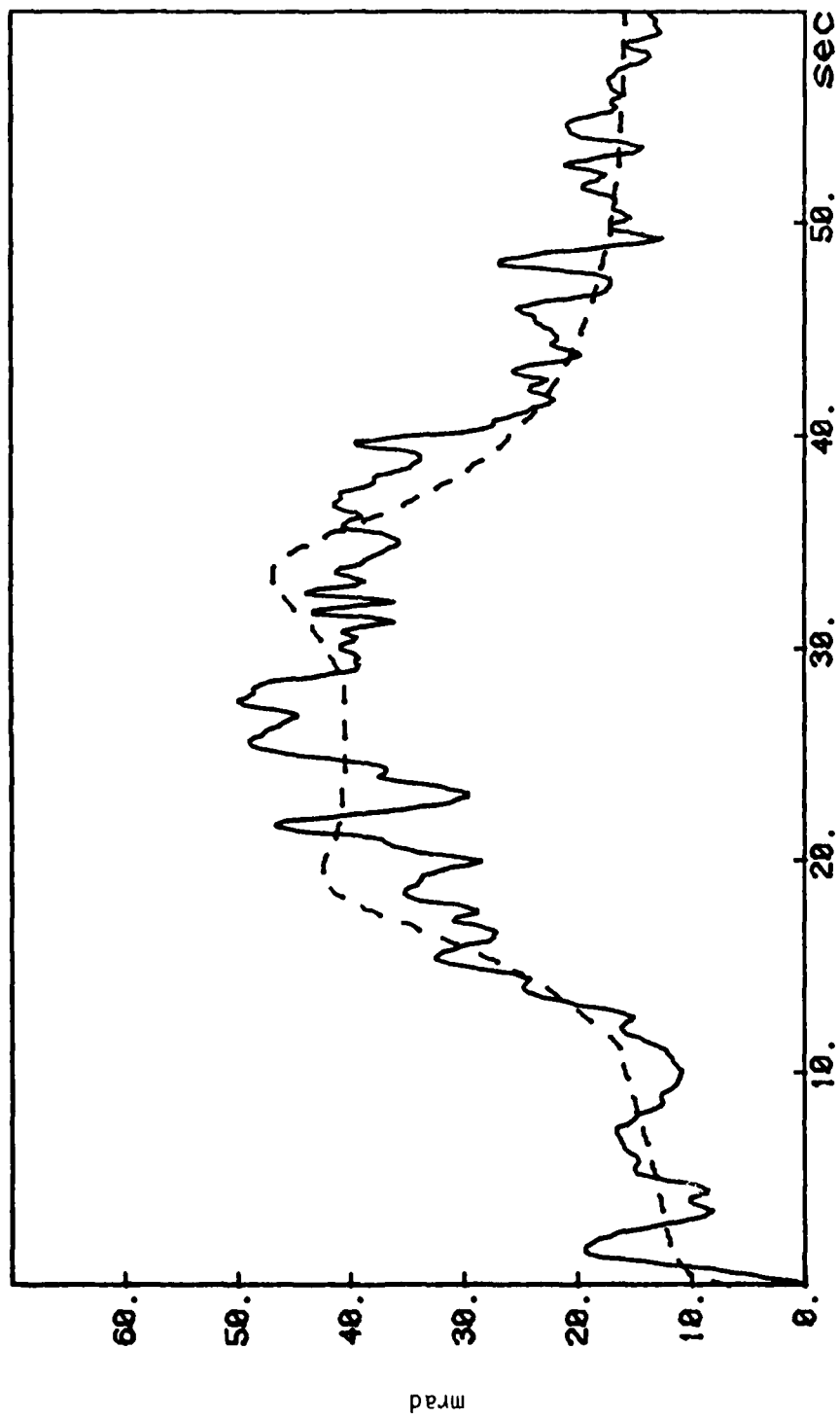


Fig. 44 MODEL-VS-DATA, PITCH ERROR SD, DYNAMIC G

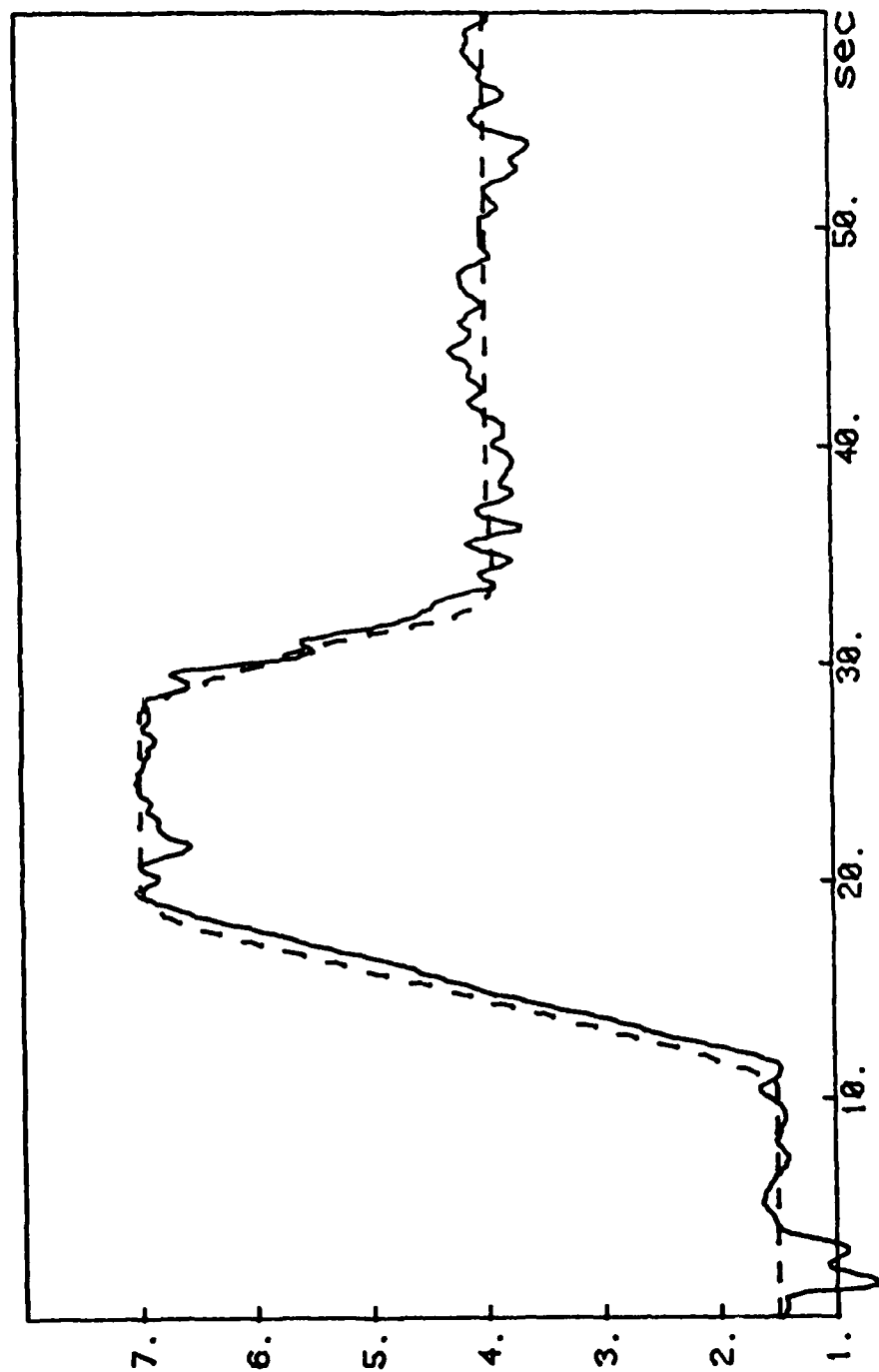


Fig. 45 MODEL-Vs-DATA, COMMANDED G_z , STATIC G CONDITION

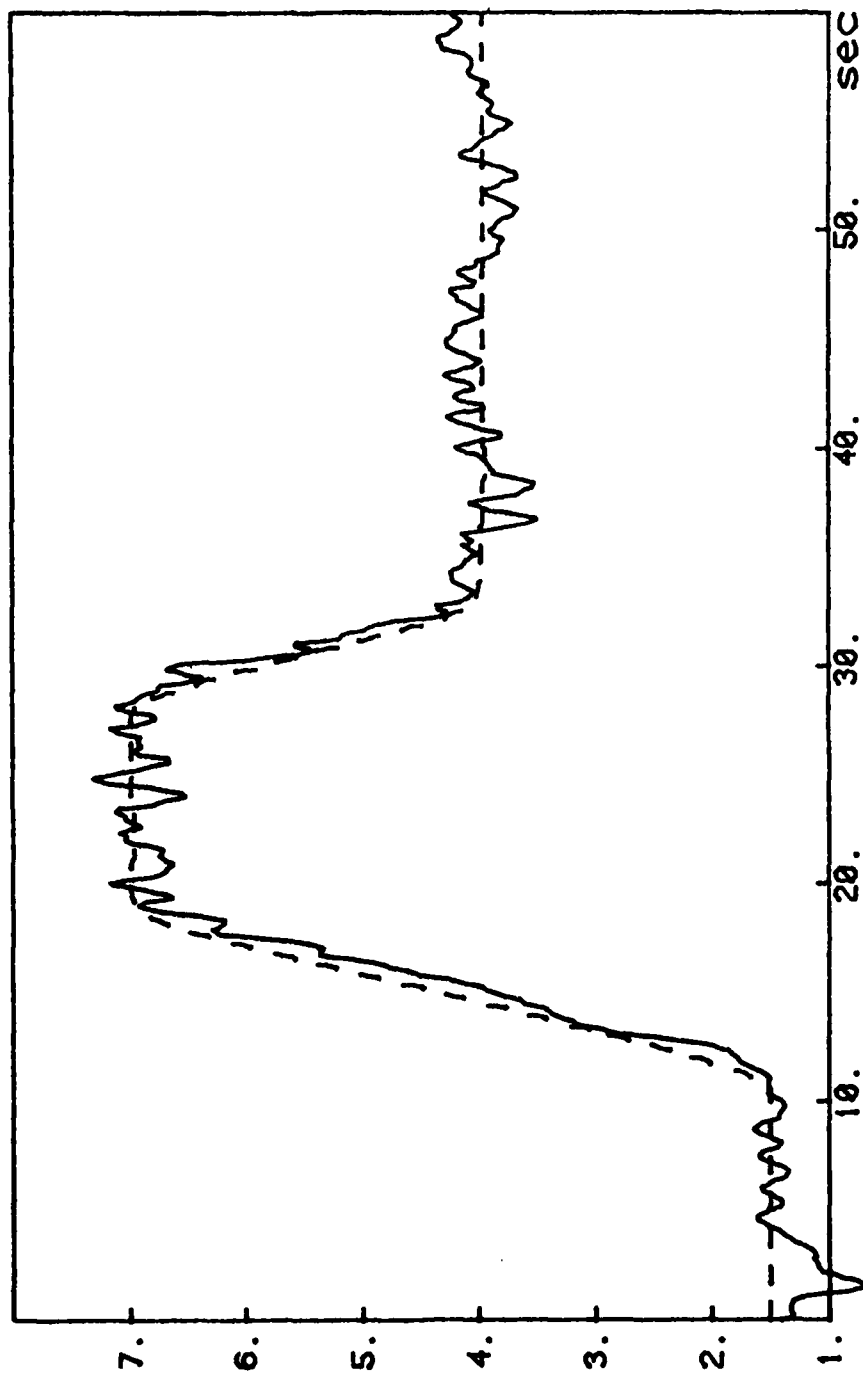


Fig. 46 MODEL-VS-DATA, COMMANDED G_z , DYNAMIC G CONDITION

- (1) One can observe a slower recovery of the tracking error during the transition period between the 7 G peak to the 4 G final plateau, when under G-stress.

This model prediction is attributed to the increase in the indifference threshold on the tracking error, a_1 , in the Dynamic-G condition. The major effect of increasing a_1 is to decrease $N_1(a_1)$, which in turn decreases the relative weighting on the tracking error in Equation (2.58). The resulting feedback gain on the tracking error is lower in magnitude, allowing the introduction of larger tracking errors, thus permitting a slow error recovery. Notice (figure 40) that the peak Attained-G level occurs during this transition interval.

- (2) A secondary effect of the increase in a_1 under G-stress, is to effect higher observation noise $V_{ep}(t)$ (Equation (2.54)).

- (3) Another indication of performance degradation under G-stress is larger standard deviations of tracking error. This is demonstrated in Figure 38. The model predicts a larger and persisting tracking error variance in the Dynamic-G condition, which is attributable to higher motor-noise. Indeed, a 40% higher motor noise ($\rho_\delta = -16.5$ dB in Dynamic-versus $\rho_\delta = -18$ dB in Static-G) was necessary to fit the ensemble tracking error SD. (From the covariance propagation equations of Section 1.4, one can see that increasing the motor-and/or observation noise results in higher variances.)

The modeling assumptions prove to be in excellent agreement with past G-stress performance research, as summarized in Section 1.2. Virtually all of these efforts conclude that the performance decrements are ascribed to larger motor and observation noises, as well as to such psychomotor response as tolerating larger tracking errors when operating under sustained acceleration stress.

2.4 Modeling the Lateral Tracking Task

2.4.1 Application of the Optimal Control Model

Similar to the longitudinal tracking dynamics, the lateral task has to be expressed in the state space,

$$\dot{\underline{x}}_o(t) = A_o \underline{x}_o(t) + \underline{b}_o \delta_a(t) \quad (2.60)$$

$$\underline{y}(t) = C_o \underline{x}_o(t)$$

where A_o , \underline{b}_o and C_o are the system matrices of the lateral dynamics, $\underline{x}_o(t)$ is the state and $\delta_a(t)$ is the aileron deflection. Notice the absence of the driving terms $w_o(t)$ and $z(t)$. In accordance with the simulated roll dynamics as represented by $G_r(s)$ in Section 2.1.5, we define the state as

$$\begin{aligned} x_1 &= e_r(t) = \text{lateral tracking error} \\ x_2 &= \dot{e}_r(t) = \frac{V}{D} \psi \\ x_3 &= K(t) \psi \\ x_4 &= K(t) \dot{\psi} \end{aligned} \quad (2.61)$$

It should be noted that these definitions are valid only when $K(t)$ is constant or slowly varying. This has been the usual assumption when considering time-varying system parameters in pilot modeling efforts.

This 4-th order system can be reduced to third order by combining the first order lag of Equation (2.26), $(\tau_\phi s + 1)^{-1}$, with the first order lag $(\tau_N s + 1)^{-1}$ which is introduced by the neuromotor dynamics in the OCM. Thus we set

$$\tau_{N, \text{equiv}} \cong \tau_N + \tau_\phi = \tau_N + \frac{1}{5.55} \quad (2.62)$$

in the subsequent modeling process, and the system then becomes

$$\begin{aligned} \dot{x}_1 &= x_2 \\ \dot{x}_2 &= x_3 \\ \dot{x}_3 &= K(t)\delta'_a(t) \end{aligned} \quad (2.63)$$

where $\delta'_a(t) = \dot{\psi}$, and x_1, x_2, x_3 are as defined previously. In matrix form, we obtain,

$$\dot{\underline{x}}_0 = \begin{bmatrix} 0 & 1 & 0 \\ 0 & 0 & 1 \\ 0 & 0 & 0 \end{bmatrix} \underline{x}_0 + \begin{bmatrix} 0 \\ 0 \\ 1 \end{bmatrix} K(t) \delta'_a(t) \quad (2.64)$$

Note that $K(t)$ enters only as a scalar multiplier on the control $\delta'_a(t)$. This means that the control $\delta'_a(t)$ can be computed for $K(t) = 1$ and then adjusted for arbitrary $K(t)$ via inverse scaling. It will be seen that $K(t)$ has an effect on the pilot's additive motor noise. For notational purposes we define $K(t)\delta'_a(t) = u(t)$.

The observations that are available to the pilot to minimize lateral tracking error are

$$\begin{aligned} y_1 &= x_1 &&= \text{tracking error } e(t) \\ y_2 &= x_2 &&= \text{error rate, } \dot{e}(t) \\ y_3 &= x_3/K(t) &&= \text{relative roll angle, } \phi \\ y_4 &= u/K(t) &&= \text{roll rate, } \dot{\phi} \end{aligned} \quad (2.65)$$

The observation y_3 of roll angle is critical for the control task. If this information is absent it is virtually impossible for a subject to control the K/s^3 system. The rule-of-thumb control logic of "keep your wings aligned with those of the target aircraft" is testimony to this fact. The information y_4 is not very important here inasmuch as the control signal $u(t)$ is essentially "known." It would be of importance if the target aircraft were free to move laterally.

2.4.2 G-Submodel for Lateral Tracking Task

Similar to the longitudinal tracking task, our modeling approach was first to isolate the G-stress-dependent OCM parameters and cost functional components, and then to determine the structure of that dependency. Below we list all OCM parameters and indicate how they are affected by acceleration stress:

Threshold Effects: The threshold nonlinearities were applied here in a fashion similar to that of Section 2.3.2. The nominal indifference threshold values on y_2 , y_3 and y_4 were selected from simulation considerations as $a_2 = 2$ mrad/sec, $a_3 = 5$ mrad, $a_4 = 2.5$ mrad/sec. These values remained unchanged in the dynamic condition. The threshold level on the observed lateral tracking error was chosen here, as in Section 2.3.2, to reflect the pilot-adopted tracking strategy. In the nominal static condition we select

$$t < t_s \quad a_1(t) = th_1 = 35 \text{ mrad} = \text{maximum angular error allowable}$$

$$t > t_s \quad a_1(t) = th_0 = 25 \text{ mrad} \approx \text{pipper radius.}$$

In the G-stress condition $th_1 = 50$ mrad, and the value of th_0 is unchanged. In the presence of G-stress, there is assumed to be a further increase in the model's

indifference threshold, viz:

$$a_1(t, G_A) = a_1(t) [1 + \rho_g \cdot \max^2(0, G_A - G_{\min})] \quad (2.66)$$

where $G_{\min} = 4g$ and $\rho_g = .3$ is chosen to match the $\sigma_{er}(t) = \sigma_{y1}(t)$ data. The rationale for this assumption is as before: under high G-stress the subject tends to tolerate larger tracking errors. These, in turn, result in a lower relative weighting on the error in the cost functional.

Observation Noise: This parameter was applied precisely in the same manner as in the longitudinal case:

$$v_{yi}(t) = \pi \rho_{yi} \frac{\sigma_{yi}^2}{f_i \cdot N_i} \quad i=1,2,3,4 \quad (2.67)$$

The nominal ρ_{yi} values are -21.5 dB as before, and $f_i = 1/4$. Notice, however, that the \bar{y}_i term is absent from Equation (2.66) as there is no target input excitation, and, strictly speaking, $\bar{y}_i = 0$.

Motor Noise: In the Optimal Control Modeling process, the control $\delta'_a(t)$ is generated as

$$\tau_{N, \text{equiv}} \dot{\delta}'_a(t) + \delta'_a(t) = \underline{L}'(t) \underline{x}(t) + v_u(t). \quad (2.68)$$

The gains $\underline{L}(t)$ are computed via

$$\underline{L}(t) = \underline{L}^*/K(t) \quad (2.69)$$

where \underline{L}^* are the optimal gains corresponding to $K(t) = 1$. The quantity $v_u(t)$ is the

human's motor noise. The motor noise consists of two parts: a purely additive component $v_u^0(t)$ [†] and a multiplicative component that scales with the control $\delta_a'(t)$.

Thus,

$$v_u(t) = \rho_a(t)v_u^0(t) + \xi(t)|\delta_a'(t)| \quad (2.70)$$

where $\xi(t)$ and $v_u^0(t)$ are assumed to be white and $\rho_a(t)$ is a known time function that modifies the additive motor noise covariance (see subsequent discussion). Multiplying Equation (2.68) through by $K(t)$, noting Equation (2.69) and defining $\delta_a(t)K(t) \triangleq u(t)$, we obtain

$$\dot{\underline{x}}_0 = A_0 \underline{x}_0 + \underline{b}_0 u(t) \quad (2.71)$$

$$\tau_{N, \text{equiv}} \dot{u}(t) + u(t) = -L^* \underline{x}(t) + \rho_a(t)K(t)v_u^0(t) + \xi(t)|u(t)| \quad (2.72)$$

Thus, the only effect of the gain $K(t)$ is to increase the effective additive motor noise component, the variance of which increases with $K^2(t)$. The motor noise covariance becomes therefore

$$V_u(t) = V_u^0(t) + \pi \rho_u(t) \text{cov}[u(t)] = \rho_a^2(t) K^2(t) V_u^0 + \pi \rho_u(t) \text{cov}[u(t)] \quad (2.73)$$

where $\rho_u(t)$ is the motor noise/signal ratio, and $\pi \rho_u(t)$ is identified as the covariance of $\xi(t)$. The multiplicative part of the motor-noise scales with the effective control $u(t)$, which is convenient for modeling. The net result is as expected: A constant motor noise input will have a greater effect on lateral tracking error during periods of high pitch rate since the system sensitivity, $K(t)$, increases as $q = \dot{\gamma}$ increases.

In addition, one has to consider the crossfeed effect in the manipulator. It

[†] Notice that an additive component must be assumed here, as there would be no other excitation to the system.

appears that during the "active" target maneuver intervals (i.e., when $\dot{G}_T = z(t) \neq 0$), the additive motor noise should increase. During these tracking periods, the pilot commands $\dot{G}_A^C \approx .75 \text{ g/sec}^2$ (see Figure 27, $t \in [10., 17.34]$ sec and $t \in [27.34, 31.34]$ sec). Because of this longitudinal control-rate, some additive noise is injected into the lateral axis, introducing random lateral errors.

The above discussion is relative to the interdependencies between the system dynamics and the motor noise. The effect of G-stress on this motor noise remained to be determined. In the course of the modeling work, it became apparent that model predictions were quite sensitive to variations in ρ_a and ρ_u . Increases in these parameters greatly increased the magnitude of the model-predicted $\sigma_{er}(t)$. Large increases in $\sigma_{er}(t)$ are observed between the static and the dynamic-G conditions (Figures 24, 26). We postulate therefore that G and/or \dot{G} stress increases the motor-noise. In a previous effort to model pilot performance under vibration stress, Levison [44] also needed to increase the motor noise to match the data. Although vibration is a form of physical stress different from sustained acceleration, it is possible to extrapolate from Levison's results to our study. The following approach was taken.

1. The nominal value of $\rho_u = -18.0 \text{ dB}$. In the dynamic conditions we select $\rho_u = -16.5$ in accordance with the longitudinal tracking task model.
2. In the static condition the nominal value of $V_u^0 = 1. (\text{rad/sec})^2$ was chosen on the basis of the manipulator dead-zone characteristics. In the dynamic conditions $V_u^0 = 2$. The value of ρ_a is nominally selected as 1.
3. Because of the crossfeed phenomenon we increase the motor noises at the times for which $z(t) \neq 0$. This is illustrated in Figure 47. Basically, ρ_u remains unchanged in the static condition but it increases to -13 dB under G-stress.

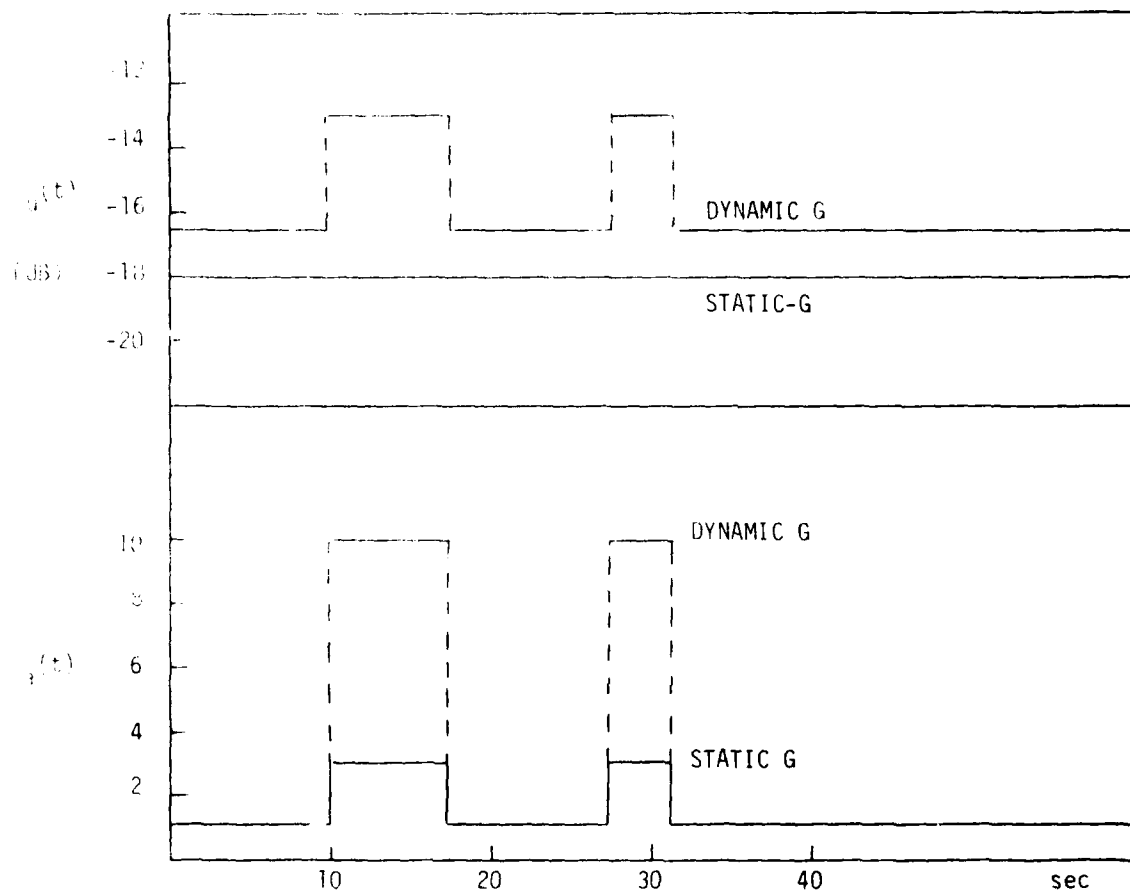


Fig. 47 MOTOR NOISES IN THE LATERAL TRACKING TASK

In the static condition we set $\rho_a = 3$ and in the dynamic $\rho_a = 10$. These increases reflect nine - and 100 - times higher levels of $V_u^0(t)$, respectively (see Equations 2.72 and 2.73). This indicates, perhaps, that sustained acceleration stress enhances the manipulator crossfeed effect.

The approach taken here modifies somewhat the preliminary model of [45].

Neuromotor Time Constant: The model was found to be quite insensitive to variations in the neuromuscular time constant, τ_N . The effective time constant used in this study was

$$\tau_{N, \text{equiv.}} = \tau_N + \tau_{\dot{\phi}} = .3 \text{ sec.}$$

Performance Index: The optimal control policy is that which minimizes the cost functional

$$J(u) = \lim_{T \rightarrow \infty} \frac{1}{T} E \left\{ \int_0^T [q_e N_1^2(a_1) e_r^2(t) + q_{\phi} \phi^2(t) + g \dot{u}^2(t)] dt \right\} \quad (2.74)$$

This is in accordance with the assumption that the subject weighs the perceived, rather than the displayed, error. The weightings that were chosen to obtain the optimal control gains were $q_e = .01$, $q_{\phi} = .1$ in the static condition, and $q_e = .01$, $q_{\phi} = .25$ in the dynamic one. Notice the much higher $\phi(t)$ weighting which indicates the higher relative importance of the roll angle in the control. Also, it is evident that under G-stress the relative weighting on $e_r(t)$ is lower than in the static condition (.01:.25 vs .01:.1). The net effect is similar to that of increasing the indifference threshold: both decrease the control gain on the error, thus generating higher $\sigma_{er}(t)$.

2.4.3 Modeling Results of the Lateral Tracking Task

An excellent indication of performance degradation under G-stress is the higher magnitude of $\sigma_{er}(t)$. We observe that $\sigma_{er}(t)$ in the Dynamic-G condition is about 60 milliradians during the peak G period, whereas in the Static condition it is about 30 mrad. The model reproduces these trends; the modeling results are illustrated in

Figures 48 - 51. (All figures relate to the first 60-second period of the 1-peak target profile.)

- Figure 48: SD of tracking error, Static G.
- Figure 49: SD of tracking error, Dynamic-G.
- Figures 50 - 51 illustrate the model-vs-data comparisons of $\sigma_{er}(t)$ under the two conditions.

2.4.4 Discussion

It is quite evident that the model reproduces the experimental data very well. It should be emphasized that no modifications to the OCM nominal parameters were necessary in the static condition. This reaffirms the validity of the OCM when nominal conditions are considered. Similarly to the longitudinal task, the increase in the model-predicted $\sigma_{er}(t)$ in the dynamic condition is attributed mainly to the increase in the human motor-noise, the lower error weighting in the cost functional, and the increase in the tracking error threshold parameter.

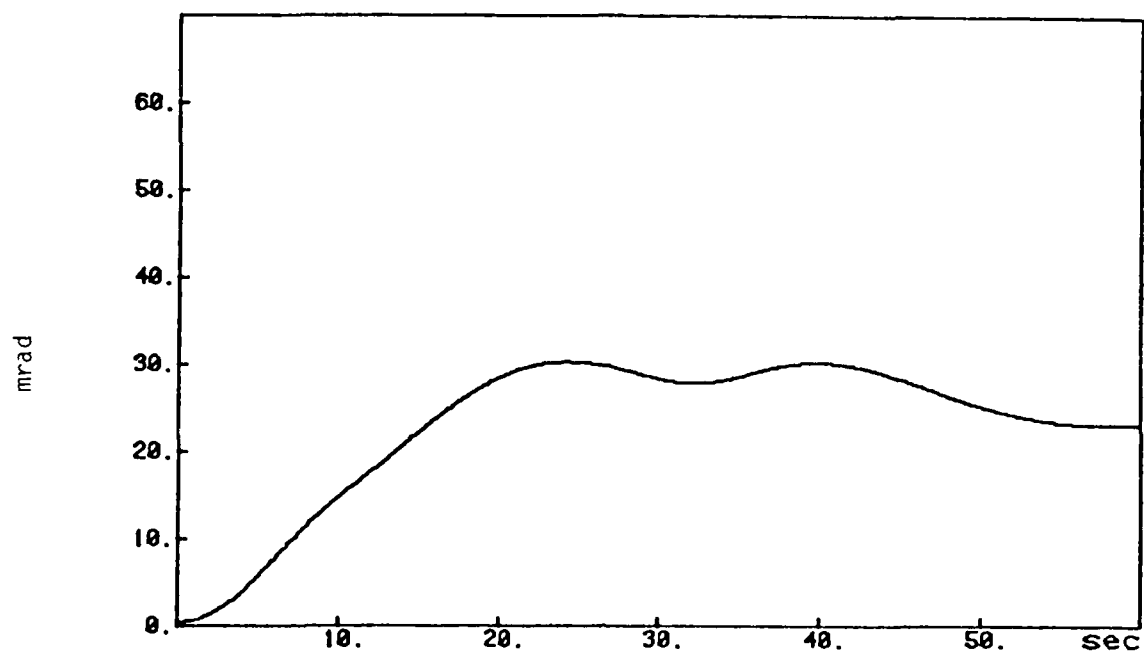


Fig. 48 STANDARD DEVIATION HEADING ERROR, 1 PEAK, STATIC G

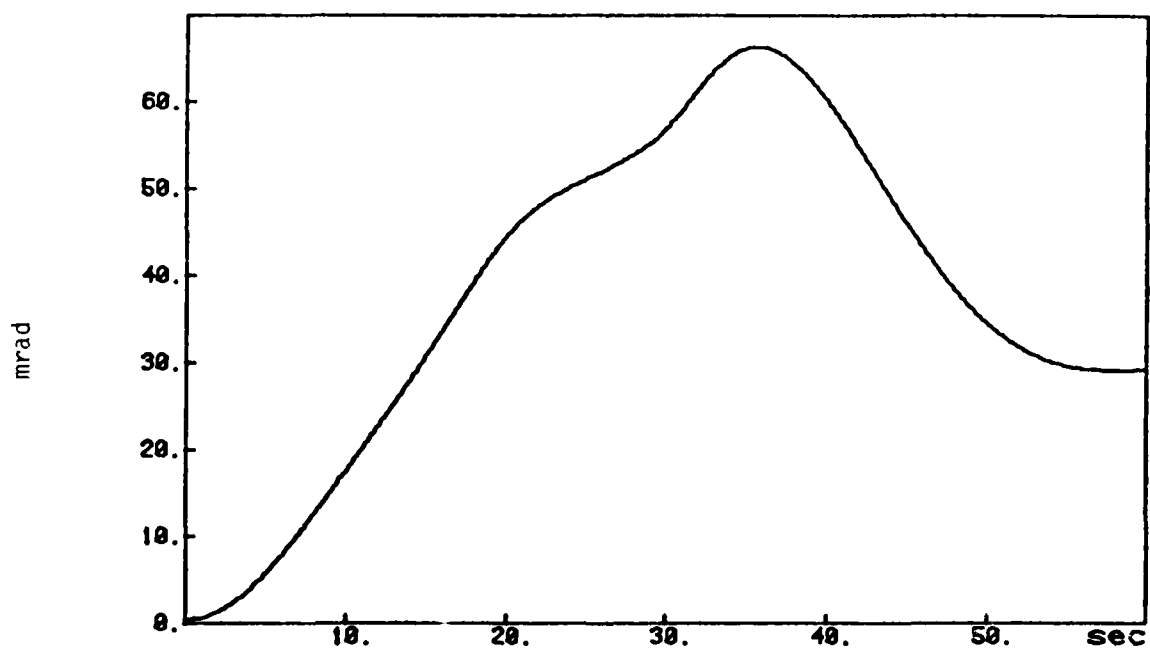


Fig. 49 STANDARD DEVIATION HEADING ERROR, 1 PEAK, DYNAMIC G

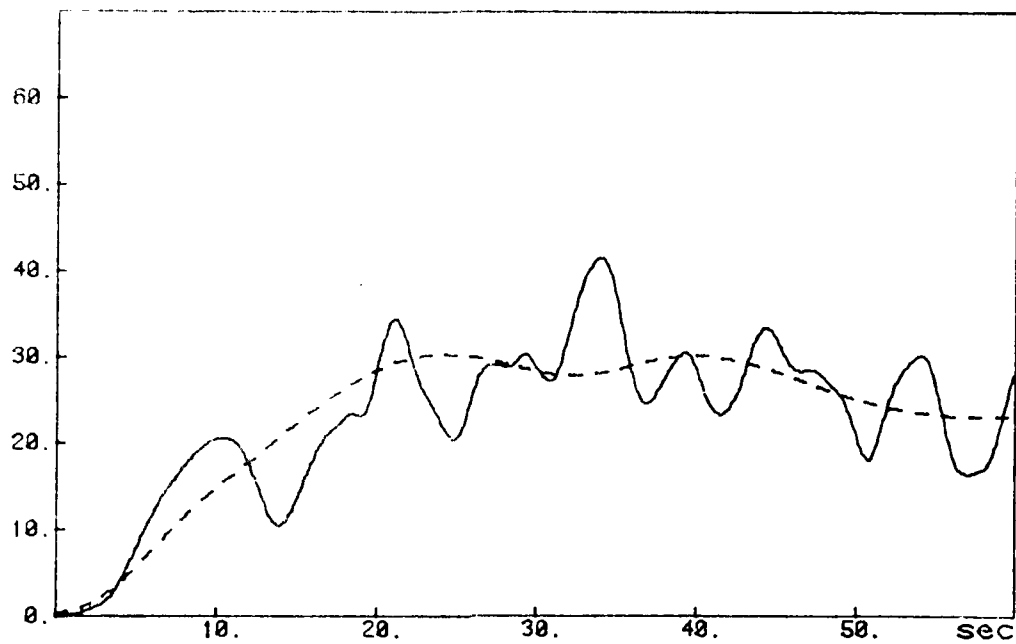


FIG. 50 MODEL-VS-DATA, HEADING ERROR SD, STATIC

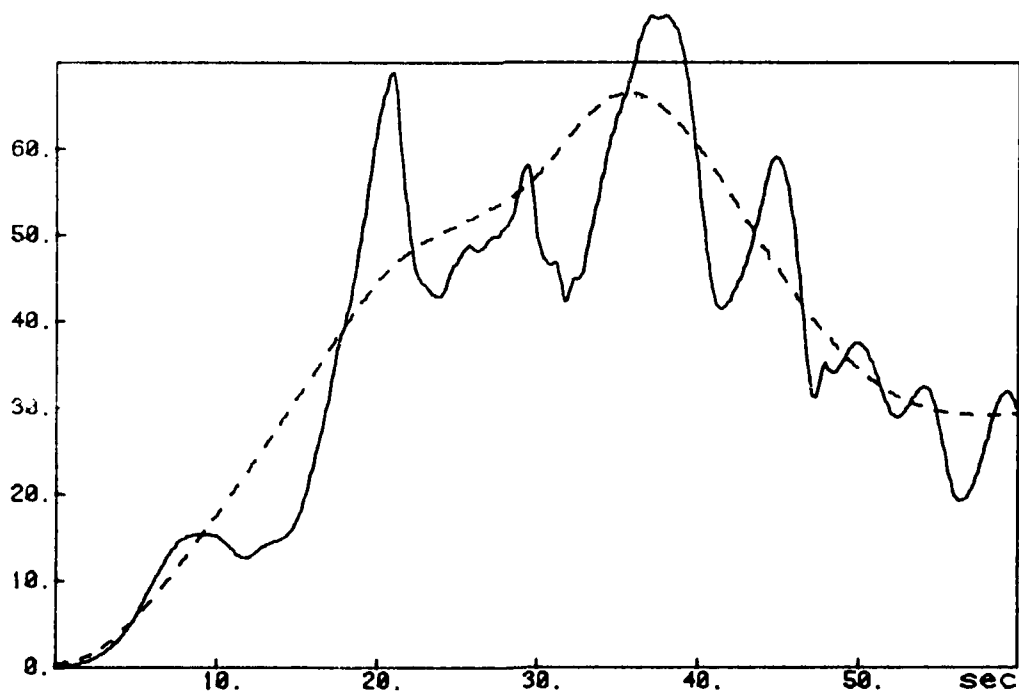


FIG. 51 MODEL-VS-DATA, HEADING ERROR SD, DYNAMIC

AD-A097 329 CONNECTICUT UNIV STORRS DEPT OF ELECTRICAL ENGINEERING--ETC F/6 5/9
HUMAN OPERATOR MODELING FOR AERIAL TRACKING.(U)
DEC 80 J KORN, A R EPHRATH, D L KLEINMAN F33615-78-C-0517
UNCLASSIFIED EECS-TR-79-16 AFAHRL-TR-80-44 NL

2 OF 2
AD
2007/5/29

END
DATE
FILMED
5 81
DTIC

III. FREQUENCY DOMAIN MEASURES OF HUMAN PERFORMANCE UNDER G-STRESS.

In Chapter II, the development of a "Time-Domain" G-model is discussed. Although this performance model is successful in the sense that it was validated by the experimental data, the information it furnishes is somewhat limited. It is intrinsically incapable of providing any frequency measures, such as power spectra, transfer functions, remnants. In fact, this model is only effective in predicting pilot performance in the presence of transients in the target profile; steady-state analysis is excluded.

It was imperative, therefore, to build a stationary performance model that will complement the nonstationary one. In this chapter, a steady-state model of pilot performance under constant sustained-G stress is presented. The experimental program leading to this G-model development is still in progress at AMRL. Results of the initial DES runs have become available and they comprise the data base for the present model building effort. Three experimental conditions are employed, and are designated as (1) Static (fixed-base), (2) Semi-dynamic (5 G open-loop stress) and (3) Post-runs (static runs immediately following the semi-dynamic condition). The control task is compensatory tracking in the lateral plane. The target input excitation is a psuedo-random signal (sum of sine waves), providing a rich set of measures amenable to FFT analysis. This is discussed in detail in section 3.1. The performance model is based upon the Optimal Control Model (OCM). Section 3.2 describes the modeling effort.

The experimental data exhibit significant tracking performance decrements under G-stress. The pilot's control remnant increases by as much as 5 db at some frequencies, and his tracking RMS error increases by some 15%. In addition, the pilot's describing function magnitude decreases by nearly 1.5 db, particularly in the post-runs condition.

[†]This Chapter is based upon a 1979 CDC paper [48].

The model reproduces these trends quite well, by properly adjusting its parameters. A discussion of the empirical and modeling results follows in Section 3.3.

3.1 Experimental Design

The constant- G_z experiments that provide the data base for the modeling effort reported herein were not designed as G_z experiments per se. In fact, they are embodied in a larger experimental program designed to investigate the combined G_z - G_y effects on pilots in the new Vectored Force Fighter (VFF) aircraft. The AMRL DES centrifuge was the motion simulator used in these experiments. The subjects were seated in the cab, which represents an aircraft cockpit, and was equipped with a sidearm control stick. The visual tracking loop included a compensatory tracking task in the lateral plane as shown in Figure 52. The display included a stationary gunsight reticle and a target aircraft, represented by a dot.

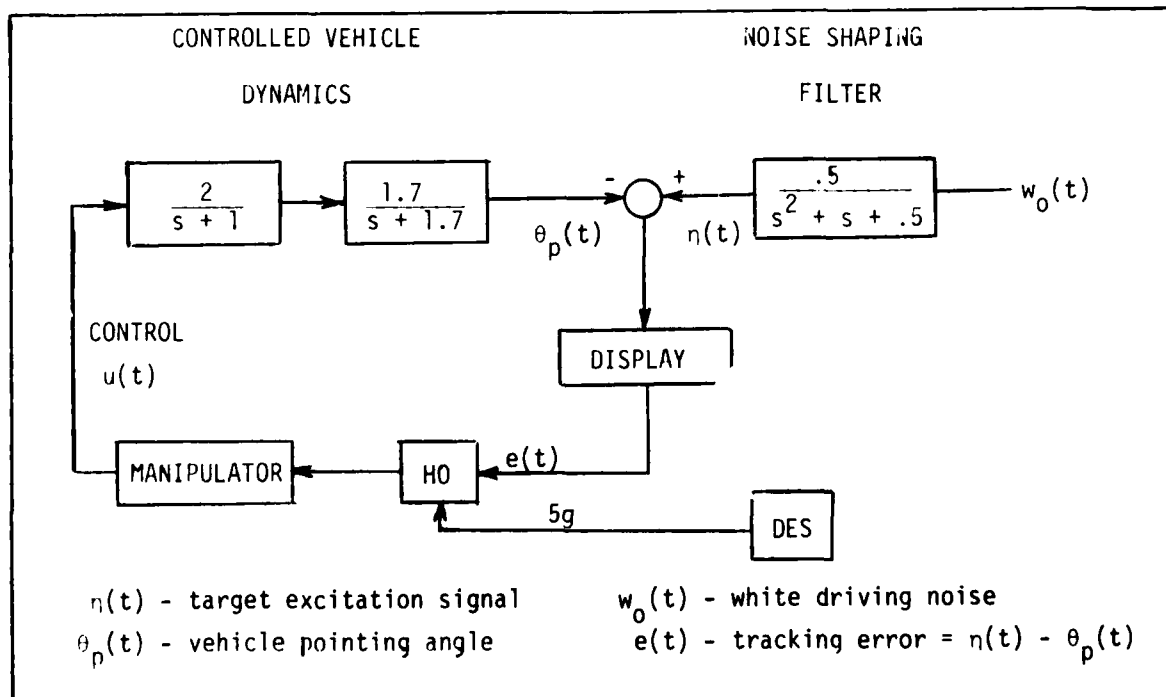


Fig. 52 TRACKING TASK CONFIGURATION

and solve the covariance equation

$$X_S A_S' + A_S X_S + \frac{E_S W E_S'}{S} = 0, \quad X_S \triangleq E\{x_S x_S'\} \quad (3.4)$$

we obtain $W = .36$, which corresponds to the specified σ_η .

The random signal $\eta(t)$ was simulated by combining 11 sine waves into psuedo-random forcing function,

$$\eta(t) = \sum_{i=1}^{11} A_i \cos(\omega_i t + \theta_i) \quad (3.5)$$

for each run, the phases, θ_i , of the sinusoids were randomized in order to eliminate cognitive response, and the frequencies, ω_i , were chosen to span the range of the human response (.15 : 15.57 rad/sec). The amplitudes, A_i , were selected to approximate $\phi_{\eta\eta}(\omega)$. A summary of the frequency components comprising the pseudo-random signal is given in Table 1. A detailed description of how to generate the approximated amplitudes can be found elsewhere [46].

No.	Frequency (rad/sec)	Amplitude
1	0.15	0.2376
2	0.38	0.2404
3	0.69	0.2023
4	1.00	0.1330
5	1.46	0.0854
6	2.22	0.0482
7	3.30	0.0259
8	4.76	0.0147
9	7.29	0.0081
10	10.51	0.0044
11	15.57	0.0025

Table 1 SUMMARY OF FREQUENCY COMPONENTS

The VFF is designed in such a way that the pilot's lateral commands generate a transient direct side force, i.e., a G_y acceleration. In order to simulate the desired G_y levels, it was necessary to centrifuge the subjects to an (almost) constant G_z , and to rotate the DES cab (in conjunction with the pilot tracking commands) to produce an off-normal G component. The present study deals only with the constant G_z runs (5G level) and no G_y acceleration. The tracking task was designed to be used both in the present constant G_z study as well as in future (closed-loop) G_y applications. This design constrained the driving signal and the plant dynamics to parameters comensurate with the DES cab's bandwidth. The design specifics are listed below.

Target Input Excitation Signal: The target driving signal was chosen to be a second order colored noise $\eta(t)$ with the power spectral density

$$\phi_{\eta\eta}(\omega) = \frac{.25W}{\omega^4 + .25} \quad (3.1)$$

and with the prescribed RMS value of $\sigma_\eta = \sqrt{E\{\eta^2\}} = .3$. Such noise is normally generated as the output of a linear time invariant system, $T(s)$, driven by white noise $w_o(t)$ with $E\{w_o^2(t)\} = W$. For the given $\phi_{\eta\eta}(\omega)$, this system is

$$T(s) = \frac{.5}{s^2 + s + .5} \quad (3.2)$$

which is nothing but a Butterworth filter with a cutoff frequency of .707 rad/sec.

If we represent $T(s)$ in the state space,

$$\begin{aligned} \dot{\underline{x}}_s &= \underline{A}_s \underline{x}_s + \underline{E}_s w_o(t) = \begin{bmatrix} 0 & 1 \\ -.5 & -1 \end{bmatrix} \cdot \underline{x}_s + \begin{bmatrix} 0 \\ .5 \end{bmatrix} \cdot w_o(t) \\ \eta(t) &= \underline{H}'_s \underline{x}_s = [1 \ 0] \underline{x}_s \end{aligned} \quad (3.3)$$

Controlled Vehicle Dynamics: The chosen plant had a second-order, overdamped transfer function, which was dictated by the DES cab dynamics, viz.,

$$G(s) = \frac{3.4}{(s+1)(s+1.7)} \quad (3.6)$$

Run Length: In order to comply with medical safety requirements, the run duration had to be limited. A run length of 81.92 seconds was chosen; with a sampling period of 40 msec, each run resulted in 2048 datum points, facilitating the FFT analysis.

Independent Variables: There were three experimental conditions (excluding the Dynamic G_y case).

1. "Static" - The centrifuge cab served as a fixed-base simulator (no G_z -stress). The subject's stick inputs effected a displayed tracking error with no actual acceleration.
2. "Semi-dynamic" - The centrifuge cab served as a moving-base simulator. The pilot nominal G_z level was 5 G. As in 1, the subject's control corrected the displayed tracking error, but no off-normal accelerations were present.
3. "Post-runs" - Same as 1, but these runs immediately followed condition 2.

Each session included two static runs, followed by two semi-dynamic runs, immediately followed by two post-runs. By this arrangement it was hoped to uncover some of the sustained-, as well as the accumulative-G effects on tracking performance.

Replications: Five subjects participated in a total of nine sessions. With two runs per condition per session, 18 runs per condition resulted.

Data Analysis: Numerous quantities, ranging from tracking error to heart rate time histories were recorded, but only a subset of these quantities was required for the performance model. The measurements that are of consequence to the modeling effort were the tracking error, $e(t)$, and the pilot stick command, $u(t)$.

When analysing the experimental data, the following steps were taken:

1. The raw data of each of the individual runs were transformed to frequency domain via an FFT program, which produced the following quantities (evaluated at the input frequencies):
 - (a) Ensembles of the individual power spectra of the tracking error, $e(t)$, and of the pilot control, $u(t)$ ($\phi_{ee}(\omega)$ and $\phi_{uu}(\omega)$, respectively).
 - (b) The spectra $\phi_{ee}(\omega)$ and $\phi_{uu}(\omega)$ are given in two parts, the input - correlated and the input - uncorrelated:

$$\begin{aligned}\phi_{ee}(\omega) &= \phi_{ee}^c(\omega) + \phi_{ee}^{uc}(\omega) \\ \phi_{uu}(\omega) &= \phi_{uu}^c(\omega) + \phi_{uu}^{uc}(\omega)\end{aligned}\tag{3.7}$$

- (c) The cross-power-spectral densities of $e(t)$ and of $u(t)$ with the input signal $\eta(t)$ ($\phi_{\eta e}(j\omega)$ and $\phi_{\eta u}(j\omega)$, respectively) were computed, and an ensemble of the equivalent pilot describing functions, $H(j\omega)$, (magnitude and phase) was obtained

$$H(j\omega) = \frac{\phi_{\eta u}(j\omega)}{\phi_{\eta e}(j\omega)}\tag{3.8}$$

- (d) The pilot control remnant, $R(\omega)$, was next obtained from the ratio of $\phi_{uu}^{uc}(\omega)$ to $\phi_{uu}^c(\omega)$,

$$R(\omega) = \frac{\phi_{uu}^{uc}(\omega)}{\phi_{uu}^c(\omega)}\tag{3.9}$$

This quantity is crucial in any performance-modeling efforts. As performance degrades under G-stress, it is reasonable to expect an increase in the remnant's magnitude, indicating perhaps involuntary motor activity. This, indeed, is the case in the present work, as seen in the subsequent sections.

(e) In addition, the performance "scores," i.e., the RMS values of $e(t)$ and of $u(t)$ (or alternately, the total power in $\phi_{ee}(\omega)$, and $\phi_{uu}(\omega)$ were computed. These quantities prove to be indicative of pilot-tracking performance, as they increase under G-stress, as might be expected.

2. The data were ensemble averaged, utilizing techniques similar to those of Section 2.2. The final product was first- and second-order statistics of:
 - a. Pilot describing function, $H(j\omega)$ (magnitude and phase),
 - b. Pilot remnant, $R(\omega)$,
 - c. RMS scores.

These results are illustrated in Figures 53 - 61 and in table 2.

Discussion of the experimental, as well as the modeling results follows in Section 3.3.

3.2 Modeling Approach

The base-line model adopted here was the "Steady-State" OCM, as explained in Section 1.4.2.2. The system being controlled is described by the state space equation

$$\dot{\underline{x}}_0(t) = \underline{A}_0 \underline{x}_0(t) + \underline{b}_0 u(t) + \underline{E}_0 w_0(t) \quad (3.10)$$

$$= \begin{bmatrix} 0 & 1 & 0 & 0 \\ -1.5 & -1 & 0 & 0 \\ 0 & 0 & -1.7 & 1.7 \\ 0 & 0 & 0 & -1 \end{bmatrix} \underline{x}_0(t) + \begin{bmatrix} 0 \\ 0 \\ 0 \\ 2 \end{bmatrix} u(t) + \begin{bmatrix} 0 \\ .5 \\ 0 \\ 0 \end{bmatrix} w_0(t),$$

where the first two states are associated with the input noise shaping, $u(t)$ is the pilot's control input and $w_0(t)$ is a zero-mean white Gaussian noise, with

$$E \{w_0(t) w_0(\sigma)\} = W\delta(t-\sigma), \quad W = .36 \quad (3.11)$$

The displayed variables consist of the paired tracking error/error rate, viz.,

$$\underline{y}(t) = \begin{bmatrix} e \\ \dot{e} \end{bmatrix} = C_{00} \underline{x}_0(t) = \begin{bmatrix} 1 & 0 & -1 & 0 \\ 0 & 1 & 1.7 & -1.7 \end{bmatrix} \underline{x}_0(t) \quad (3.12)$$

The OCM assumes that the well-trained and motivated human operator adopts an optimal control strategy, subject to his inherent psycho-physiological limitations. The mathematical interpretation of this statement is that the pilot, in the case at hand, will minimize the following cost functional:

$$J(u) = E \left\{ \lim_{T \rightarrow \infty} \frac{1}{T} \int_0^T (e^2(t) + g \dot{u}^2(t)) dt \right\}, \quad (3.13)$$

where g is the relative weighting on the control rate. Obtaining the optimal control law is accomplished by solving the steady-state Riccati equation pertaining to (3.13).

The well-known solution to this problem is

$$\tau_N \dot{u} + u = -L_{opt}' \hat{\underline{x}}_0(t) + v_u(t) \quad (3.14)$$

where τ_N is the human operator (HO) neuromuscular time constant, $v_u(t)$ is an additive motor noise, L_{opt} is the optimal control gains vector and $\hat{x}_0(t)$ is the estimated state. There is a one-to-one correspondence between q_r and τ_N ; usually the latter is specified and q_r is adjusted accordingly.

Human Limitations: The neuromuscular time constant, τ_N , is just one of the OCM parameters that reflect the human inherent constraints. It represents the human's neuromotor bandwidth limitation in generating the control input.

Another human constraint stems from the fact that the human estimates the system state on the basis of a delayed and noisy perceived information,

$$y_{pi}(t) = y_i(t-\tau) + v_{yi}(t-\tau) \quad i=1,2 \quad (3.15)$$

where

τ = human's lumped time delay,

$v_{yi}(t)$ = observation noise of the i -th indicator.

The observation (or sensor) noise $v_{yi}(t)$ is a zero-mean, white Gaussian noise with covariance

$$E \{v_{yi}(t) v_{yi}(\sigma)\} = V_{yi} \delta(t-\sigma) \quad (3.16)$$

$$V_{yi} = \pi \rho_{yi} E\{y_i^2(t)\},$$

and ρ_{yi} is the noise/signal ratio of the i -th observed variable.

The driving motor noise of Equation (3.14) is also zero-mean, white and Gaussian. Its covariance is

$$\begin{aligned} E\{v_u(t)v_u(\sigma)\} &= V_u \delta(t-\sigma) \\ V_u &= \pi \rho_u E\{u^2(t)\} , \end{aligned} \tag{3.17}$$

where ρ_u is the motor noise/signal ratio.

In the modeling work, τ_N , τ , ρ_{yi} , and ρ_u are of major interest, since these are the only parameters that need to be tuned in order to match the experimental data. A comprehensive OCM parameter identification program that was developed at the University of Connecticut [47] facilitated this task. The application of this identification procedure to the case at hand can be found in the Appendix. The experimental and the modeling results are discussed in the following section.

3.3 Results and Discussion

Figures 53 and 61 present the model-data comparisons for all three conditions. The data are represented by the ensemble means and the standard deviations at the input frequencies, and the model predictions -- by the continuous lines. In addition, the predicted RMS control and tracking error scores are compared with the experimental ones in Table 2. The following observations can be made, regarding the empirical data:

Describing Function Magnitude: The highest magnitude among the three conditions is observed in the static case. It is 0.5 - 1.0 dB larger than the magnitude in the semi-dynamic condition, and 1.0 - 1.5 dB larger than in the post-run condition. These differences are present at almost all input frequencies.

Describing Function Phase: Here, no significant differences are apparent among the three conditions.

Control Remnant: The most pronounced difference exists here. Whereas there is hardly any difference in the remnant between the static and the post-run conditions, the semi-dynamic case (G_z - stress, Figure 3.7) exhibits an increase by as much as 3 to 5 dB throughout the entire frequency range.

Tracking Scores: Table 2 lists the empirical RMS values (\pm one standard deviation) of $e(t)$ and of $u(t)$ for the three conditions. The following observations are made:

1. The lowest RMS error value is in the static condition, and the highest--in the G_z -stress condition.
2. The lowest control levels were applied during the post-runs, and the highest--during the G_z runs.

Figures 53 through 61 show the modeling results, which are the major achievement of this effort. The experimental data validate the model in all three cases, throughout the entire frequency range. Some discrepancies exist at low frequencies, between the phases in particular: the model is unable to reproduce the phase droops below 0.7 rad/sec. This has traditionally been the case in all past modeling works.

The model predicted scores match the experimental RMS values as well. The predicted scores, both error and control, deviate no more than half a standard deviation from the ensemble score means.

Table 3 summarizes the OCM parameters that were identified from the data. It is apparent that the operator's motor mechanism is impaired by G_z -stress. The highest motor noise/signal ratio, ρ_u , was identified for the semi-dynamic condition. The increase in ρ_u under G-stress is by as much as 4.5 dB. This result is in excellent agreement with past psycho-motor research [13, 19], and may be attributed to a phenomenon such as tremor. It is quite interesting, however, that the post-runs effect lower motor noise.

Moreover, the observation noise/signal coefficient, ρ_e , under G-stress increases from -19.6 dB to a level as high as -15.1 dB. This again is consistent with past research concerning G-effects on vision. The increase ρ_e may be accounted for by decrements in visual acuity under G-stress, blur, etc., as reported by Grether [9] and many others. Alternately, this increase in ρ_e can be ascribed to a decrease in the attentional allocation or to an increase in the indifference threshold on the observed error due to G-stress, or both. This is readily evident if we replace Equation (3.16) with

$$V_e = \frac{\pi \rho_e E\{e^2(t)\}}{f_e \cdot N_e} \quad (3.18)$$

where $f_e \leq 1$ is the fractional attention allocated to $e(t)$. The term

$$N_e = N_e [a_e, E\{e^2(t)\}] \leq 1 \quad (3.19)$$

is a statistically linearized function, arising from a thresholded error observation with threshold level a_e (see [43]). It has been shown [44, 45] that the error indifference threshold is indeed affected by G-stress.

The trends in ρ_e^* are not as clear as in ρ_e , but the model proved quite insensitive to the former. Therefore, ρ_e^* may be assigned a prescribed nominal value.

Another parameter which is affected by G-stress is the lumped time delay, τ . There is some increase in τ in the semi-dynamic condition but it decreases slightly in the post-run case. The increase in human reaction time under G-stress is again in accordance with previous research (e.g. [13]). The neuromuscular time constant, τ_N , increases both for G and post-G runs; this validates the hypothesis of accumulative G_z -effects. This decrease in the human control bandwidth, combined with a significant

decrease both in the describing function gain (Figure 59) and in control activity, (Table 2 - post run condition), suggest a hysteresis effect of fatigue induced by an accumulated G_z -stress.

TABLE 2 - RMS SCORES

SCORES (RMS) CONDITION	TRACKING ERROR, e		CONTROL, u	
	EXPERIMENTAL	PREDICTED	EXPERIMENTAL	PREDICTED
STATIC	.093 \pm .014	.090	.37 \pm .10	.32
G_z -STRESS	.107 \pm .015	.102	.42 \pm .18	.33
POST-RUNS	.095 \pm .021	.088	.33 \pm .09	.29

Table 3 - MODEL PARAMETERS

CONDITION PARAMETERS	STATIC	G_z - STRESS	POST-RUNS
ρ_u , dB	-17.5	-15.3	-20.1
ρ_e , dB	-19.6	-15.1	-21.3
ρ_e^* , dB	-29.5	-30.8	-24.5
τ , SEC	.257	.266	.236
τ_N , SEC	.159	.176	.165

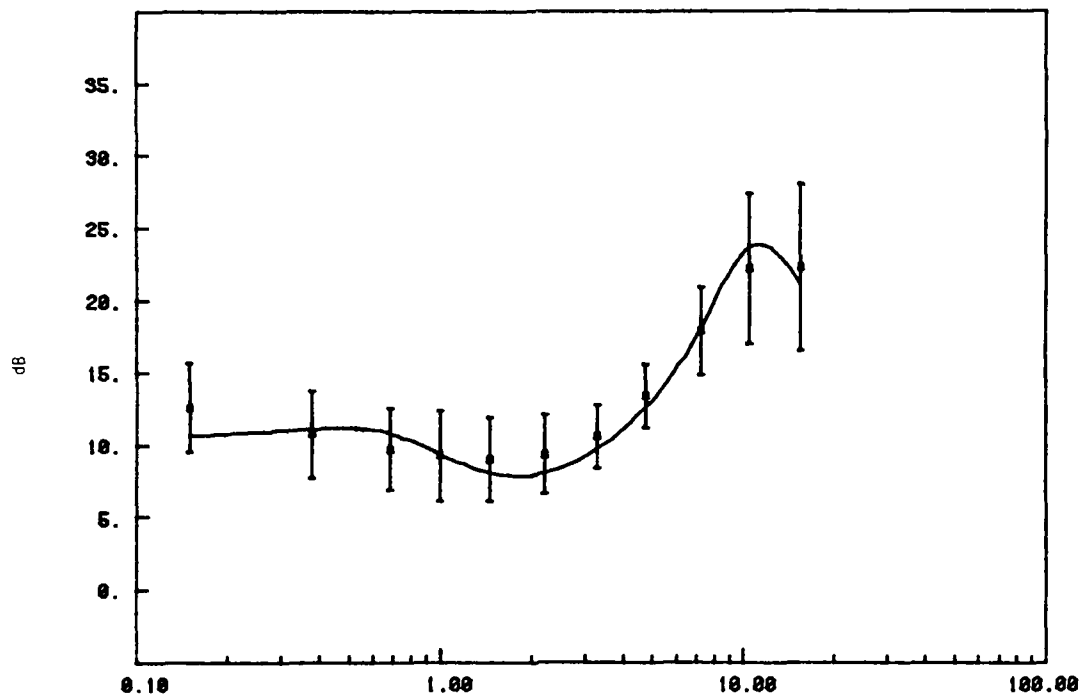


Fig. 53 PILOT DESCRIBING FUNCTION MAGNITUDE $|H(j\omega)|$, STATIC CONDITION

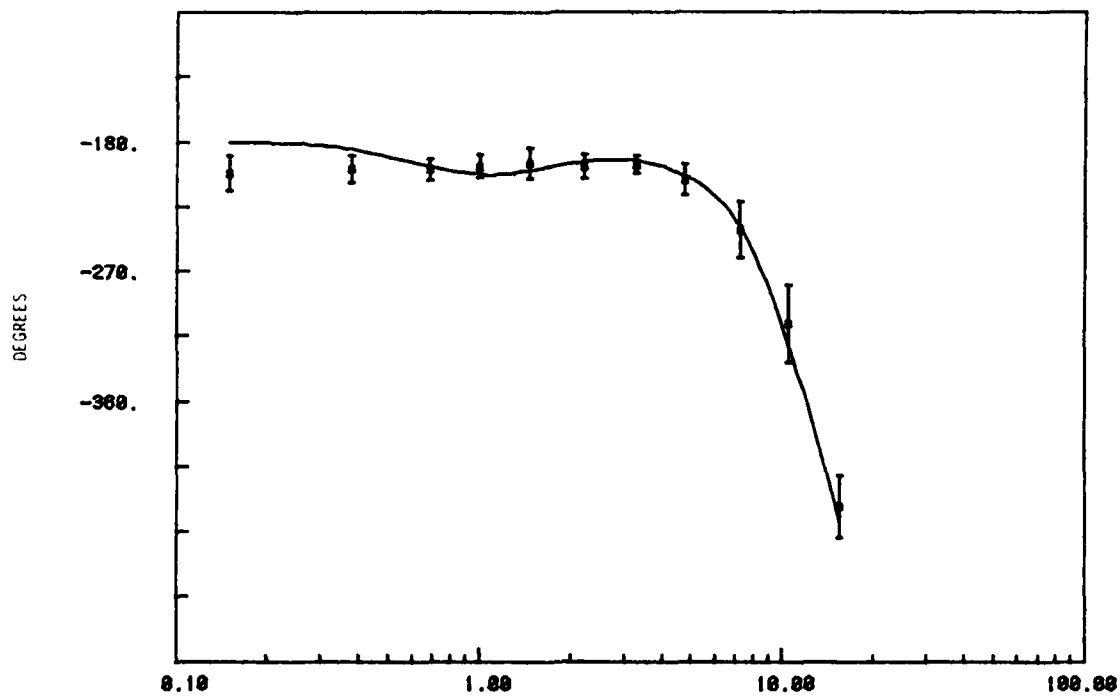


Fig. 54 PILOT DESCRIBING FUNCTION PHASE $\angle H(j\omega)$ STATIC CONDITION

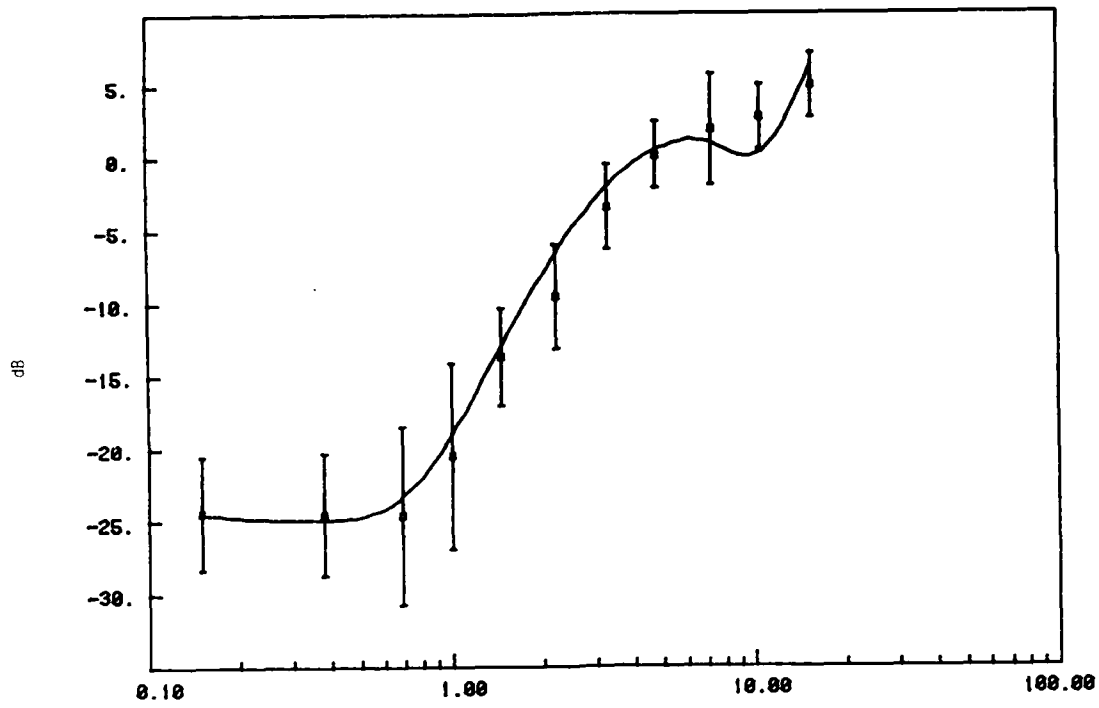


Fig. 55 CONTROL REMNANT $R(\omega)$, STATIC CONDITION

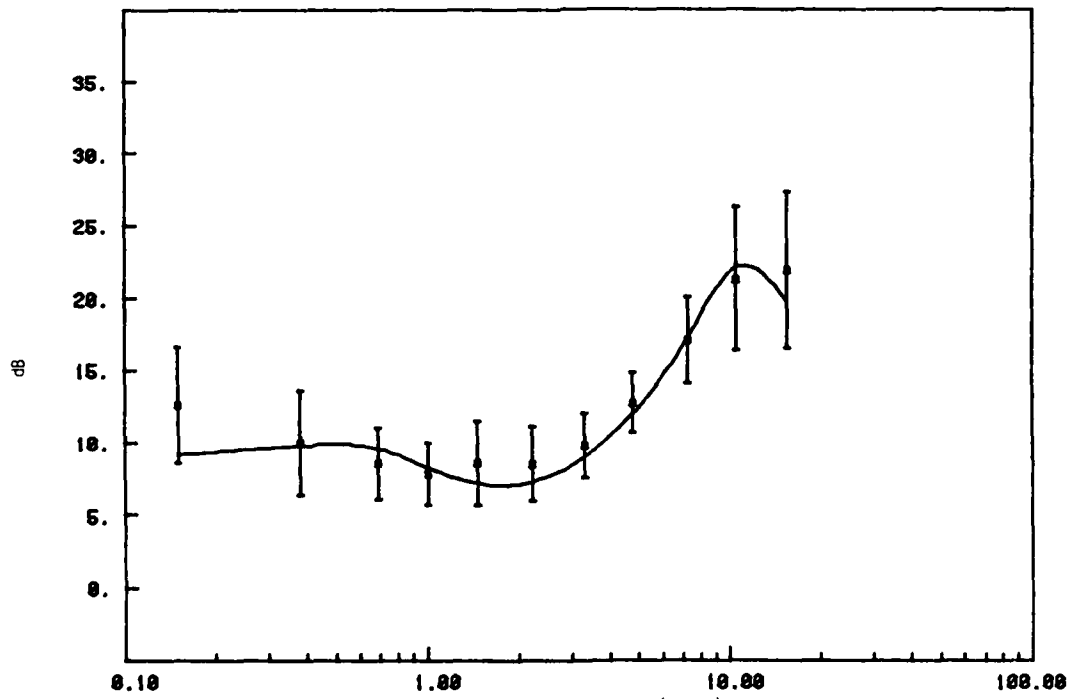


Fig. 56 PILOT DESCRIBING FUNCTION MAGNITUDE $|H(j\omega)|$, DYNAMIC CONDITION

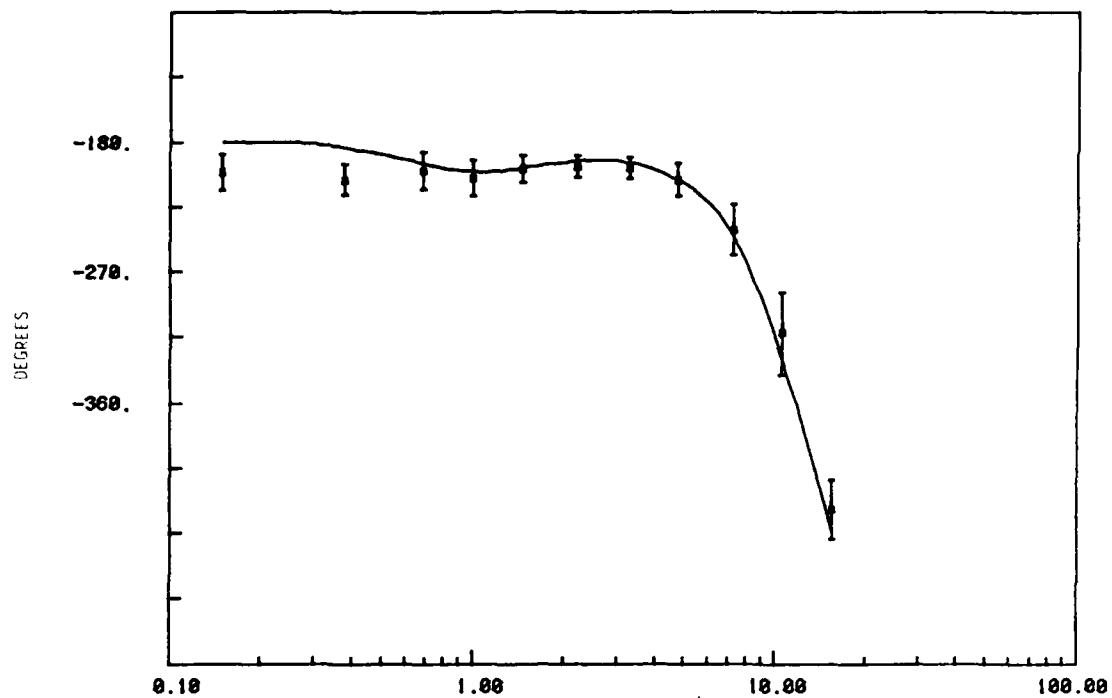


Fig. 57 PILOT DESCRIBING FUNCTION PHASE $\angle H(j\omega)$, DYNAMIC CONDITION

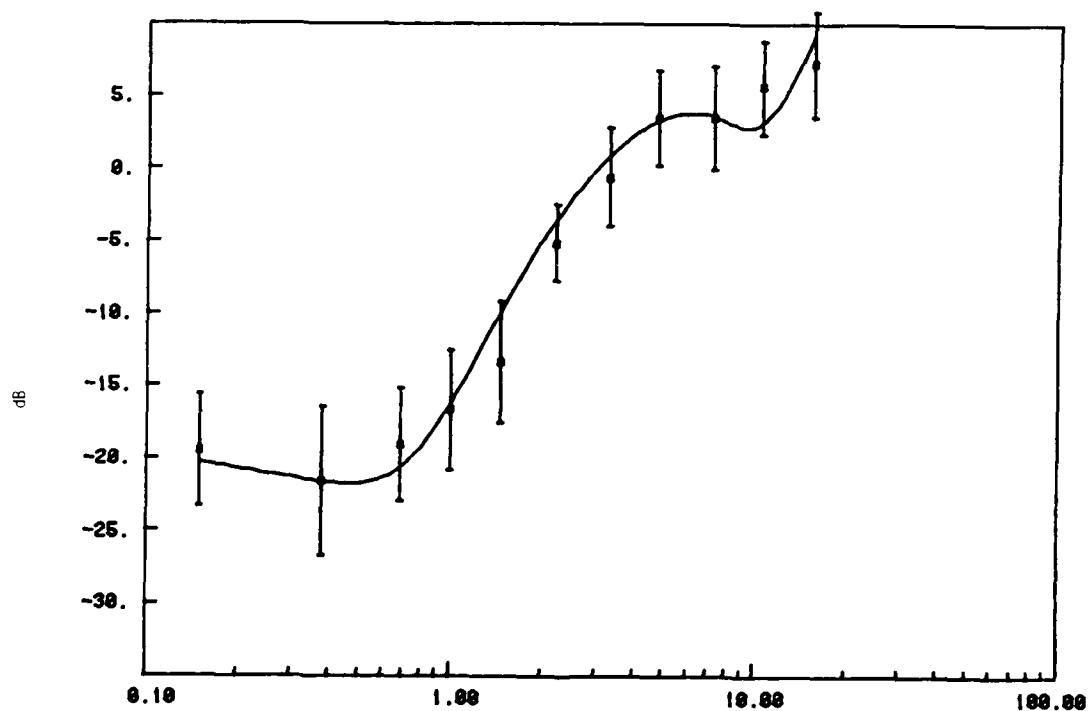


Fig. 58 CONTROL REMNANT $R(\omega)$, DYNAMIC CONDITION

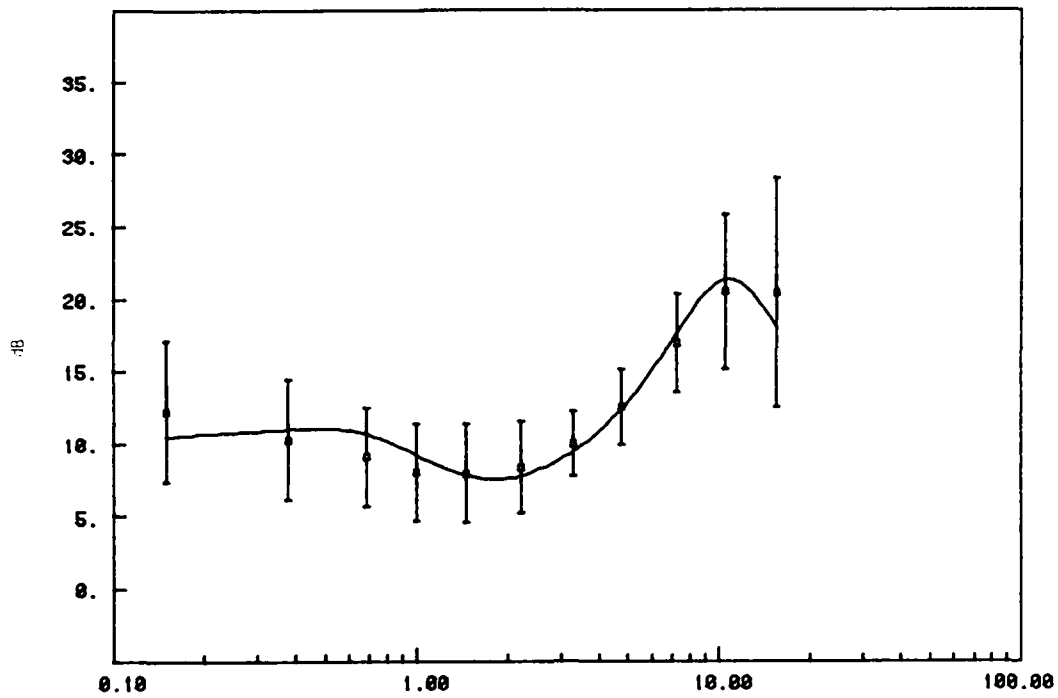


Fig. 59 PILOT DESCRIBING FUNCTION MAGNITUDE $|H(j\omega)|$, POST RUN CONDITION

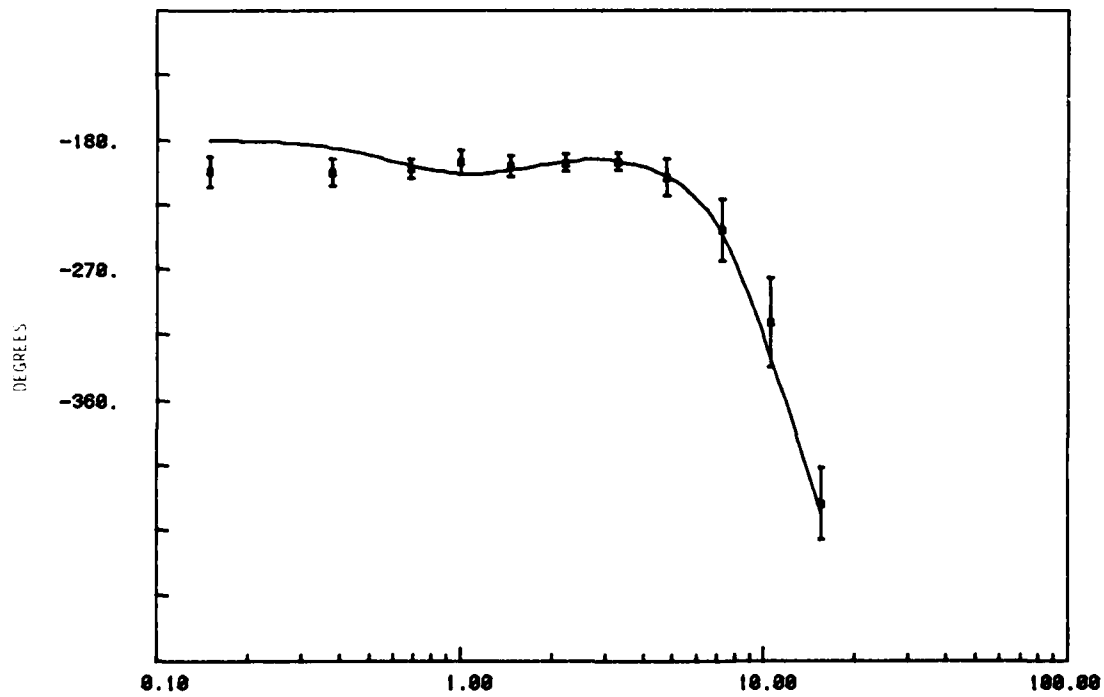


Fig. 60 PILOT DESCRIBING FUNCTION PHASE $\angle H(j\omega)$, POST-RUN CONDITION

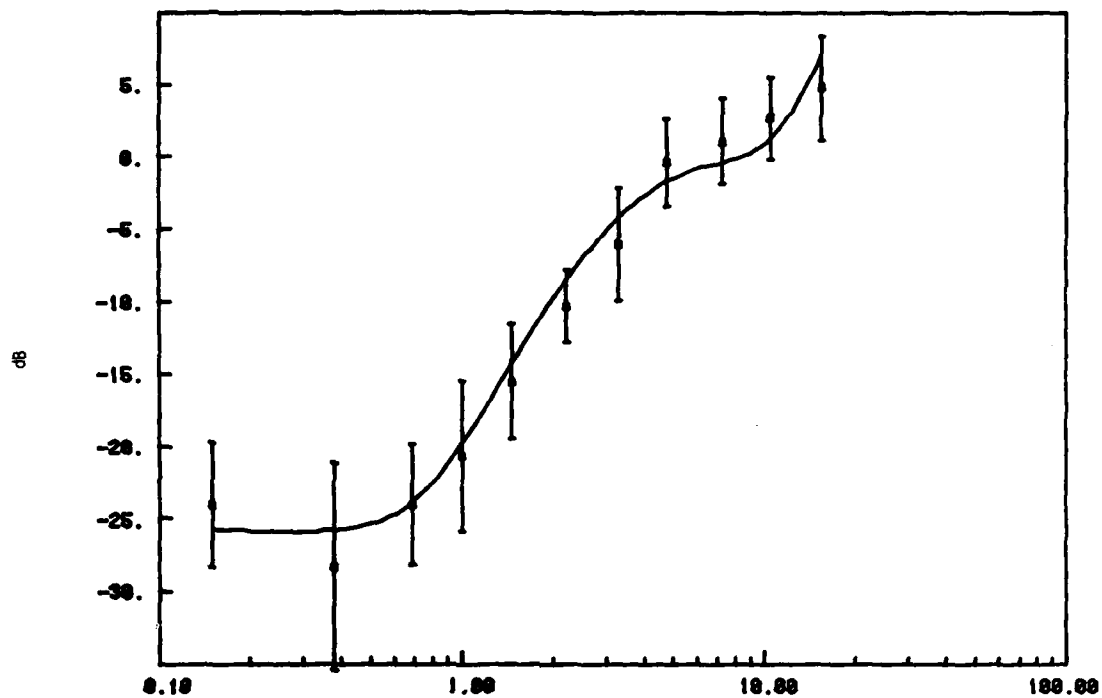


Fig. 61 CONTROL REMNANT $R(\omega)$, POST-RUN CONDITION

IV CONCLUSIONS

It has become a well-established fact that linear acceleration stress effects substantial degradation in pilot performance. The results of the compensatory tracking/sustained acceleration research program, jointly undertaken by Air Force Aerospace Medical Research Laboratory and the University of Connecticut-CYBERLAB, substantiates this contention. Statistical analyses performed on the experimental data prove that significant differences exist between G_z versus no- G_z -stress conditions. The acceleration stress data exhibit trends which are clearly a manifestation of performance impairment:

1. The variability in the tracking errors increases significantly under G_z -stress. This is demonstrated by high levels and enduring periods of tracking-error-variance time histories, and by larger RMS tracking scores.
2. Pilot's involuntary motor activity increases in the presence of sustained G_z -stress. The data show large increase in the input-uncorrelated control power, and higher control RMS values.
3. It is evident from the data that G_z -stress effect slow tracking error recovery and lower magnitude of the human describing function. This is, perhaps, an indication of a lower control bandwidth on the part of the pilot under positive acceleration stress.

The analytical phase, on its part, has resulted in a normative performance model which has been validated by the experimental data. The model is based upon the Optimal Control Model (OCM) and it has been augmented by a G-submodel to include the acceleration effects. The model parameters, which reflect a person's inherent limitations, depart from their nominal values to account for the performance degradation under strenuous acceleration conditions.

Virtually all the model parameters need to be perturbed in order to replicate the data trends. It is shown that the model parameters which are affected are the observation noise, neuromotor time constant τ_N , and reaction time-delay, all of which exhibit a significant increase under G_z -stress. In addition, some accumulative G-effects are evident as τ_N remains higher than nominal in the post-G runs, reflecting a lower control bandwidth, and perhaps fatigue.

The most noteworthy deviations from the nominal, however, are the increases in the motor noise and in the error indifference threshold parameters. The first results in higher control remnant levels and tracking error variances, which are observed from the empirical data. The latter effects a slow tracking - error recovery in the closed-loop G-stress condition.

At present, we are pursuing a G_y -stress research program which is an extension of this study. The G_y program, in addition to lateral accelerations, involves positive vertical acceleration stress of up to 5G. As the experimental data of this program become available, the performance model under G_z -stress may be refined further.

APPENDIX

IDENTIFICATION OF OCM PARAMETERS UNDER G-STRESS

The application of the Optimal Control Model (OCM) to a manual-control task usually involves matching model predictions to available experimental data. Traditionally, this has been done by tediously varying the model parameters until a suitable model-data match has been obtained. In the past year, a comprehensive Parameter Identification Program for the OCM (OCMID) has been developed [47]. This program provides an automated technology for the model-building process.

The OCMID is a modular computer package designed to identify parameters of the OCM. User-supplied routines determine the parameters to be identified and the form of the program output. The package is designed with flexibility to allow any routine to be interchanged with user - supplied routines, so the package can be tailored to specific needs. In conjunction with the present G-model research, the OCMID has been extended with additional routines, incorporating a graphics display subprogram.

Approach:

The objective is to identify the pilot describing function (magnitude and phase), the remnant, and the model predicted performance scores. The OCM parameters that generate these predictions are to be identified from experimental frequency measures data so as to minimize a weighted least-squares objective functional. The minimization of this cost functional provides a scalar metric, which in turn, reflects how closely the currently obtained model matches the measured describing function's magnitude and phase, control remnant and performance RMS scores. We choose, therefore, the cost functional

$$J = \frac{1}{2} \left[q_{se} \left(\frac{s_e - \hat{s}_e}{\sigma_{se}} \right)^2 + q_{su} \left(\frac{s_u - \hat{s}_u}{\sigma_{su}} \right)^2 \right] \quad (A.1)$$

$$+ \frac{1}{N_f} \sum_{i=1}^{N_f} \left[q_{Mi} \left(\frac{|H(j\omega_i)| - |\hat{H}(j\omega_i)|}{\sigma_{Mi}} \right)^2 + q_{Pi} \left(\frac{\angle H(j\omega_i) - \angle \hat{H}(j\omega_i)}{\sigma_{Pi}} \right)^2 + q_{Ri} \left(\frac{R(\omega_i) - \hat{R}(\omega_i)}{\sigma_{Ri}} \right)^2 \right]$$

s_e = RMS score of tracking error

s_u = RMS score of control input

$H(j\omega_i)$ = Pilot describing function @ i-th input frequency

$R(\omega_i)$ = Pilot remnant @ i-th input frequency

$\sigma(\cdot)$ = Ensemble standard deviation of the pertinent variable

$\hat{(\cdot)}$ = Represents the OCMID current estimates

$q(\cdot)$ = Relative weightings (at present = 1.)

N_f = Number of frequencies = 11

The choice of this cost functional gives a weighted least-squares fit to the data. Notice that each squared difference in J is divided by the appropriate ensemble standard deviation. In this way, datum points with larger $\sigma(\cdot)$ are automatically given less weight.

The minimization of J is carried out by applying Powell's non-gradient optimization method [49]. Basically, Powell's method finds pseudo-conjugate gradient search directions by perturbing the parameters in the Euclidean space. A bivariate quadratic line search is used to minimize J in each search direction, such that the parameters "move" a step along each orthogonal direction. This means that in one Powell iteration the parameters "move" along the average direction of all the individual orthogonal directions.

After the program has converged, a single quasi-Newton step is taken to ensure convergence and to provide approximate confidence intervals for the identified parameters. To see this step we rewrite J as:

$$J = \frac{1}{2} \sum_{i=1}^{NT} f_i^2(\theta) = \frac{1}{2} f(\theta)' f(\theta) \quad (A.2)$$

where:

NT = total number of the weighted squared differences

$\underline{\theta}$ = parameter vector to be identified

f_i^2 = i-th squared term.

The quasi-Newton step is

$$\underline{\theta}^{k+1} = \underline{\theta}^k - \alpha \left[\frac{\partial f'}{\partial \underline{\theta}} \cdot \frac{\partial f}{\partial \underline{\theta}} \right]^{-1} \frac{\partial f}{\partial \underline{\theta}} \underline{f} \bigg|_{\underline{\theta}=\underline{\theta}^k} \quad (A.3)$$

where α is the one-dimensional line search minimizing element. In the case at hand,

$$NT = 2 + 3 \cdot N_f = 35$$

$$\underline{\theta}' = (\rho_u, \rho_e, \rho_e^*, \tau_N, \tau)$$

and the $f_i(\underline{\theta})$ terms are given by Equation (A.1). Note that the term inside the squared brackets of Equation (A.3) is the approximated Hessian. The approximate confidence interval for the identified parameter set is then given by the square-root of the diagonal elements of the inverse Hessian.

References

1. Brown, J. L. and Lechner, M., "Acceleration and Human Performance - A Survey of Research," Aviation Medicine, February 1956.
2. Roth, E. M., "Acceleration," Section 6 in Compendium of Human Responses to Aerospace Environment, NASA CR-1205(II), November 1968.
3. Code, C. F., Wood, E. H., Sturm, R. E., Lambert, E. H. and Baldes, E. J., "The Sequence of Physiological Events in Man during Exposure to Positive Acceleration," Federation Proceedings, 1945, 4, (14).
4. Wood, E. H., Lambert, E. H., Baldes, E. J. and Code, C. F., "Effects of Acceleration in Relation to Aviation," Federation Proceedings, 1946, 5, 327-344.
5. Lindberg, E. F. and Wood, E. H., "Acceleration," in Physiology of Man in Space, by J. H. W. Brown (ed.), Academic Press, 1963.
6. Fraser, T. M., "Sustained Linear Acceleration," in Bioastronautics Data Book,
7. Little, V. Z., Leverett, S. D. and Hartman, B. O., "Psychomotor and Physiologic Changes During Accelerations of 5, 7, and 9 +G_x," Aerospace Medicine, November 1968.
8. Smedal, H. A., Rogers, T. A., Duane, T. D., Holden, G. R. and Smith, J. R., Jr. "The Physiological Limitations of Performance During Acceleration," Aerospace Medicine, January 1963.
9. Grether, W. F., "Acceleration and Human Performance," Aerospace Medicine, November 1971.
10. Newsom, W. A. and Leverett, S. D., "Retinal Circulation in Man during Centrifugal Acceleration," Transactions of the American Academy of Ophthalmology and Otolaryngology, January-February, 1968, 39-49.
11. White, W. J., Variations in Absolute Visual Threshold during Acceleration Stress, WADC-TR-60-34, WPAFB, Ohio, 1960. AD 243612
12. York, E., Oleynik, R. J. and Patton, R. M., "Human Acceleration Experience at the Aerospace Medical Research Department, U. S. Naval Air Development Center, Johnsville, 1 January 1961 - 30 December 1965," Aerospace Medicine, January 1968.
13. Frankenhaeuser, M., "Effects of Prolonged Gravitational Stress on Performance," Acta Psychologica, Vol 14., 1958.
14. White, W. J. and Jorve, W. R., The Effects of Gravitational Stress upon Visual Acuity, WADC TR 56-247, WPAFB, Ohio, 1958. AD 110444

15. Braustein, M. L. and White, W. J., "Effects of Acceleration on Brightness Discrimination," Journal of Optical Society of America, Vol. 52, No. 8, August 1962.
16. White, W. J. and Monty, R. A., "Vision and Unusual Gravitational Forces," Human Factors, June 1963.
17. Barr, P. O., "Hypoxemia in Man Induced by Prolonged Acceleration," Acta Physiologica Scandinavica, 1962, 54, 128-137.
18. Canfield, A. A., Comrey, A. L. and Wilson, R. C., "The Influence of Increased Positive G on Reaching Movements," The Journal of Applied Psychology, Vol. 37, No. 3, 1953.
19. Cohen, M. M., "Sensory-motor Adaptation and After-effects of Exposure to Increased Gravitational Forces," Aerospace Medicine, March, 1970.
20. Cohen, M. M., "Hand-Eye Coordination in Altered Gravitational Fields," Aerospace Medicine, June, 1970.
21. Kaehler, R. C. and Meehan, J. P., Human Psychomotor Performance under Varied Transverse Accelerations, WADD TR 60-621, Wright Air Development Division, WPAFB, Ohio. AD 247169
22. Canfield, A. A., Comrey, A. L. and Wilson, R. C., "A Study of Reaction Time to Light and Sound as Related to Increased Positive Radial Acceleration," Aviation Medicine, October, 1949.
23. Canfield, A. A., Comrey, A. L., Wilson, R. C., and Zimmerman, W. S., "The Effect of Increased Positive Radial Acceleration upon Discrimination Reaction Time," The Journal of Experimental Psychology, Vol. 40, 1950.
24. Ross, B. M. and Chambers, R. M., "Effects of Transverse G-Stress on Running Memory," Perceptual and Motor Skills, 1967, 24, 423-435.
25. Miller, I., Simon, G. B. and Cohen, E., A Device and Tests for Measuring Intellectual Functions during Acceleration, WADD TR 60-366, WPAFB, Ohio, 1960. AD 243635
26. Brown, J. L. and Collins, C. C., "Air-to-Air Tracking during Closed-Loop Centrifuge Operation," Aviation Medicine, November 1958, Vol. 29, 794-804.
27. Brown, J. L., "Acceleration and Motor Performance," Human Factors, Vol 2., 1960.
28. Piranian, A. G., The Influences of Buffet, Sustained Normal Accelerations, and Basic Aircraft Flying Qualities on Tracking Performance in Air Combat Maneuvering, NADC-73257-30, Naval Air Development Center, Warminster, Pennsylvania.
29. Smiles, K.A., Human Performance Capability in the Aircraft Acceleration Environment of Aerial Combat, AMRL-TR-72-60, Aerospace Medical Research Laboratory, Wright-Patterson Air Force Base, Ohio. AD 759174.

30. Fletcher, D. E., Carter, C. C. and Brown, J. L., "Effects of Positive Acceleration upon the Performance of an Air-to-Air Tracking Task," Aviation Medicine, December 1958.
31. Kaehler, R. C., The Effects of Transverse Accelerations and Exponential Time-Lag Constants on Compensatory Tracking Performance, ASD TR 61-457, Aeronautical Systems Division, WPAFB, Ohio, AD 268185.
32. Middleton, W. C. and White, W. J., "Effects of Centrifuge Radius on the Performance of Entry Task," Aerospace Medicine, August 1968.
33. Creer, B. Y., Stewart, J. D. and Douvillier, J. G., Jr., "Influence of Sustained Accelerations on Certain Pilot-Performance Capabilities," Aerospace Medicine, September 1962.
34. Chambers, R. M., Control Performance under Acceleration with Side-arm Attitude Controllers, NADC-MA-6110, Naval Air Development Center, Johnsville, Penn., 1961.
35. Guercio, J. G. and Wall, R. L., "Congruent and Spurious Motion in the Learning and Performance of a Compensatory Tracking Task," Human Factors, 1972, 14 (3), 259-269.
36. Kleinman, D. L., Baron, S. and Levison, W. H., "An Optimal Control Model of Human Response, Part I: Theory and Validation," Automatica, Vol. 6, 1970.
37. Baron, S., Kleinman, D. L. and Levison, W. H., "An Optimal Control Model of Human Response - Part II: Prediction of Human Performance in a Complex Task," Automatica, Vol. 6, 1970.
38. Kleinman, D. L., Baron, S. and Levison, W. H., "A Control Theoretic Approach to Manned-Vehicle Systems Analysis," IEEE Transactions on Automatic Control, Vol. AC-16, No. 6, 1971.
39. Kleinman, D. L. and Baron, S., Manned Vehicle Systems Analysis by Means of Modern Control Theory, NASA CR-1753, June 1971.
40. Kleinman, D. L., "Covariance Propagation in the Optimal Control Model," private communication.
41. Kleinman, D. L., "FDREP - A General Purpose Subroutine for Human Frequency Domain," private communication.
42. Harvey, T. R. and Dillow, J. D., "Application of an Optimal Control Pilot Model to Air-to-Air Combat," AIAA Guidance and Control Conference, August 1974.
43. Kleinman, D. L. and Baron, S., Analytic Evaluation of Display Requirements for Approach to Landing, BBN Report 2075, Bolt Beranek and Newman Inc., Cambridge, Mass., March 1971.

44. Levison, W. H., "Analysis of Vibration-Induced Pilot Remnant," Proceedings of the 10th Annual Conference on Manual Control, 1974.
45. Korn, J. and Kleinman, D. L., "Advances in Modeling Pilot Tracking Performance in the Presence of Sustained Linear Accelerations," Proceedings of the 15th Annual Conference on Manual Control, 1979.
46. Levison, W. H., "Techniques for Data Analysis and Input Waveform Generation for Manual Research," private communication.
47. Lancraft, R. E., and Kleinman, D. L., "On the Identification of Parameters in the Optimal Control Model," 15th Annual Conference on Manual Control, March 1979.
48. Korn, J., Kleinman, D. L. and Repperger, D. W., "Frequency Domain Measures of Human Performance under G-Stress," Proceedings of the 18th Conference on Decision and Control, December 1979.
49. Powell, M. J. D., "A Method for Minimizing a Sum of Squares of Non-linear Functions without Calculating Derivatives," Computer J., Vol. 7, 1964.

END

DATE
FILMED

5 81

DTIC